A review of electrode materials for electrochemical supercapacitors

Wang, Guoping; Zhang, Lei; Zhang, Jiujun

Publisher's version / Version de l'éditeur:
https://doi.org/10.1039/c1cs15060j
Chemical Society Reviews, 41, 2, pp. 797-828, 2011-07-21

Chem Soc Rev

Cite this: *Chem. Soc. Rev.*, 2012, **41**, 797–828

www.rsc.org/csr

CRITICAL REVIEW

A review of electrode materials for electrochemical supercapacitors

Guoping Wang,*[ab] Lei Zhang*[b] and Jiujun Zhang[b]

Received 4th March 2011
DOI: 10.1039/c1cs15060j

In this *critical review*, metal oxides-based materials for electrochemical supercapacitor (ES) electrodes are reviewed in detail together with a brief review of carbon materials and conducting polymers. Their advantages, disadvantages, and performance in ES electrodes are discussed through extensive analysis of the literature, and new trends in material development are also reviewed. Two important future research directions are indicated and summarized, based on results published in the literature: the development of composite and nanostructured ES materials to overcome the major challenge posed by the low energy density of ES (476 references).

1. Introduction

With the rapid development of the global economy, the depletion of fossil fuels, and increasing environmental pollution, there is an urgent need for efficient, clean, and sustainable sources of energy, as well as new technologies associated with energy conversion and storage.

In many application areas, some of the most effective and practical technologies for electrochemical energy conversion and storage are batteries, fuel cells, and electrochemical supercapacitors (ES). In recent years, ES or ultracapacitors have attracted significant attention, mainly due to their high power density, long lifecycle, and bridging function for the power/energy gap between traditional dielectric capacitors (which have high power output) and batteries/fuel cells (which have high energy storage).[1,2]

The earliest ES patent was filed in 1957. However, not until the 1990s did ES technology begin to draw some attention, in the field of hybrid electric vehicles.[3] It was found that the main function of an ES could be to boost the battery or fuel cell in a hybrid electric vehicle to provide the necessary power for

[a] *College of Chemical Engineering, University of South China, Hengyang 421001, China. E-mail: wgpcd@yahoo.com.cn; Fax: +86 734 8282 375; Tel: +86 734 8282 667*
[b] *Institute for Fuel Cell Innovation, National Research Council of Canada, 4250 Wesbrook Mall, Vancouver, BC V6T 1W5, Canada. E-mail: lei.zhang@nrc.gc.ca; Fax: +1 604 221 3001; Tel: +1 604 221 3087*

Guoping Wang

Dr Guoping Wang is an associate professor at the University of South China. He joined the National Research Council of Canada Institute for Fuel Cell Innovation as a visiting scholar in 2010. Dr Wang received his BE and MEng from Sichuan University and then his PhD from Chinese Academy of Science in 2005 in the field of applied chemistry, under the direction of Prof. Zuolong Yu. Since 2002, Dr Wang has been engaged in the research in the field of electrochemistry. His research interests focus on battery and supercapacitor materials, chemical engineering and processes. He has published over twenty technical papers and holds two Chinese patents.

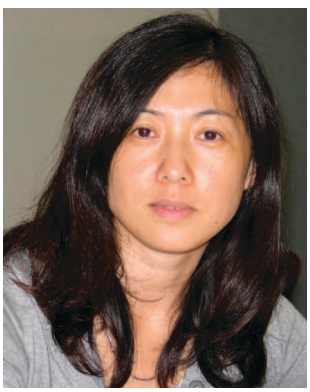

Lei Zhang

Ms Lei Zhang is a Research Council Officer at National Research Council of Canada Institute for Fuel Cell Innovation. She received her first MSc majoring in Materials Chemistry from Wuhan University, China, in 1993 and her second MSc in Materials/Physical Chemistry from Simon Fraser University, Canada, in 2000. Ms Zhang's main research interests include PEM fuel cell electrocatalysis, catalyst layer/electrode structure, metal–air batteries and supercapacitors. Ms Zhang is an adjunct professor of Federal University of Maranhao, Brazil, and Zhengzhou University, China, respectively. She is also an international advisory member of the 7th IUPAC International Conference on Novel materials and their Synthesis (NMS-VII) and an active member of the Electrochemical Society and the International Society of Electrochemistry.

acceleration, with an additional function being to recuperate brake energy.[4] Further developments have led to the recognition that ES can play an important role in complementing batteries or fuel cells in their energy storage functions by providing back-up power supplies to protect against power disruptions. As a result, the US Department of Energy has designated ES to be as important as batteries for future energy storage systems.[5] Many other governments and enterprises have also invested time and money into exploring, researching, and developing ES technologies.

Recent years have yielded major progress in the theoretical and practical research and development of ES, as evinced by a large number of research articles and technical reports.[6–14] At the same time, the disadvantages of ES—including low energy density and high production cost—have been identified as major challenges for the furtherance of ES technologies.

To overcome the obstacle of low energy density, one of the most intensive approaches is the development of new materials for ES electrodes. Most popular today are carbon particle materials, which have high surface areas for charge storage. But in spite of these large specific surface areas, the charges physically stored on the carbon particles in porous electrode layers are unfortunately limited. ES of this kind, called electrostatic or electrical double-layer supercapacitors (EDLS), have a limited specific capacitance (measured in Faradays per gram of the electrode material) and a low ES energy density. Advanced approaches to increase the ES energy density are to hybridize the electrode materials by adding electrochemically active materials to a carbon-particle-based ES electrode layer or to completely replace the carbon materials with electrochemically active materials. ES with electrochemically active materials as electrodes are called faradaic supercapacitors (FS). It has been demonstrated that faradaic or hybrid double-layer supercapacitors can yield much higher specific capacitance and ES energy density than EDLS.[15]

Regarding advanced ES materials, metal oxides such as ruthenium oxides and manganese oxides are considered the most promising materials for the next generation of ES. Therefore, in this review we pay particular attention to metal oxides and their applications in ES electrodes. First, however, we provide some introductory background on ES, which we hope will facilitate our review and analysis of the literature. Finally, we will discuss the direction that future research in ES might be expected to take.

2. Fundamentals and applications of ES

2.1 Two types of ES

An ES is a charge-storage device similar to batteries in design and manufacturing. As shown in Fig. 1, an ES consists of two electrodes, an electrolyte, and a separator that electrically isolates the two electrodes. The most important component in an ES is the electrode material. In general, the ES's electrodes are fabricated from nanoscale materials that have high surface area and high porosity. It can be seen from Fig. 1 that charges can be stored and separated at the interface between the conductive solid particles (such as carbon particles or metal oxide particles) and the electrolyte. This interface can be treated as a capacitor with an electrical double-layer capacitance, which can be expressed as eqn (1):

$$C = \frac{A\varepsilon}{4\pi d} \quad (1)$$

where A is the area of the electrode surface, which for a supercapacitor should be the active surface of the electrode porous

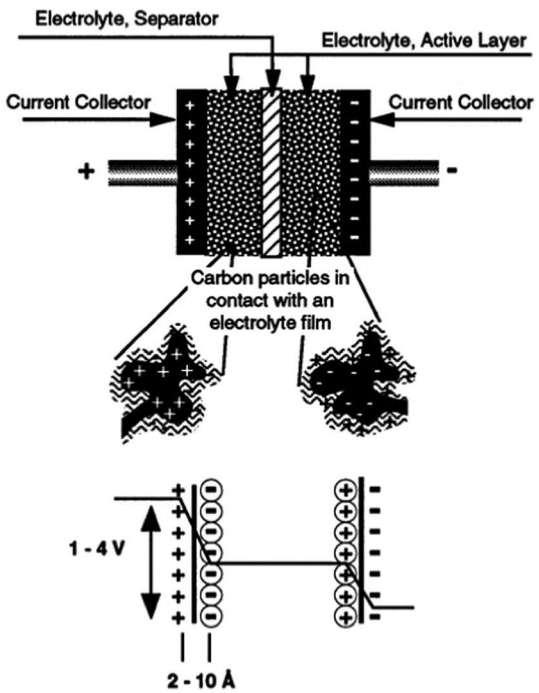

Fig. 1 Principles of a single-cell double-layer capacitor and illustration of the potential drop at the electrode/electrolyte interface.[3] (Reprinted from ref. 3 with permission from Elsevier.)

Jiujun Zhang

Dr Jiujun Zhang is a Senior Research Officer and PEM Catalysis Core Competency Leader at the National Research Council of Canada Institute for Fuel Cell Innovation (NRC-IFCI). Dr Zhang received his BS and MSc in Electrochemistry from Peking University in 1982 and 1985, respectively, and his PhD in Electrochemistry from Wuhan University in 1988. After completing his PhD, he was an associate professor at the Huazhong Normal University for two years. Starting in 1990, he carried out three terms of postdoctoral research at the California Institute of Technology, York University, and the University of British Columbia. Dr Zhang has over twenty-eight years of R&D experience in theoretical and applied electrochemistry. He holds several adjunct professorships, and is an active member of the Electrochemical Society, the International Society of Electrochemistry, and the American Chemical Society.

layer; ε is the medium (electrolyte) dielectric constant, which will be equal to 1 for a vacuum and larger than 1 for all other materials, including gases; and d is the effective thickness of the electrical double layer.

As described in the Introduction, two types of ES exist. One is the EDLS, in which the electrode material, such as carbon particles, is not electrochemically active. In other words, there is no electrochemical reaction on the electrode material during the ES charging and discharging processes, and pure physical charge accumulation occurs at the electrode/electrolyte interface. The other type is the FS, in which the electrode material is electrochemically active, *e.g.* metal oxides, which can directly store charges during the charging and discharging processes.[15–17]

2.1.1 Electrostatic supercapacitors (EDLS). The capacitance of the electrode/interface in an electrostatic or EDLS is associated with an electrode-potential-dependent accumulation of electrostatic charge at the interface. The mechanism of surface electrode charge generation includes surface dissociation as well as ion adsorption from both the electrolyte and crystal lattice defects.[5] These processes operate solely on the electrostatic accumulation of surface charge. As shown in Fig. 1, this electrical double-layer capacitance comes from electrode material particles, such as at the interface between the carbon particles and electrolyte, where an excess or a deficit of electric charges is accumulated on the electrode surfaces, and electrolyte ions with counterbalancing charge are built up on the electrolyte side in order to meet electroneutrality. During the process of charging, the electrons travel from the negative electrode to the positive electrode through an external load. Within the electrolyte, cations move towards the negative electrode while anions move towards the positive electrode. During discharge, the reverse processes take place. In this type of ES, no charge transfers across the electrode/electrolyte interface, and no net ion exchanges occur between the electrode and the electrolyte. This implies that the electrolyte concentration remains constant during the charging and discharging processes. In this way, energy is stored in the double-layer interface.

If the two electrode surfaces can be expressed as E_{S1} and E_{S2}, an anion as A^-, a cation as C^+, and the electrode/electrolyte interface as //, the electrochemical processes for charging and discharging can be expressed as eqn (2)–(5).[18,19]

On one electrode (say, a positive one):

$$E_{S1} + A^- \xrightarrow{\text{charging}} E_{S1}^+//A^- + e^- \quad (2)$$

$$E_{S1}^+//A^- + e^- \xrightarrow{\text{discharging}} E_{S1} + A^- \quad (3)$$

On the other electrode (say, a negative one):

$$E_{S2} + C^+ + e^- \xrightarrow{\text{charging}} E_{S2}^-//C^+ \quad (4)$$

$$E_{S2}^-//C^+ \xrightarrow{\text{discharging}} E_{S2} + C^+ + e^- \quad (5)$$

And the overall charging and discharging process can be expressed as eqn (6) and (7):

$$E_{S1} + E_{S2} + A^- + C^+ \xrightarrow{\text{charging}} E_{S1}^+//A^- + E_{S2}^-//C^+ \quad (6)$$

$$E_{S1}^+//A^- + E_{S2}^-//C^+ \xrightarrow{\text{discharging}} E_{S1} + E_{S2} + A^- + C^+ \quad (7)$$

2.1.2 Faradaic supercapacitors (FS). Faradaic supercapacitors (FS) or pseudocapacitors are different from electrostatic or EDLS. When a potential is applied to a FS, fast and reversible faradaic reactions (redox reactions) take place on the electrode materials and involve the passage of charge across the double layer, similar to the charging and discharging processes that occur in batteries, resulting in faradaic current passing through the supercapacitor cell. Materials undergoing such redox reactions include conducting polymers and several metal oxides, including RuO_2, MnO_2, and Co_3O_4.[15,20–22] Three types of faradaic processes occur at FS electrodes: reversible adsorption (for example, adsorption of hydrogen on the surface of platinum or gold), redox reactions of transition metal oxides (*e.g.* RuO_2), and reversible electrochemical doping–dedoping in conductive polymer based electrodes.[15]

It has been demonstrated that these faradaic electrochemical processes not only extend the working voltage but also increase the specific capacitance of the supercapacitors.[23] Since the electrochemical processes occur both on the surface and in the bulk near the surface of the solid electrode, a FS exhibits far larger capacitance values and energy density than an EDLS. As reported by Conway *et al.*,[24] the capacitance of a FS can be 10–100 times higher than the electrostatic capacitance of an EDLS. However, a FS usually suffers from relatively lower power density than an EDLS because faradaic processes are normally slower than nonfaradaic processes.[25] Moreover, because redox reactions occur at the electrode, a FS often lacks stability during cycling, similar to batteries.

It is worth mentioning that hybrid ES with an asymmetrical electrode configuration (*e.g.* one electrode consists of electrostatic carbon material while the other consists of faradaic capacitance material) have been extensively studied recently to capitalize on both electrode materials' advantages in improving overall cell voltage, energy, and power densities.[14,26,27] In this kind of hybrid supercapacitor, both electrical double-layer capacitance and faradaic capacitance mechanisms occur simultaneously, but one of them plays a greater role. In both mechanisms, large surface area, appropriate pore-size distribution, and high conductivity are essential properties of the electrode materials to achieve large capacitance, as will be discussed in a later section.

2.2 ES capacitance, voltage, power, and energy density

Fig. 1 shows that the entire cell can be treated as two capacitors in series. If the capacitances of the two electrodes, *i.e.* positive and negative, can be expressed as C_p and C_n, respectively, the overall capacitance (C_T) of the entire cell can be expressed as eqn (8):[11]

$$\frac{1}{C_T} = \frac{1}{C_p} + \frac{1}{C_n} \quad (8)$$

If the two electrodes are the same, namely, $C_p = C_n$, the overall capacitance C_T would be half of either one's capacitance, the corresponding ES is called a symmetric ES. In the case of $C_p \neq C_n$ (the anode and the cathode have two different electrode materials, the corresponding ES is called an asymmetric ES), C_T is mainly dominated by the one with smaller capacitance. In general, the capacitance and stored charge essentially depend on the electrode material used.

When the ES is charged, a voltage (V) will build up across the two electrodes. The theoretical (or maximum) energy (E) and power densities (P) of this ES can be expressed as eqn (9) and (10):[7,8]

$$E = \frac{1}{2}CV^2 = \frac{QV}{2} \quad (9)$$

$$P = \frac{1}{4R_S}V^2 \quad (10)$$

where Q denotes the stored total charges in the ES and R_S stands for the equivalent inner resistance of the ES. From these two equations, it can be seen that V, C and R_S are three important variables determining the ES's performance. In order to increase ES's energy density and power density, one has to put effort in increasing the values of both V and C or reducing the value of R_S. Here the value of the ES voltage (V) is dependent on the materials used for the electrode and electrolyte (*e.g.* when carbon is used as the electrode material for aqueous electrolytes, the cell voltage or supercapacitor voltage window is about 1 V, while in organic electrolytes the cell voltage is in the range of 3–3.5 V), whereas the operating voltage is determined by the electrolyte's stability window.

From both eqn (9) and (10), it can be seen that both energy and power densities are proportional to the square of voltage, therefore, increasing the voltage may be more effective than increasing capacitance or reducing inner resistance in terms of raising the ES's energy and power densities. To increase the ES's cell voltage within the electrolyte's stability window, selecting the type of electrode materials and optimizing electrode structures can achieve high cell voltages.

Furthermore, eqn (10) indicates that the larger the cell internal resistance, the lower the power density will be. Therefore, in order to increase the power density of ES, reducing cell's internal resistance, a sum of electrode and electrolyte resistances, should be the major focus. In general, ES's inner resistance is much smaller than that of batteries due to the rapid combination of positive and negative charges (even in a faradaic-type ES, the redox processes involving electron and ion transfers are also very fast), the power density of an ES is normally much higher than in batteries. Even so, reducing inner resistance can always benefit the ES's performance in terms of power density improvement.

Eqn (9) indicates that the energy density of ES is proportional to its capacitance, meaning that the higher the capacitance, the higher the energy density will be. Therefore, increasing the capacitance is an effective way to improve energy density. This can be achieved by improving the specific capacitance of electrode materials as well as optimizing electrode layer structures. In order to increase overall cell capacitance, both electrode capacitances have to be increased. Therefore, developing electrode materials should be one of the key approaches in ES research and development.

In evaluating an electrode material for ES, another generally used definition is the specific capacitance (C_s), with a unit of Faraday per gram (F g^{-1}), which can be expressed as eqn (11):

$$C_s = \frac{C_i}{W} \quad (11)$$

where W is the weight in grams of the electrode material in the electrode layer, and C_i is the electrode capacitance (anode or cathode). Note that this specific capacitance is the intrinsic capacitance of the material. A higher specific capacitance does not necessarily mean that this material will be a better ES electrode material, because electrode capacitance is also strongly dependent on the electrode layer structure and the electron and ion transfers within the layer. For example, a material that forms an extremely thin film on the electrode surface can yield a huge specific capacitance value because of its very low weight. However, when using this high capacitance material to construct a thick layer and thereby achieve high electrode capacitance for energy storage, the electrode capacitance may not be as high as expected; this will be discussed further in later sections. Nonetheless, the concept of specific capacitance has been adopted as an important parameter in evaluating an ES material.

2.3 Electrolyte

As shown in Fig. 1, besides the two electrodes, the electrolyte, which resides inside the separator as well as inside the active material layers, is also one of the most important ES components. The requirements for an electrolyte in ES include: wide voltage window, high electrochemical stability, high ionic concentration and low solvated ionic radius, low resistivity, low viscosity, low volatility, low toxicity, low cost as well as availability at high purity.

The electrolyte used in an ES can be classified into three types: (1) aqueous electrolyte, (2) organic electrolyte, and (3) ionic liquids (ILs).

(1) *Aqueous electrolyte*. Compared with organic electrolytes, aqueous electrolytes (such as H_2SO_4, KOH, Na_2SO_4 and NH_4Cl aqueous solution and so on) can provide a higher ionic concentration and lower resistance. ES containing aqueous electrolyte may display higher capacitance and higher power than those with organic electrolytes, probably due to higher ionic concentration and smaller ionic radius. In addition, aqueous electrolytes can be prepared and utilized without stringently controlling the preparing processes and conditions, while organic ones need strict processes and conditions to obtain ultra-pure electrolytes.

Unfortunately, a large disadvantage of aqueous electrolytes is their small voltage window as low as about 1.2 V, much lower than those of organic electrolytes. According to eqn (9) and (10), it can be seen that aqueous electrolytes have a large limitation in terms of improving both energy and power densities due to their narrow voltage window. This is the reason why organic electrolytes are often recommended.

(2) *Organic electrolyte*. Compared to aqueous electrolytes, organic electrolytes can provide a voltage window as high as 3.5 V.

This is a large advantage of organic over aqueous electrolytes. Among organic electrolytes, acetonitrile and propylene carbonate (PC) are the most commonly used solvents. Acetonitrile can dissolve larger amounts of salt than other solvents, but suffers from environmental and toxic problems. PC-based electrolytes are friendly to the environment and can offer a wide electrochemical window, a wide range of operating temperature, as well as good conductivity. Besides, organic salts such as tetraethylammonium tetrafluoroborate, tetraethylphosphonium tetrafluoroborate, and triethylmethylammonium tetrafluoroborate ($TEMABF_4$) have also been used in ES electrolytes. Salts with less symmetric structures have lower crystal-lattice energy and increased solubility. However, one issue which should be kept in mind is that the water content in organic electrolytes must be kept below 3–5 ppm. Otherwise, the ES's voltage will be significantly reduced.

(3) *Ionic liquids (ILs)*. A salt may be melted, namely, 'liquified', by providing heat to the system to counterbalance the salt lattice energy. Such a system is called molten salts or ILs. ILs can exist in liquid form at the desired temperatures. Their desirable properties make them promising candidates for ES electrolytes. These properties include low vapor pressure, high thermal and chemical stability,[28,29] low flammability, wide electrochemical stability window ranging from 2 to 6 V, typically about 4.5 V, and conductivity at a level of *ca.* 10 mS cm^{-1}.[30] Since ILs are solvent-free, there is no solvation shell in ILs, and thus ILs can offer a well identified ion size.[1]

The main ILs studied for ES applications are imidazolium, pyrrolidinium, as well as asymmetric, aliphatic quaternary ammonium salts with anions such as tetrafluoroborate, trifluoromethanesulfonate, bis(trifluoromethanesulfonyl)imide, bis(fluorosulfonyl)imide or hexafluorophosphate.[30–32] Room temperature ILs are usually quaternary ammonium salts such as tetralkylammonium $[R_4N]^+$, and cyclic amines such as aromatic pyridinium, imidazolium and saturated piperidinium, pyrrolidinium. Low temperature molten salts based on sulfonium $[R_3S]^+$ as well as phosphonium $[R_4P]^+$ cations are also explored in the literature.[30]

The chemical–physical properties of these ILs strongly depend on the type of cation and anion. For example, aliphatic quaternary ammonium and pyrrolidinium salts display a wider potential range, sometimes exceeding 5 V, but their conductivity is generally lower than that of 1-ethyl-3-methylimidazolium-based ILs which remain liquid down to low temperature (< -50 °C) and display higher conductivities as high as 10^{-2} S cm^{-1} at room temperature.[31]

A number of electrodes and devices have been prepared using ILs. For example, ethyl-methyl-imidazolium-bis(trifluoromethane-sulfonyl)imide was used to investigate the relationship between the pore size of carbon electrodes, ion size of the electrolyte, and the capacitance.[1] *N*-Butyl-*N*-methyl pyrrolidinium bis-(trifluoromethane sulfonyl)imide (NBNMPBTSI), which has low melting temperature, hydrophobic and highly cycleable properties within a wide voltage window, allowed hybrid ES to be operated between 3.4 and 1.5 V.[33] 1-Ethyl 3-methyl imidizolium bistrifluoromethylsulfonyl imide showed better fluidity than NBNMPBTSI.[34] The use of solvent-free 1-butyl-3-methyl imidazolium hexafluorophosphate,[35] with good conductivity, wide electrochemical window and low vapor pressure, could help mesoporous nickel-based mixed rare-earth oxide electrodes to reach a higher power density of 458 W kg^{-1}, a higher energy density of 50 W h kg^{-1}, as well as an excellent cycle life (no apparent capacity loss during 500 cycles). It was also reported that *N*-methyl-*N*-propyl-pyrrolidinium bis(fluorosulfonyl)imide might be a very promising IL because it possesses a wider potential range together with high conductivity at room temperature.[31]

The challenge for ILs is to design ILs having a wider potential range together with high conductivity in a wide temperature range. To extend the temperature range, the methoxyethyl group has been introduced on the N atom, resulting in *N*-methyl-(2-methyoxyethyl)ammonium tetrafluoroborate, and *N*-methoxyethyl-*N*-methylpyrrolidinium bis(trifluoro-methanesulfonyl)imide, which made them remain in the liquid state down to −35 and −95 °C, respectively.[31]

To overcome the issue of insufficient electrolyte conductivity of ILs, particularly at the temperatures lower than room temperature, a dilution of ILs with organic solvents (such as acetonitrile, propylene carbonate or γ-butyrolactone) might be feasible. For example, ILs mixed with the commonly used $PC/TEMABF_4$ electrolytes showed some improvement in conductivity and therefore higher capacity and enhanced low-temperature power density. However, this approach may give rise to other problems such as safety, toxicity, flammability and narrow temperature regimes and so on. Furthermore, to achieve a high wettability of electrodes by ILs, the interface properties of electrode–IL need to be optimized.

2.4 ES Fabrication and manufacturing

Main processes in the fabrication of cells include five steps: (1) coating the electrode; (2) winding; (3) filling with an electrolyte; (4) testing; and (5) welding and sealing.

The electrode, the heart of the cell, determines the ES performance in terms of self-discharge, life expectancy, capacity, resistance, and so on. Therefore, the electrode fabrication including an active material coating process is the most important step. As a result, strictly controlling the preparation process is necessary for achieving both high performance and durability. Normally, aluminium foil is used as the current collector because of its high current-carrying capability, chemical stability and low cost. In the process of coating electrodes, firstly, binders, active materials and conductive additives are mixed to obtain a homogeneous slurry with the desired density, and then the slurry is spread onto an etched aluminium foil, followed by drying the electrode and roll-pressing to achieve a uniform electrode coating layer. Once the electrodes are prepared, they are brought into a glove box with ultra-low moisture. A pair of such electrodes, with a separator layer inserted between them, is wound around a central mandrel into the desired shape. Then the electrolyte is filled into this separator. The electrolyte-filling process generally requires special care. The amount of electrolyte in the cell is critical, because excess electrolyte can lead to excessive gassing and leakage in operation. Generally, the process is slow, typically taking one to two days, and is relatively labor intensive. This is because of the nanopore level of internal porosity of active materials, making the wetting process slow. After the completion of electrolyte filling, the cell is subjected to

cycling test (for two to five formation cycles). During formation, the abnormal cells are removed away. Some manufacturers will follow formation with evacuation and final welding and sealing, while others will pre-seal the cell prior to formation. The cells may be cycled further to establish stable capacity, depending on applications.

In order to match different applications, ES cells are connected in series or in parallel to obtain the desired output voltage or energy capacity. Several ES cells are connected to be one module, which may be connected with other modules. However, the difference in self-discharge will make the voltages of all cells unequal. Under extreme situations, some cells' voltages may be even negative (called "cell reversal"). These differences among cell voltages can also alter with the change of operating voltage of the ES module. If measures are not taken to balance the voltages, the life expectancy of ES will be shortened significantly. The principles of voltage balancing have two types: passive and active balancing. Passive voltage balancing, which can cause large power loss, refers to instantly balancing the voltage difference. Active voltage balancing is instructed using a controller with an individual charging system.

2.5 ES electrode material evaluation

2.5.1 Cyclic voltammetry. The normal way to carry out material capacitance measurements is to coat the chosen material onto an inert electrode surface, then measure this electrode in the chosen electrolyte using electrochemical cyclic voltammetry (CV) to record cyclic voltammograms of the material, from which the capacitance can be calculated. If the charge (Q in eqn (9)) accumulated inside the electrode layer is measured using the area under the cyclic voltammogram in either direction in a potential window from E_1 to E_2, the capacitance, C_i ($=C_p$ or C_n), of this electrode layer can be obtained by eqn (12):

$$C_i = \left|\frac{Q}{E_2 - E_1}\right| \qquad (12)$$

2.5.2 Electrochemical impedance spectroscopy (EIS). In addition to cyclic voltammetry, electrochemical impedance spectroscopy (EIS) is also a useful tool for determining the capacitance of ES materials.[19,29]

The most popular way to run EIS measurements is collecting the ES impedance data at the open-circuit potential by applying a small amplitude of alternative interrupting potential (*e.g.*, ±5 to ±10 mV) over a wide range of frequency f (*e.g.*, 1 mHz to 1 MHz). It can provide the relationship between the imaginary part of impedance $|Z|$ and f. The capacitance can be calculated using $C = 1/(2\pi f|Z|)$ using a linear portion of a $\log|Z|$ *vs.* $\log f$ curve, which is called the Bode plot. This Bode plot shows that the capacitance decreases with increasing frequency, and at the high frequency region the supercapacitors behave like a pure resistance, indicating that the electrolyte ions probably cannot penetrate into micropores under high frequencies. The EIS can also be expressed as a Nyquist diagram, where the imaginary part of impedance, $Z(f)''$, is plotted against the real part of impedance, $Z(f)'$.[9] From the Nyquist plot, a charge transfer resistance can be obtained from the diameter of the semicircle on this plot. At high frequency (larger than 10^4 Hz), the impedance implies the conductivity of both active materials and electrolyte. The high-to-medium frequency region (10^4 to 1 Hz) shows pseudocharge transfer resistance, which is associated with the porous structure of the electrodes. At low frequency ranges (less than 1 Hz), the impedance plot is the characteristic feature of pure capacitive behavior. Theoretically, a pure capacitor should display a parallel line to the imaginary axis of the Nyquist plot. However, in normal cases, the plot shows a line with the inclined angle between 45° and 90° against the real axis, corresponding to the ion diffusion mechanism between Warburg diffusion and ideal capacitive ion diffusion (pseudo capacitance).[36,37] This deviation from the parallel line may be attributed to two reasons: one is the different penetration depth of the alternating current signal in virtue of pore size distribution at both electrodes, leading to abnormal capacitance, the other is the redox reaction at the electrode, giving rise to pseudocapacitance.[35,38]

2.6 Advantages, challenges, and applications of ES

2.6.1 Advantages of ES. Compared to batteries, ES have several advantages:

(1) *High power density*. Fig. 2 compares specific power *versus* specific energy of modern storage devices. It is clear that ES display a much higher power delivery (1–10 kW kg^{-1}) when compared to lithium ion batteries (150 W kg^{-1}). Since an ES stores electrical charges both at the electrode surface and in the bulk near the surface of the solid electrode, rather than within the entire electrode, the charge–discharge reaction will not necessarily be limited by ionic conduction into the electrode bulk, so the charging and discharging rates are much faster than the electrochemical redox reactions inside batteries. These rapid rates lead to high power density in ES. For example, an ES can be fully charged or discharged in seconds (~30 s), and the energy can be taken from it very rapidly, within 0.1 s.[39,40] For batteries, the charging time is normally on the scale of hours.

(2) *Long life expectancy*. The storage of electrochemical energy in batteries is realized through faradaic reactions, which often involve irreversible interconversion of the chemical electrode reagents and irreversible phase changes.

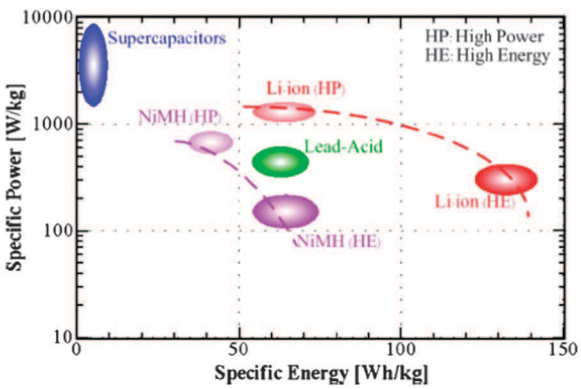

Fig. 2 Specific power *versus* specific energy of modern storage devices.[41] (Cited from the permission of Database ©2009 IEEE.)

In contrast, when energy is stored in an ES, no or negligibly small chemical charge transfer reactions and phase changes are involved in charging and discharging, so an ES can have almost unlimited cyclability. ES do not need any maintenance during their lifetimes and can withstand a huge number of charge–discharge cycles, up to 1 000 000. Moreover, ES can run deeply at high rates for 500 000–1 000 000 cycles with only small changes in their characteristics. Such longevity is impossible for batteries even if the depth of discharge is as small as 10–20% of the overall energy. The life expectancy for ES is estimated to be up to 30 years, which is much longer than for lithium ion batteries (1000–10 000 cycles and a life expectancy of only 5–10 years). Even for FS, although fast redox reactions are involved during charging and recharging, their life expectancy is also much longer than that of batteries.[9,14,15,23]

(3) *Long shelf life*. Another advantage of supercapacitors is their long shelf life. Most rechargeable batteries if left on the shelf unused for months will degrade and become useless due to self-discharge and corrosion. In contrast, ES maintain their capacitance and thus are capable of being recharged to their original condition, although self-discharge over a period of time can lead to a lower voltage. It is reported that ES can sit unused for several years but still remain close to their original condition.[14]

(4) *High efficiency*. ES are reversible with respect to charging and discharging throughout their complete operating range of voltage, and the energy loss to heat during each cycle is relatively small and readily removed (*i.e.*, heat management is easy). This means that the cycle efficiency of ES is high (around 95%) even when operating at rates above 1 kW kg^{-1}.[42]

(5) *Wide range of operating temperatures*. ES can function effectively at extremely high and low temperatures. The typical operating temperature for ES ranges from −40 to 70 °C. This is advantageous for military applications, where reliable energy storage is required to run proprietary electronic devices under all temperature conditions during war.

(6) *Environmental friendliness*. ES, in general, do not contain hazardous or toxic materials, and their waste materials are easily disposed.

(7) *Safety*. In normal circumstances, ES are much safer than batteries, in particular lithium-ion batteries.

In summary, compared to other energy storage systems such as batteries and fuel cells, ES are superior in the areas of life expectancy (without any noticeable performance degradation after long-term operation), reversibility, power density, shelf life, efficiency, operating temperatures, environmental friendliness, and safety.[3,14–17,23,43–46]

2.6.2 Challenges for ES. Although ES have many advantages over batteries and fuel cells, they also face some challenges at the current stage of technology.

(1) *Low energy density*. ES suffer from limited energy density (about 5 W h kg^{-1}) when compared with batteries (> 50 W h kg^{-1}), as shown in Fig. 2. Commercially available ES can provide energy densities of only 3–4 W h kg^{-1}. If a large energy capacity is required for an application, a larger supercapacitor must be constructed, driving up the cost. Low energy density is the major challenge for ES applications in the short and medium terms.

(2) *High cost*. The costs of raw materials and manufacturing continue to be major challenges for ES commercialization. The main cost of an ES arises from its electrode materials. At present, for practical purposes carbon and RuO_2 are the most common electrode materials used in commercial ES. However, carbon materials, in particular those with a high surface area, are presently expensive (US$50–100 per kg),[14] not to mention the cost of a rare metal oxide such as RuO_2. In addition, the separator and the electrolyte can also boost the expense. For example, if ES use organic electrolytes, their cost is far from negligible.

(3) *High self-discharging rate*. ES have a low duration and a high self-discharging rate of 10–40% per day.[43] In some applications, this has been considered a major obstacle to their practical use.

(4) *Industrial standards for commercialization*. Currently, carbon/carbon ES with capacitance of 50–5000 F have become commercially available, the electrolyte used in such kind of ES is acetonitrile, which can give a cell voltage of 2.7 V with a typical specific energy of 4 W h kg^{-1}. This performance was achieved when charging the device at 400 W kg^{-1} from 100% to 50% of the rated voltage. Although this kind of ES is commercially available, it is necessary to establish some general industrial standards such as performance, electrode structure, electrode layer thickness and porosity and so on. However, due to the variety of applications as well as limited commercial products, we are still not able to search out generally available industrial standards for ES at this moment. Gore's commercial electrode may give us some sense what the standards may look like. Gore's electrode, which is prepared by coating the activated carbon–PTFE composite on an etched aluminium collector, exhibits a BET surface density of ~1800 m^2 g^{-1}, a thickness of 0.3 mm and an average pore diameter of ~2 nm.[31] Actually, the requirement for electrode thicknesses should be strongly dependent on the ES applications. For example, for energy sensitive applications, the coating may be around 150 microns, while for power sensitive applications, the thickness is probably about 100 microns. Therefore, it is necessary to put some effort on ES standard establishment for different applications.

2.6.3 Applications of ES. With their many advantages, ES have become very competitive choices for applications such as electric vehicles, electric hybrid vehicles, digital communication devices, digital cameras, mobile phones, electrical tools, pulse laser techniques, uninterruptible power supplies, and storage of the energy generated by solar cells.[25,47–54]

For example, in memory back-up, batteries' poorer cycle life makes their frequent replacement expensive (adding 20% onto the price of battery operated appliances).[55] In addition, in battery powered electric vehicles, batteries with lower power density cannot meet peak load requirements, originating from accelerating or climbing. With advantages such as long lifetime and high power density, ES can solve these problems.[23] Combining ES with batteries can yield improved performance in hybrid electric vehicles, including powerful acceleration, braking energy recovery, excellent cold weather starting, and increased battery life. Thus, ES has the potential to play an important role in complementing or replacing batteries in the

energy conversion and storage fields.[1] The main market targeted by ES manufacturers in the coming decades may be transportation, including hybrid electric vehicles and metro trains.[54,56]

Due to their relatively low energy density and high cost, the market development of ES is still in the early commercialization stage. Currently, ES occupy less than 1% of the world market for electrical energy storage (batteries and supercapacitors). In 2007, the total supercapacitors market generated revenues of about $99.6 million. At present, NEC (Japan), Elna (Japan), and Panasonic (Japan) occupy a large share of the ES market.[23] Other manufacturers of ES include SAFT (France), Cap-XX (Australia), NESS (South Korea), Korchip (South Korea), Econd (Russia), ESMA (Russia), ELIT (Russia), Maxwell (USA), AVX (USA), Copper (USA), EPCOS (USA), EVANS (USA), Kold Ban (USA), PowerSystem Co. (Japan), and Chubu Electric Power (Japan).[14,43,57] The ES market is moving ahead steadily and changing significantly every year. It is expected that a compound annual growth rate of 10.9% will be achieved for the next ten years, with $205.9 million in revenue generated by 2014. Continuing improvements will open new markets, leading to a bright future for ES.[3]

3. Electrode materials

As discussed above, the capacitance and charge storage of ES intimately depend on the electrode materials used. Therefore, further developing new materials with high capacitance and improved performance relative to existing electrode materials is the most important method to overcome these challenges.[58]

Apparently, the capacitance of ES heavily depends on the specific surface area of the electrode materials. Since not all the specific surface area is electrochemically accessible when the material is in contact with an electrolyte, the measured capacitance of various materials does not linearly increase with increasing specific surface area. Thus, for those electrochemically accessible surface area or useful surface area, a definition called the electrochemical active surface area may be more accurate in describing the electrode capacitance behavior. The pore size of the electrode material plays an important role in the electrochemical active surface area. According to Largeot *et al.*,[1] the pore size of electrode materials that yielded maximum double-layer capacitance was very close to the ion size of the electrolyte (with respect to an ionic liquid electrolyte), and both larger and smaller pores led to a significant drop in capacitance. However, increasing the pore size can also increase the average distance d between the pore wall and the center of an ion, then make the capacitance of materials with larger pores decreased according to eqn (1).[1] The porosity relevant to the development of high capacitance is itself not a simple parameter, involving both pore sizes and pore-size distribution for a given overall specific area ($m^2\ g^{-1}$) of the material. Therefore, ES capacitance strongly depends on the surface area of the electrode accessible to the electrolyte.

In general, the electrode materials of ES can be categorized into three types:[15,59,60] (1) carbon materials with high specific surface area,[61,62] (2) conducting polymers,[63–67] and (3) metal oxides, such as RuO_2,[68,69] IrO_2,[70] MnO_2,[71,72] NiO,[73,74] Co_2O_3,[75] SnO_2,[76] V_2O_5,[77–79] and MoO.[45,80]

3.1 Carbon materials

Carbon materials are considered prospective electrode materials for industrialization. The advantages of carbon materials include abundance, lower cost, easy processing, non-toxicity, higher specific surface area, good electronic conductivity, high chemical stability, and wide operating temperature range.[23] Carbon-based electrochemical capacitors are close to electrochemical double-layer capacitors. As shown in Fig. 3,[81] cyclic voltammetry curves of carbon materials have good rectangular shapes, suggesting that they are appropriate capacitive materials for ES. Their galvanostatic charge–discharge profile, with its triangular symmetrical distribution, also indicates good capacitive properties for ES. Normally, carbon materials store charges mainly in an electrochemical double-layer formed at the interface between the electrode and the electrolyte, rather than storing them in the bulk of the capacitive material. Therefore, the capacitance predominantly depends on the surface area accessible to the electrolyte ions. The important factors influencing their electrochemical performance are specific surface area, pore-size distribution, pore shape and structure, electrical conductivity, and surface functionality. Among these, specific surface area and pore-size

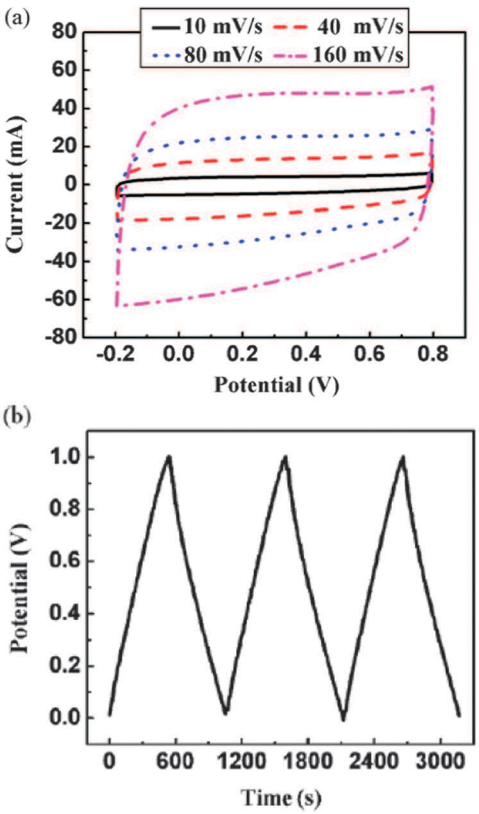

Fig. 3 (a) Cyclic voltammetry curves of an activated mesocarbon microbeads (AMCMBs)/CNTs compound electrode at different scan rates (10, 40, 80, and 160 mV s^{-1}); (b) galvanostatic charge–discharge curves of the AMCMBs/CNTs compound electrode at a constant specific current of 0.5 A g^{-1}.[81] (Reprinted from ref. 81 with permission from Elsevier.)

distribution are the two most important factors affecting the performance of carbon materials.

As suggested by Conway,[15] the carbon for double-layer type supercapacitors must have three properties: (1) high specific areas, in the order of 1000 m^2 g^{-1}, (2) good intra- and interparticle conductivity in porous matrices, and (3) good electrolyte accessibility to the intrapore space of carbon materials. According to these three properties, in the process of selecting supercapacitor electrode materials the general rule is to obtain a high and accessible specific surface area with good electrical conductivity.

High surface area carbon materials mainly include activated carbon,[82–87] carbon aerogels,[88] carbon nanotubes (CNTs),[89,90] templated porous carbons,[91–94] and carbon nanofibres.[95] The performance of these carbons as ES electrode materials has been described in detail in the literature.[9] However, in most cases[14] the measured specific capacitances of carbon materials in real supercapacitors are less than those stated in the literature, with values in the range of 75–175 F g^{-1} for aqueous electrolytes and 40–100 F g^{-1} for organic electrolytes.

In general, carbon materials with larger specific surface areas have a higher capability for charge accumulation at the electrode/electrolyte interface.[6] Many methods have been investigated to increase the specific surface area, including heat treatment, alkaline treatment, steam or CO_2 activation, and plasma surface treatment with NH_3.[61,84,96–104] These methods can effectively make micropores and defects on the carbon surface, leading to an increase in the specific surface area.

However, specific capacitance is sometimes not directly proportional to the specific surface area. This is because not all micropores in the electrode layer are necessarily accessible to electrolyte ions. Even today, there is still no common understanding or agreement about the effect of optimal pore size on the performance of carbon electrode materials. Some studies have reported that pore sizes of either 0.4 or 0.7 nm could be suitable for aqueous electrolytes, while a pore size of around 0.8 nm might be better for organic electrolytes.[84,86] In recent papers,[1,105] the match between pore size and ion size was demonstrated through achieving a maximum capacitance.

In addition to high specific surface area and appropriate pore size, surface functionalization has also been considered an effective way to improve the specific capacitance of carbon materials.[6,106–115] It is believed that surface functional groups or heteroatoms can help the adsorption of ions and then improve the hydrophilicity/lipophilicity of the carbon materials, leading to enhanced wettability and facilitated rapid electrolyte ion transport within the micropores. At the same time, the presence of functional groups on the surface of carbonaceous materials may induce faradaic redox reactions,[3] leading to a 5–10% increase in the total capacitance. As shown in Fig. 4,[116] redox peaks, which lead to a remarkable pseudocapacitance, come from the redox reaction (a faradaic process) of oxygenated groups on the surface of carbon nanostructures.

Thus, introducing surface functional groups or heteroatoms on the surface of carbon materials appears to be an effective way of improving an electrode's capacitance.

The heteroatoms commonly present in a carbon framework are oxygen, nitrogen, boron, and sulfur. Among these, the introduction of nitrogen has been investigated most extensively

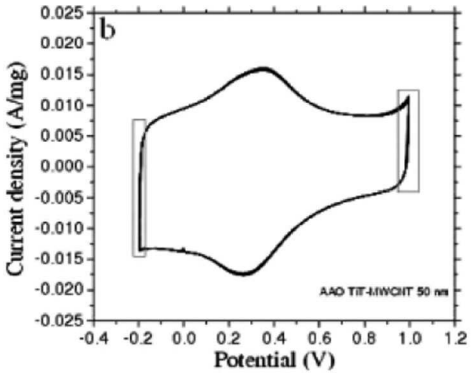

Fig. 4 CV plots in 0.5 M H_2SO_4 at a scan rate of 50 mV s^{-1} for multiwalled carbon nanotubes.[116] (Reprinted from ref. 116 with permission from American Chemical Society.)

in the literature.[110,114,117–120] It must be noted that the risk of electrolyte decomposition induced by active surface functional groups (especially oxygen-containing acidic groups) is also increased, particularly in an organic electrolyte, depending on the concentration of functional groups, the electrode surface area, and the operating ES voltage.[112] In addition, the intrinsic electrical resistance of the material may increase because the bonded heteroatoms possess higher reactivity, resulting in barriers to electron transfer.

Another way to increase the capacitance is to introduce conducting polymers into the carbon materials. For example, specific capacitance can reach 170 F g^{-1} by introducing a polypyrrole into multiwalled carbon nanotubes (MCNTs).[121,122] However, due to the rapid degradation of conducting polymers, a high cycle life ($>100\,000$) might not be achievable. Moreover, the degradation of these materials may be accelerated by possible over-charging/discharging during sustained operation. In this situation, carbon-supported transition metal oxides may be used for their enhanced stability. For example, introducing 1 wt% of RuO_2 into a carbon electrode material can increase the capacitance of the MCNTs from 30 to 80 F g^{-1} owing to the pseudocapacitive behavior of RuO_2. Besides enhanced capacitance, an electrode modified with RuO_2 has also exhibited a longer cycle life compared to that of carbon-polymer composite materials.[123]

In summary, carbon materials with high surface area and suitable porous structures seem to be ideal materials for ES in terms of specific power and cycle life. Unfortunately, their high resistivity, due to the contact resistance between carbon particles, gives rise to a high internal series resistance, leading to reduced ES performance.[23] In addition, the surface area inaccessible to electrolyte ions[124] also impedes the capacitance performance of carbon materials, resulting in limited capacitance values of only 40–160 F g^{-1} for both activated carbon and carbon aerogels,[125] and 10–35 F g^{-1} for CNTs.[123] Note that these values are strongly dependent on the microtexture of the nanotubes, number of defects, micropore volume, and contamination. It is believed that future research areas in carbon materials are development of carbon electrodes with higher specific surface area, rational pore distribution, and moderate surface modification so as to optimize overall capacitance and conductivity without compromising stability.

3.2 Faradaic materials

As mentioned above, materials based on an electrical double-layer mechanism have limited specific capacitance, typically in the range of 10–50 μF cm^{-2} for a real electrode surface. Because pseudocapacitance may be 10–100 times greater, supercapacitors made of redox-active materials bearing pseudocapacitance are highly desirable[126] as the next generation of ES. They not only store charges in the double layer, as a conventional supercapacitor electrode does, but also undergo fast and reversible surface redox reactions (faradaic reactions). Therefore, considerable efforts have been devoted in recent years to developing electrode materials with pseudocapacitance. This kind of material is generally classified into two types: conducting polymers and electroactive metal oxides.

3.2.1 Conducting polymers (CPs). CPs possess many advantages that make them suitable materials for ES, such as low cost, low environmental impact, high conductivity in a doped state, high voltage window, high storage capacity/porosity/reversibility, and adjustable redox activity through chemical modification.[127–131]

CPs offer capacitance behavior through the redox process. When oxidation takes place, ions are transferred to the polymer backbone, and when reduction occurs, the ions are released from this backbone into the electrolyte. These redox reactions in the conducting polymer come about throughout its entire bulk, not just on the surface.[57] Because the charging and discharging reactions do not involve any structural alterations such as phase changes, the processes are highly reversible.[15]

CPs can be positively or negatively charged with ion insertion in the polymer matrix to balance the injected charge. A typical example is poly(cyclopenta(2,1-*b*;3,4-*b*′-dithiophen-4-one)).[132,133] Electronic conductivity can thus be induced in such a kind of polymers by oxidation or reduction reactions, which generate delocalized 'n' electrons on the polymer chains. Early researchers termed the oxidation–reduction processes of these polymers as 'doping'. The positively-charged polymers, introduced by oxidation on the repeating units of polymer chains, are termed as 'p-doped', while negatively-charged polymers generated by reduction are termed as 'n-doped'. The potentials of these doping processes are determined by the electronic state of π electrons.

CPs-based ES systems have three configurations:[15,19,134–139] (1) Type I (symmetric). This type of ES is named as a p–p ES in which both electrodes use the same p-dopable polymer. When fully charged, one electrode is in the full p-doped (positive) state and the other in the uncharged state. The voltage window is 0.8–1 V; (2) Type II (asymmetric). This type is a p–p′ ES. Two different p-dopable polymers with a different range of oxidation and reduction electroactivities are used, such as polypyrrole/polythiophene; and (3) Type III (symmetric). This is an n–p type ES. Electrodes use the same polymer which can be both p- and n-doped in the same molecule, such as poly(3-fluorophenyl)thiophene. The voltage window is up to 3.1 V in nonaqueous solutions. Type III is considered a significant advance in CPs-based ES in terms of materials design and the stored energy density.

The common electrical CPs in supercapacitor applications are polyaniline (PANI),[140] polypyrrol (PPy),[141] polythiophene (PTh),[142,143] and their corresponding derivatives. PANI and PPy can only be p-doped since their n-doping potentials are much lower than the reduction potential of common electrolyte solutions. This is the reason why they often find use as cathode materials. PTh and its derivatives are both n- and p-dopable.[133,144] Substitution at the 3-position of PTh with an aryl group can result in more positive n-doping potentials. However, these polymers show poor conductivity in the reduced state (at more negative potentials) and produce a low capacitance. Consequently, they are usually employed as the positive electrode with a negative electrode made from another material such as carbon.[29] It should be noted that PANI requires a proton to be properly charged and discharged, therefore, a protic solvent, an acidic solution or a protic ionic liquid is required.[145] It seems that all CPs can only work (supplying charges) within a strict potential window. Beyond this strict potential range, the polymer may be degraded at more positive potential, and as the potential is too negative, the polymer may be switched to an insulating state (un-doped state). Hence, the selection of a suitable potential range for ES performance is crucial.[146] Table 1 shows the potential windows for various conductive polymers for ES applications.

There are many reports on applying the above CPs to ES. For example, Kim *et al.*[147] synthesized a composite material containing PPy, vapor-grown carbon fibres, and carbon with a thickness of 5–10 nm by *in situ* chemical polymerization, and achieved specific capacitances of ~588 and ~550 F g^{-1} at potential scan rates of 30 and 200 mV s^{-1}, respectively.

Recently, the specific capacitance of an electrode modified with pure PANI was reported by Li *et al.* to be 815 F g^{-1}.[148] In addition, poly(3,4-ethylene-dioxythiophene) (PEDOT)[146,149] was explored as a candidate material for ES because of its high stability. Using an electrochemical deposition method, a highly porous, amorphous polymer film on a gold plate was obtained, as shown in Fig. 5. The corresponding cyclic voltammetry curves are shown in Fig. 6, where a platinum mesh was used as the counter electrode. The results indicate that dendritic CPs, based on a bithiophene–triarylamine backbone, are capable of achieving a peak specific capacitance of over 990 F g^{-1} for a single electrode in an organic electrolyte at a potential scan rate of 50 mV s^{-1}.[150] These values are much higher than the capacitance of electrodes based on commercial activated carbons.

Unfortunately, swelling and shrinking of CPs may occur during the intercalating/deintercalating process. These problems often lead to mechanical degradation of the electrode and fading electrochemical performance during cycling, and then compromise CPs as electrode materials.

CP-based ES often remarkably degrade under less than a thousand cycles. For example, the ES device formed with PPy electrodes showed an initial capacitance of 120 F g^{-1}, which was degraded by ~50% in the first 1000 cycles at a constant current density of ~2 mA cm^{-2}.[151] For polythiophenes, the relatively poor stability of the n-doped state could lead to a continuous decrease of its ES performance upon cycling.[152,153] As shown by P. Sivaraman *et al.*, the specific capacitance of

Table 1 Specific capacitance of CPs-based composites

CPs-based composite	Specific capacitance/F g^{-1}	Electrolyte	Voltage window/V	Current load or scan rate	Reference
Ppy-20wt%MWNTs/ PANI-20wt% MWNTs	320 (Type II)	1.0 M H_2SO_4	0–0.6	5 mV s^{-1}	163
PANI-20 wt% MWNTs	670 (3-Electrode)	1.0 M H_2SO_4	−0.8–0.4	2 mV s^{-1}	
	344 (Type I)		0–0.6		
Ppy-20 wt% MWNTs	506 (3-Electrode)	1.0 M H_2SO_4	−0.6–0.2	5 mV s^{-1}	
	192 (Type I)		0–0.5 (*vs.* Hg|Hg_2SO_4)		
PEDOT-Ppy (5 : 1)	230 (3-Electrode)	1.0 M $LiClO_4$	−0.4–0.6 (*vs.* SCE)	2 mV s^{-1}	168
	290 (3-Electrode)	1.0 M KCl	−0.4–0.6 (*vs.* SCE)	2 mV s^{-1}	
	276 (Type I)	1.0 M KCl	0–1.0 (*vs.* SCE)	3 mA cm^{-2}	
Ppy-CNTs//PmeT-CNTs	87 (Type II)	1.0 M $LiClO_4$ in AC	0–1.0	0.62 A g^{-1}	169
PPy-65 wt% carbon	433 (3-Electrode)	6.0 M KOH	−1.0–0(*vs.* Hg|HgO)	1 mV s^{-1}	170
Ppy-graphene	165 (Type I)	1.0 M NaCl	0–1.0	1 A g^{-1}	171
Ppy-MCNTs	427 (3-Electrode)	1.0 M Na_2SO_4	−0.4–0.6 (*vs.* Ag|AgCl)	5 mV s^{-1}	172
Ppy-29.22 wt% mica	197 (3-Electrode)	0.5 M Na_2SO_4	−0.2–0.8 (*vs.* SCE)	10 mA cm^{-2}	173
Ppy-67.36 wt% mica	103 (3-Electrode)				
Ppy-RuO_2	302 (3-Electrode)	1.0 M H_2SO_4	−0.2–0.7 (*vs.* Hg|HgO)	0.5 mA cm^{-2}	174
Ppy-MnO_2	602 (3-Electrode)	0.5 M Na_2SO_4	−0.5–0.5 (*vs.* Ag|AgCl)	50 mV s^{-1}	151
PANI-Ti	740 (3-Electrode)	0.5 M H_2SO_4	−0.2–0.8 (*vs.* Ag|Ag^+)	3 A g^{-1}	175
PANI-80wt% graphene	158 (3-Electrode)	2.0 M H_2SO_4	0–0.8 (*vs.* AgCl|Ag)	0.1 A g^{-1}	176
PANI-50wt% graphene	207 (3-Electrode)				
PANI-10wt% graphene	320 (3-Electrode)				
MPANI/CNTs	1030 (3-Electrode)	1.0 M H_2SO_4	−0.2–0.7 (*vs.* SCE)	5.9 A g^{-1}	164
PANI-Si	409 (3-Electrode)	0.5 M H_2SO_4	0–0.8 (*vs.* AgCl|Ag)	40 mA cm^{-2}	177
PEDOT-MCNTs (70 : 30)	120 (Type I)	1.0 M H_2SO_4		2 mV s^{-1}	146
	80	6.0 M KOH			
	60	1.0 M $TEABF_4$ in AN			
PEDOT-MCNTs (80 : 20)	160 (AC as the negative electrode)	1.0 M $TEABF_4$ in AN	0–1.5	0.2 A g^{-1}	

Note: PPy: polypyrrole; PANI: polyaniline; Type I, II: defined by A. Rudge *et al.*;[139] PEDOT: poly(3,4-ethylenedioxythiophene); PTh: poly(thiophene); PMeT: poly(3-methylthiophene); PFPT: poly[3-(4-fluorophenyl)thiophene]; AN: acetonitrile; $TEABF_4$: tetraethylammonium terafluoroborate; PC: propylene carbonate; 3-electrode: standard 3-electrode cell; SCE: saturated calomel electrode; AC: activated carbon.

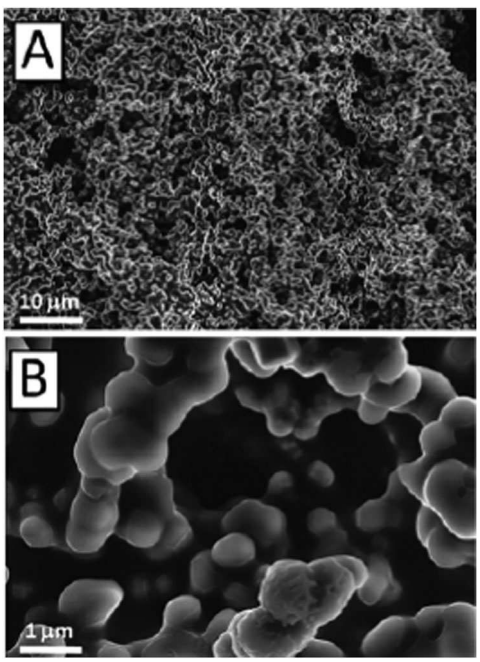

Fig. 5 Scanning electron microscopy image of pTTPA films electrochemically deposited with cyclic voltammetry between 0 and 1 V at a rate of 100 mV s^{-1} (A) and enhanced magnification image (B).[150] (Reproduced by permission of the Royal Society of Chemistry.)

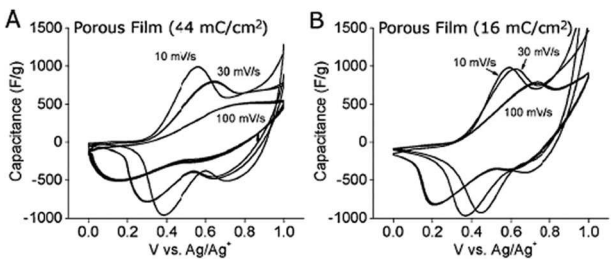

Fig. 6 Cyclic voltammetry curves normalized to specific capacitance (F g^{-1}) for TTPA electrochemically polymerized on Au/PI with charge densities of 44 mC cm^{-2} (A) and 16 mC cm^{-2} (B).[150] (Reproduced by permission of the Royal Society of Chemistry.)

the poly(3–methyl thiophene)(PMeT) ES could be decreased by 16.2% during the first 200 cycles.[138] Another report showed that the PMeT polymer, which was synthesized with a template by electrochemical polymerization of 3-methyl thiophene, decreased by ~16% the specific capacitance of the PMeT/PVDF|PC/EC/1 M $LiClO_4$|PMeT/PVDF ES (type III) within 150 cycles.[154] PANI could also suffer from a similar serious problem derived from the volumetric changes during the doping/dedoping process. The loss of specific capacitance of the PANI nanorods could be as high as 29.5% after only 1000 cycles between 0.2 and 0.8 V.[155] Apparently, low cycling stability is a very serious problem for CP materials when they are used in ES.

To mitigate the challenge of low stability, the following ways have been investigated:

(1) *Improving CP materials' structures and morphologies*. It seems that nanostructured CPs such as nanofibers, nanorods,

nanowires, and nanotubes could reduce cycling degradation problems caused by volumetric changes or mechanical forces through providing a relatively short diffusion length to enhance the utilization of electrode materials. For example, in a three-electrode cell with a 1 M H_2SO_4 solution as the electrolyte, ordered nanometre-scale PANI whiskers only showed about 5% of capacitance loss after 3000 consecutive cycles at a current density of 5 A g^{-1}.[156]

(2) *Hybridizing ES*. Since CPs in the n-doped state possess poorer stability than those in the p-doped state,[137,157] replacing an n-doped polymer at the negative electrode by a carbon electrode seemed feasible.[143,158,159] For example, a hybridized ES with a p-doped polythiophene derivative as the positive electrode and activated carbon as the negative electrode could maintain a good performance cyclability of over 10 000 cycles with a better performance than double-layer carbon-based ES in terms of power density.[160]

(3) *Fabricating composite electrode materials*. It was demonstrated that composite CP electrodes could enhance the cycling stability by improving their chain structure, conductivity, mechanical stability and processability, as well as mitigating mechanical stress.[146] For example, in comparison with pure PPy electrodes whose loss in specific capacitance was close to 50%, the ES based on two identical MnO_2/PPy nanocomposite electrodes, initially gave a much higher specific capacity of ~180 F g^{-1}, and also showed a relatively stable performance degrading only by ~10% in the initial 1000 cycles. Furthermore, a relatively stable performance was seen for the subsequent 4000 cycles at a constant current density of 2 mA cm^{-2}.[151]

Regarding composite electrodes, adding carbon, especially carbon nanotubes, into CPs is also believed to be an effective solution for improving the mechanical and electrochemical properties of electrodes.[147,161–163] For example, the sulfonated multi-wall carbon nanotube (MWCNT) in the composites can greatly improve the cycle stability of PANI, only showing 5.4% loss from their initial specific capacitance after 1000 cycles. This was attributed to the use of MWCNT with exceptional mechanical properties as a support and the formation of the charge-transfer complex, which could reduce the cycle degradation problems of PANI caused by volume changes or mechanical problems.[155] Zhang *et al.*[164] showed that a PANI/CNT composite electrode (Fig. 7) with nanostructure, hierarchical porous structure, large surface area, and superior conductivity had high specific capacitance (1030 F g^{-1}), superior rate capability (95% capacity retention at 118 A g^{-1}), and high stability (5.5% capacity loss after

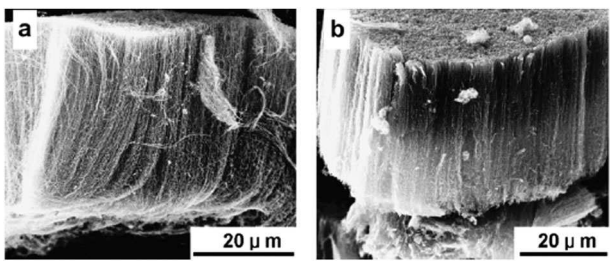

Fig. 7 SEM images of (a) CNT array and (b) polyaniline/CNT array composite.[164] (Reprinted from ref. 164 with permission from Elsevier.)

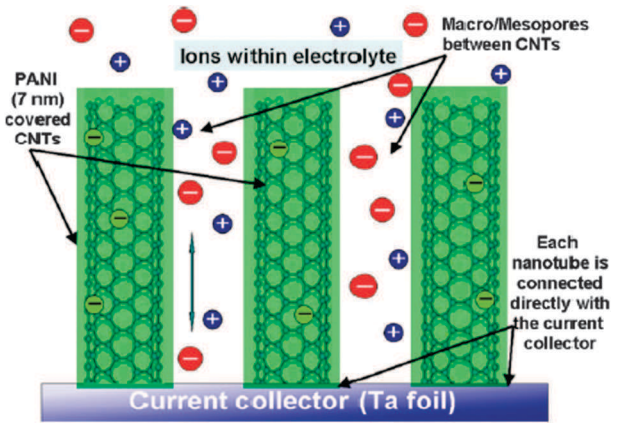

Fig. 8 Schematic representation of the microstructure and energy storage characteristics of a polyaniline/carbon nanotube (PANI/CNT) composite electrode.[164] (Reprinted from ref. 164 with permission from Elsevier.)

5000 cycles) between −0.2 and 0.7 V (*vs.* SCE) at 10 mA in a 1 M H_2SO_4 electrolyte.

The roles of the CNT array in this composite are schematically shown in Fig. 8.[164] From this figure, four points can be summarized:[164–167] (1) the superior conducting network consisting of CNTs allows for efficient charge transport in the composite electrode, (2) the high specific surface area and the nanometre size ensure high utilization of electrode materials, and then a high specific capacity, (3) the hierarchically porous structure can enhance the ionic conductivity, and (4) using CNTs with special mechanical properties as a support can reduce the cycle degradation caused by mechanical problems or volume changes.

Because the properties of CPs can be greatly improved through preparing a CP-based composite, recent studies mainly focus on CP-based composites which involve carbon, inorganic oxides/hydroxides, and other metal compounds. Some examples of these composites and their electrochemical properties are given in Table 1. From Table 1, one can see that the composite materials can give a wide distribution of capacitance values, which are also dependent on the parameters such as the constituents of composites, electrolytes used, scan rate, current load, and mass ratio of the components as well as cell configuration. Therefore, more effort is still needed to optimize these parameters to achieve optimized electrochemical properties for these CP-based composites for ES applications.

3.2.2 Metal oxides/hydroxides. In general, metal oxides can provide higher energy density for ES than conventional carbon materials and better electrochemical stability than polymer materials. They not only store energy like electrostatic carbon materials but also exhibit electrochemical faradaic reactions between electrode materials and ions within appropriate potential windows.[178]

The general requirements for metal oxides in ES applications are:[15] (1) the oxide should be electronically conductive, (2) the metal can exist in two or more oxidation states that coexist over a continuous range with no phase changes involving irreversible modifications of a 3-dimensional structure,

and (3) the protons can freely intercalate into the oxide lattice on reduction (and out of the lattice on oxidation), allowing facile interconversion of $O^{2-} \leftrightarrow OH^-$. To date, those investigated include ruthenium oxide, manganese oxide, cobalt oxide, nickel oxide, and vanadium oxide.

3.2.2.1 RuO_2. Among the transition metal oxides, RuO_x has been the most extensively studied candidate due to its wide potential window, highly reversible redox reactions, three distinct oxidation states accessible within a 1.2 V voltage window, high proton conductivity, remarkably high specific capacitance, good thermal stability, long cycle life, metallic-type conductivity, and high rate capability.[59,179–181] With RuO_2 electrodes, double-layer charging only contributes to about 10% of the accumulated charge, in parallel with which the redox pseudocapacitance mechanism can occur.

The pseudocapacitive behaviors of ruthenium oxides in acidic and alkaline environments involve different reactions, which in turn show different sensitivities toward crystallinity. For example, amorphous ruthenium oxide materials in the H_2SO_4 electrolyte exhibited a maximum capacitance of 720 F g^{-1} upon calcination at 150 °C.[182] For a crystalline state in a KOH electrolyte, a maximum capacitance of 710 F g^{-1} was obtained by calcinating ruthenium oxide at 200 °C.[183] The corresponding mechanisms were suggested to be as follows. In acidic electrolyte solution, according to eqn (13), rapid reversible electron transfer is accompanied by electro-adsorption of protons on the surface of RuO_2 particles, where Ru oxidation states can change from Ru(II) to Ru(IV):[15,182,184–188]

$$RuO_2 + xH^+ + xe^- \leftrightarrow RuO_{2-x}(OH)_x \qquad (13)$$

However, in an alkaline solution, the changes in the valency state of RuO_2 are quite different. It has been suggested that when the carbon/ruthenium composite is charged the RuO_2 in the composite electrode will be oxidized to RuO_4^{2-}, RuO_4^-, and RuO_4, and when it is discharged these high valency state compounds will be reduced to RuO_2.[183,189]

No matter what kind of electrolyte is used, the following factors play key roles in the electrochemical behavior of Ru oxides:

(1) *Specific surface area*. The pseudocapacitance of RuO_x comes mainly from the surface reactions. The higher the specific surface area, the more the metal centers will be capable of providing multiple redox reactions and the higher the specific capacitance will then be. Obviously, one of the most effective ways to increase the specific capacitance is to increase the specific surface area of RuO_x.[182] Several approaches, such as depositing RuO_2 films on substrates with a rough surface, coating a thin RuO_2 film on high-surface-area materials, making nanometre-sized oxide electrodes, *etc*. have been explored to maximize the surface area of RuO_2 by creating micropores large enough for ion diffusion.[125,190–194] For example, hydrous ruthenium oxide ($RuO_2{\cdot}xH_2O$) thin-film electrodes electrodeposited on titanium substrates exhibited high reversible characteristics, excellent cycle stability, and superior power characteristics. The maximum specific capacitance of the $RuO_2{\cdot}xH_2O$ film electrode was as high as 786 F g^{-1}.[191] Elsewhere, metal particles prepared using the polyol method were small and uniform in size as well as highly dispersed on a carbon surface, leading to a redox specific capacitance of 914 F g^{-1}.[125] A specific capacitance as high as 1300 F g^{-1} was also reported for nanotubular arrayed electrodes incorporated with hydrous ruthenium oxide.[195]

(2) *The combined water in RuO_x*. As implied by eqn (13), the reversible redox transitions strongly depend on the processes of proton/cation exchange and electron-hopping. The quasi-metallic conductivity of RuO_2 allows facile electron transfer into and through the electrode matrix, so the transfer of cations in the solid phase is critical for a RuO_2 electrode. It was reported that cation diffusion in hydrated electrodes could occur *via* hopping of alkaline ions and H^+ ions between H_2O and OH^- sites, suggesting that the hydrogen atoms were relatively mobile in $RuO_2{\cdot}xH_2O$ samples as compared to those in rigid samples.[196] Thus, the combined water in RuO_2 is expected to enhance the diffusion of cations inside the electrode layer.

In fact, hydrous ruthenium oxide is a good proton conductor (H^+ diffusion coefficient reaches 10^{-8}–10^{-12} cm^2 s^{-1}),[197–199] and fast ionic conduction *via* hydrous micropores, mesopores, or the interlayer does lead to an increase in the capacitive behavior.[200] As reported in the literature,[201] hydrous ruthenium oxide ($RuO_2{\cdot}0.5H_2O$) showed a capacitance as high as ~900 F g^{-1}. However, when the water content was decreased to $RuO_2{\cdot}0.03H_2O$, the capacitance dropped to 29 F g^{-1} and the anhydrous phase displayed a capacitance of only 0.5 F g^{-1}. Sugimoto *et al.*[202] also demonstrated the importance of hydrous regions (either interparticle or interlayer). These hydrous regions can allow appreciable protonic conduction for high-energy and high-power electrochemical capacitors. The results are shown in Table 2.

The water content in $RuO_2{\cdot}xH_2O$ strongly depends on the preparation process and conditions. Normally, chemically formed RuO_2 is redox active only within a fraction of the surface Ru atoms, while electrolytically formed RuO_2 can have more hydrated oxide states in which a substantial volume fraction of Ru atoms is redox active.[15] The water content, x, of $RuO_2{\cdot}xH_2O$ is typically 0.9 for a room-temperature dried product, and tri- and dihydrated phases can also be obtained, depending on the conditions.[200] Increasing the annealing temperature can result in a lack of chemically bound water, inhibiting proton intercalation and leading to a decrease in specific capacitance.[203,204]

(3) *The crystallinity of $RuO_2{\cdot}xH_2O$*. The pseudocapacitance of $RuO_2{\cdot}xH_2O$ materials is also closely related to the degree of crystallinity. A well crystallized structure has difficulty in expanding or contracting, so it prevents protons from

Table 2 Specific capacitance obtained by cyclic voltammetry at various scan rates for $RuO_2{\cdot}xH_2O$[202] (reprinted from ref. 202 with permission from American Chemical Society)

	Specific capacitance/F (g-RuO_2)$^{-1}$		
Scan rate/mV s^{-1}	RuO_2	$RuO_2{\cdot}0.3H_2O$	$RuO_2{\cdot}0.5H_2O$
2	24	124	342
5	22	112	331
20	19	93	316
50	18	82	304
200	16	68	280
500	15	61	256

permeating the bulk material, leading to a diffusion limitation. As a result, the fast, continuous, and reversible faradaic reactions are compromised, and the capacitance of RuO_2 with good crystallinity comes mainly from the surface reaction.[205] In contrast, the redox reaction of an amorphous composite occurs not only on the surface but also in the bulk of the powder, which is why an amorphous composite exhibits far superior performance when compared with crystallized structures.[182]

The crystallinity of $RuO_2{\cdot}xH_2O$ depends on the synthesis procedure. $RuO_2{\cdot}xH_2O$ obtained *via* a vapor procedure has exhibited better crystallinity and lower specific capacitance than that obtained *via* a solution procedure.[206]

Temperature is another important factor controlling the crystallinity and water content of $RuO_2{\cdot}xH_2O$ materials. Although active sites can be obtained at a lower heat treatment temperature, their activities are quite low due to their low conductivity, even though water is still retained in the oxide. Under a higher heat treatment temperature, the number of active sites is decreased due to crystallization and water loss. For example, when the annealing temperature exceeds 175 °C, the specific capacitance will drop rapidly due to the formation of a crystalline phase. A similar trend was also observed by Kim and Popov.[207]

In a word, a disordered form is an essential parameter improving the capacitance of $RuO_2{\cdot}xH_2O$. According to the literature, when the temperature is close to the crystallization temperature of ruthenium oxide, $RuO_2{\cdot}xH_2O$ can remain amorphous and hydrous.[182,190,208] The optimal annealing temperature is reported to be about 150 °C.[182]

(4) *The size of $RuO_2{\cdot}xH_2O$*. Smaller sized particles not only can shorten the diffusion distance but also can facilitate proton transport in the bulk of ruthenium oxide, increase the specific surface area, and enhance the electro-active sites. Thus, the smaller the particle size, the higher the gravimetric capacitance and utilization efficiency.[200,206,207] For example, assuming the particle is spherical (where redox reactions can occur to a depth of 2 nm from the surface of the particle), when the particle diameter is 10 nm only 49% of the total particle volume can contribute to the total capacitance. However, for a particle with a diameter of 3 nm, this value can reach 96%. Therefore, one of the key points is to cut RuO_2 particles down to a nanosize and maintain high electrical and protonic conduction throughout the particles. For example, a nanometre-sized crystalline RuO_2, anchored on CNTs using a simple supercritical fluid deposition method, has shown a specific capacitance of up to 900 F g^{-1}, close to its theoretical value.[209] By deploying RuO_2 into a nanostructure to increase its surface area and paths for diffusion, specific capacitance values as high as 1300 F g^{-1} were achieved.[21,195,200,201,210] The presence of ordered nanopores can also lead to better electrolyte diffusion into the electrode material and then improve the completion of the redox reaction, resulting in higher pseudocapacitance.[211]

The particle size of $RuO_2{\cdot}xH_2O$ can be controlled in different ways, depending on the preparation method. Using a colloidal method, the particle size of $RuO_2{\cdot}xH_2O$ can be altered by the amount of $NaHCO_3$ and the reaction time.[207] With a conventional sol–gel method, the size of RuO_2 particles can be adjusted by the RuO_2 content in the composites as well as the alkali used in the preparation procedure. It was also reported that RuO_2 particles prepared *via* $NaHCO_3$ titration were smaller than those produced by NaOH titration.[212] According to Ramani *et al.*,[213] varying the deposition temperature and/or pH can control the cluster size in the process of electroless deposition. Using a template method, the particle size of $RuO_2{\cdot}xH_2O$ can be controlled by altering the template size. Cui *et al.* and Lin *et al.*[214,215] reported that nanostructured crystalline RuO_2 particles prepared using a SiO_2 hard template had a narrow size distribution. However, it should be noted that a hard template is often accompanied by a higher pyrolysis temperature, which can lead to well crystallized RuO_2 with a small amount of water, and a relatively low specific capacity of 229 F g^{-1} for 40 wt% Ru at 10 mV s^{-1}.[214] Therefore, a soft template is advisable for preparing nanosized RuO_2 composites, although the particles and pores are not as regular and ordered as in those samples prepared using a hard template. For example, in a soft template situation, the annealing temperature can be as low as 100 °C, and the specific capacitance of a composite with 50 wt% RuO_2 can reach 642 F g^{-1}.[208] In addition to the soft template method, the polyol process also appears to be a promising alternative for preparing nanosized RuO_2. Particles prepared from this process were found to be uniform in size and distribution, and displayed a specific capacitance of 914 F g^{-1} when the Ru loading was 20 wt%.[125]

Obviously, ruthenium oxide can be brought close to its theoretical capacitance by deploying the RuO_2 in a nanostructure to increase its surface area and pathways for diffusion.[21,195,200,202,210]

(5) *Electrolytes used*. The specific capacitance values of RuO_x electrodes can be changed by using different electrolytes in the surpercapacitor.[212] In some electrolytes, the RuO_2 electrode may behave like a double-layer capacitor, regardless of the RuO_2 loading in the electrode layer. However, in other electrolytes, RuO_x materials can display pseudocapacitance behavior that is dependent on the RuO_x content. Electrolyte concentration can also have an effect on the performance of RuO_x electrodes. For example, when KOH electrolyte concentration was higher than 0.5 M, the capacitance increased linearly with increasing KOH concentration, whereas when the concentration was lower than 0.5 M, the capacitance decreased sharply with declining concentration.[215] Therefore, the ionic concentration in electrolytes must match the needs of both the electrical double layer and the faradaic reactions.

3.2.2.2 RuO_2-based composites. Despite the exceptional properties of ruthenium oxide and its high theoretical capacitances (1360 F g^{-1} for $RuO_2{\cdot}0.5H_2O$), its costliness is a practical impediment. Rough calculation has indicated that 90% of a superconductor's cost comes from the electrode material.[3] Therefore, many researchers[216–222] have focused their efforts on reducing Ru usage and increasing its utilization.

Two approaches have been demonstrated in the literature: synthesis of mixed-oxide composites by doping base metal oxides into ruthenium oxide (*e.g.* MnO_2, NiO *etc.*),[183,221,223–228] and fabrication of ruthenium-based composite materials in which particles of hydrous ruthenium oxide are deposited on other

low-cost materials (*e.g.* carbons with different surface textures and conductive polymers).[186,207,218,229–234]

3.2.2.2.1 Mixed-oxide composites. In the attempt to reduce the cost of precious metal use, many studies have focused on combining RuO_2 with cheap metal oxides such as SnO_2, MnO_2, NiO, VO_x, TiO_2, MoO_3, WO_3, and CaO to form composite oxide electrodes.[183,184,227,228] For instance, a specific capacitance of 710 F g^{-1} in a KOH electrolyte[183] was reported for a SnO_2–RuO_2 composite electrode wherein RuO_2 was deposited by an incipient wetness precipitation method. Takasu *et al.*[223] reported that the specific charge of a RuO_2 (33%)–VO_2 (67%)/Ti electrode was about 50 times higher than for a RuO_2/Ti electrode. Sugimoto *et al.*[227] also demonstrated enhanced supercapacitive properties by doping with vanadium. The introduction of V not only extended the electrochemical window of the $Ru_{0.36}V_{0.64}O_2$ electrode from much less than 1.0 V to 1.1 V but also increased the utilization of Ru species as well as the electrode's electrochemical stability.[49]

Amorphous $Ru_{1-y}Cr_yO_2/TiO_2$ nanotube composites were also synthesized by loading various amounts of $Ru_{1-y}Cr_yO_2$ on TiO_2 nanotubes *via* a reduction reaction of aqueous $Ru_{1-y}Cr_yO_2$ with $RuCl_3$.[235] The results demonstrated that the three-dimensional nanotube network of TiO_2 offered a solid support structure for $Ru_{1-y}Cr_yO_2$, allowing the active material to be readily available for electrochemical reactions while at the same time improving the active material's utilization. It was reported that a maximum specific capacitance of 1272.5 F g^{-1} was obtained with the proper amount of $Ru_{1-y}Cr_yO_2$ loaded on the TiO_2 nanotubes. With their large surface area TiO_2 nanotubes not only help the transportation of ions but also facilitate double-layer charging. As a result, the utilization of RuO_2 can be greatly enhanced by loading it on TiO_2 nanotubes.[226]

In summary, the following five key factors have been proposed to determine the capacitive performance of Ru-based oxide composites:[21,179,182,195,236–240] (i) the electrochemical kinetics of electron transfer for active materials, (ii) "in-particle" electron-hopping resistance within every RuO_2 particulate, (iii) "between-particle" electron-hopping resistance between particulates, (iv) electron-hopping resistance at the interface between active materials and current collectors, and (v) barriers to proton diffusion within oxide composites and particulates.

In addition to providing extra pseudocapacitance, the additive metal oxides can simultaneously function in the composite as follows:

(a) *To facilitate electron and proton conduction in the oxides.* One of the functions of the additive metal oxides is to aid in electron and proton conduction. It was reported that the structural support from Co species facilitated electronic conduction within the metal oxide. As a result, at higher potential scan rates (500 mV s^{-1}), a Ru–Co mixed oxide electrode exhibited a superior performance of 570 F g^{-1} when compared to a RuO_2 electrode (475 F g^{-1}).[241]

In composites of ruthenium oxide and niobium hydroxide, RuO_2 particles can provide electrically conductive pathways and niobium oxide possesses good proton diffusion.[242] Hence, there is an optimization among electrical conduction through interconnected RuO_2 grains, proton conduction through the mixed oxide, and efficient utilization of ruthenium. Only if concentrations of mixed metals are moderate can a higher specific capacitance be expected. It was reported that the optimum composite consisted of roughly equal amounts of ruthenium and niobium. At the same time, the Ru/Nb oxide composite maintained a high specific capacitance with increasing potential scan rate, and the overall capacitance loss of these mixed oxides was much less significant than for pure RuO_2.

(b) *To enhance the dispersion of ruthenium oxide.* The dispersion of ruthenium oxide can benefit from doping with other metal oxides. As shown in Fig. 9,[242] with a greater niobium content, the dispersion of ruthenium increases significantly. For example, at 33.3% niobium (1 : 2 Nb : Ru), the aggregation of RuO_2 grains exists in the composite. However, when niobium contents reached 50% (1 : 1 Nb : Ru) and 66.7% (2 : 1 Nb : Ru), the ruthenium and niobium oxide species could homogenously disperse throughout the film. Furthermore, ~95% niobium could result in a film without discernable RuO_2 grains. Kuo and Wu[225] successfully developed an electrochemical capacitor electrode containing highly dispersed RuO_2 electroplated on a conductive mesoporous tin oxide substrate.

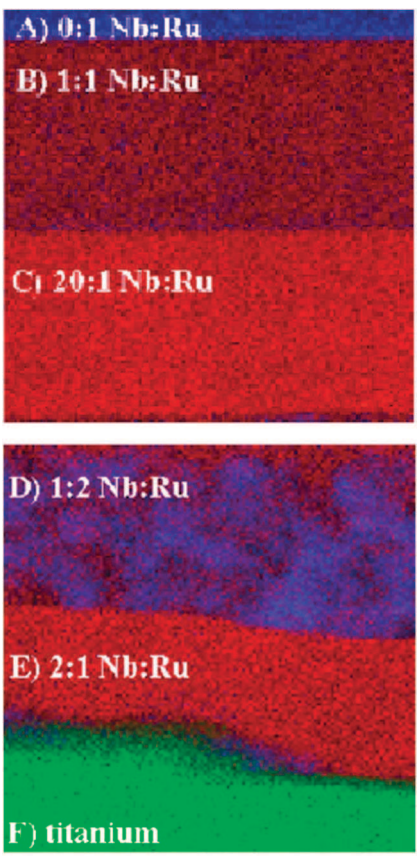

Fig. 9 Compositional mapping using TEM-EDS, showing layers of mixed Nb:Ru oxides (500 nm field of view).[242] (Reprinted from ref. 242 with permission from Elsevier.)

(c) *To minimize the RuO_2 particle size*. The addition of other metal oxides can affect the particle size of RuO_2. For instance, niobium can induce a decrease in RuO_2 particle sizes, placing more RuO_2 in electroactive regions, *i.e.* near grain surfaces.[242] In addition, the incorporation of vanadium diminished the particle size of Ru oxide, giving rise to a higher specific surface area. Accordingly, its redox capacitance and surface utilization were dramatically increased.[243] According to Hu *et al.*,[126] the average particle size of RuO_2 can be decreased by increasing the Sn content. For example, in a series of Ru oxide materials—$RuO_2{\cdot}xH_2O$, $Ru_{0.8}Sn_{0.2}O_2{\cdot}xH_2O$, $Ru_{0.6}Sn_{0.4}O_2{\cdot}xH_2O$, and $SnO_2{\cdot}xH_2O$—the mean particle sizes of the primary particulates, which decreased with increasing Sn content, were 3.0, 2.2, 1.9, and 1.6 nm, respectively. It was also observed that when RuO_2 was electroplated and dispersed onto a highly conductive mesoporous SnO_2 matrix, RuO_2 existed in the form of particles with sizes less than 0.2 mm either on SnO_2 crystalline surfaces or forming skeletal structures within voids. In a supercapacitor test, a RuO_2–SnO_2 composite electrode achieved a specific capacitance of 930 F g^{-1} in 1 M H_2SO_4 and an overall specific energy of $\sim$0.5 W h kg^{-1} at a specific power $>$ 1.5 kW kg^{-1}.[225]

It can be seen from the above-mentioned roles of doping metal oxides that the capacitive performance (*e.g.* specific capacitance and power characteristics) of binary oxides is strongly affected by their molar ratio.[244] Liu *et al.*[208] obtained a capacitance of 642 F g^{-1} from a composite with a molar ratio of Co : Ru = 1 : 1 at 150 °C. For materials like $RuO_2{\cdot}xH_2O$, $Ru_{0.8}Sn_{0.2}O_2{\cdot}xH_2O$, $Ru_{0.6}Sn_{0.4}O_2{\cdot}xH_2O$, and $SnO_2{\cdot}xH_2O$, the main factor influencing the total specific capacitance is their composition, and a higher specific capacitance of 850 F g^{-1} is obtainable with a Sn content of 0.2.[126]

3.2.2.2.2 RuO_2/carbon composites. In recent years, composites containing RuO_2 and carbon materials (such as carbon, carbon aerogels, CNTs, carbon nanofibres, *etc.*) have been intensively studied as ES materials.[123,192,193,209,213,221,223,231,233,234,245–262] The quantity of RuO_2 required in the electrode layer has thereby been reduced significantly, and higher specific capacitances have been achieved, such as 256 F g^{-1} with 14% Ru in a carbon aerogel,[247] 647 F g^{-1} with 60% RuO_2 in Ketjenblack,[256] 628 F g^{-1} with RuO_2/MCNTs in a ratio of 2 : 1,[193] $\sim$850 F g^{-1} for carbon–RuO_2 composite electrodes,[186] and 900 F g^{-1} for RuO_2 oxide powder pressed on conductive carbon.[201] It is necessary to point out that many investigators utilized a very high annealing temperature to obtain RuO_2/carbon composites.[247] Obviously, as mentioned previously, high temperature will lead to higher crystallinity, compromising the utilization of RuO_2. Therefore, synthesis conditions need to be optimized.

In RuO_2/carbon composites, a carbon support mainly plays the following roles:

(i) A carbon support seems to favor the dispersion of amorphous $RuO_2{\cdot}xH_2O$ particles, usually 3–15 nm in size.[263] As shown by Kim *et al.*,[192] carboxylated carbon nanotubes can prevent RuO_2 particles from agglomerating and contribute to the high dispersion of RuO_2 nanoparticles by forming a bond between RuO_2 and the surface carboxyl groups of the carbon nanotubes. Kim *et al.* showed a strong interaction between RuO_2 and the surface carboxyl groups of carbon, which contributed to the high dispersion of RuO_2 nanoparticles. It was also observed that the highly dispersed RuO_2 nanoparticles exhibited increased capacitance, because the protons were able to access the inner part of RuO_2. (ii) A carbon support can facilitate the transfer of ions and electrons in the electrode layers. By inducing more porosity,[263] the carbon support can enable easy penetration of the electrolyte up to the oxide primary particles. The porous morphology of MCNTs allows excellent electrolyte access in three dimensions, reducing the ion intercalation distance to nanometres when a thin layer of RuO_2 was coated on CNTs.[193] Besides introducing more porosity to the electrode, the surface functional groups of CNTs may also enable the electrode to easily transport the solvated ions to the electrode/electrolyte interfaces, increasing the faradaic reaction sites of the RuO_2 nanoparticles, and then affecting the pseudofaradaic reactions of those nanoparticles.[260] The conductivity of the dispersed MCNTs can also increase the electrical conductivity of the composite.[193]

For RuO_2/carbon composites, two points should be noted:

(a) Carbons with different porosity, crystallinity, and specific surface area will exert different influences on the electrochemical behavior of RuO_2. For instance, for microporous carbon-derived composites, the specific capacitance remains nearly constant in the range of 0–20 wt% RuO_2. This is because the increase in specific capacitance due to the increased RuO_2 content is balanced out by the decrease in specific capacitance owing to the decrease in the carbon's specific surface area. When the RuO_2 content is greater than 20 wt%, the contribution of RuO_2 increases the specific capacitance.[206] In the case of mesoporous carbon-derived composites, their specific capacitance increases linearly with increasing RuO_2 content. When carbon nanofibres were used to construct a RuO_2 composite, even though their specific surface areas were small, the specific capacitance of the composites also increased with increasing RuO_2 content.[262]

It was reported that oxide deposited on crystalline carbons is texturally different from oxide deposited on amorphous carbons.[262,263] The former showed some crystallization and larger particle size (2–4 nm), while the latter was amorphous with a smaller particle size (1–1.5 nm) and had a large specific surface area (450 m^2 g^{-1}). Although the RuO_2 composites with amorphous carbon exhibited lower conductivity than those with crystalline carbon, their specific capacitances were found to be larger.

(b) The particle size of supported RuO_2 often increases with increased RuO_2 loading, within a range that depends on the type of carbon used. For carbon nanofibres, when RuO_2 loading was 0–11 wt%,[262] the particle size increased from 2 to 4 nm. When microporous and mesoporous carbons were used as supports, and the RuO_2 loading was increased from 0 to 15 wt% on microporous carbon and from 0 to 40 wt% on mesoporous carbon, the corresponding particle sizes grew from 1.4 to 4 nm and from 1.4 to 1.8 nm, respectively. However when loading was increased beyond these ranges, the particle size of $RuO_2{\cdot}xH_2O$ was found to remain constant (generally 4 nm).[206] Increase in RuO_2 particle size is often

associated with decreased specific capacitance. Fortunately, particle size can be conveniently tuned by adjusting the mass ratio of the carbon precursor.[183,206,207,209]

In conclusion, the addition of carbon to an Ru oxide based electrode layer may improve the homogeneity of the electrochemical reaction, reduce the ionic resistance of the metal oxide, expand the active sites, increase electrical conductivity, and consequently further increase the power and energy densities of the corresponding supercapacitor.[218]

3.2.2.2.3 RuO_2/polymer. Recently, RuO_2/polymer composites have also received more attention. For example, hydrous RuO_2 particles, electrochemically loaded into poly(3,4-ethylenedioxythiophene)-doped poly(styrene sulfonic acid) exhibited a high specific capacitance of 653 F g^{-1}.[264] Zang *et al.*[174] reported a nanostructured polypyrrole/RuO_2 composite that achieved a specific capacitance of 302 F g^{-1}. Liu *et al.*[265] synthesized a RuO_2/poly(3,4-ethylenedioxythiophene) nanotube composite that displayed a high specific capacitance and rapid charging/discharging capability. This RuO_2-based composite reached a high specific capacitance of 1217 F g^{-1}, and when it was used as the electrode material in a supercapacitor, a high power density of 20 kW kg^{-1} was achieved, maintaining 80% of the maximum energy density (28 W h kg^{-1}). The high power capability and specific capacitance were attributed to the special hollow nanotube structures and their thin walls, which allowed ions to readily penetrate into the composite material and access their internal surfaces, and then provided a short diffusion distance for ion transport.

Polymers are claimed to play several roles in RuO_2/polymer composites: (i) preventing the aggregation of $RuO_2{\cdot}xH_2O$ particles by steric and electrostatic stabilization mechanisms; (ii) uniformly distributing $RuO_2{\cdot}xH_2O$ particles on the polymer matrix; (iii) increasing the active surface area of $RuO_2{\cdot}xH_2O$; (iv) providing an efficient route to deliver proton species; and (v) improving the adhesion of $RuO_2{\cdot}xH_2O$ to the current collector.[264]

Unfortunately, the accompanying volume increase caused by the polymer in the RuO_2 composite is undesirable for light and compact energy devices, as the polymer's density is relatively low compared with that of hydrous ruthenium oxide. Another critical problem is swelling and shrinking of the polymer during the supercapacitor cycling process.

In summary, when RuO_2-based composites are used as ES electrode materials for practical applications, they should possess the following properties: (i) nanosized, amorphous, hydrous structures (solid-state proton diffusion), (ii) networked particles with good connections (electronic conductivity), (iii) networked pores inside electrode layers (proton conduction), (iv) high packing density (volumetric energy density), and (v) mechanical stability (cycle stability).[266]

3.2.2.3 MnO_2. Although amorphous hydrous RuO_2 can provide extremely high specific capacitance, its drawbacks, such as relatively high cost and environmental harmfulness, prevent it from being used in the commercialization of supercapacitors.[267] As an alternative approach, researchers have put significant effort into finding cheaper and environmentally friendly materials that exhibit electrochemical behavior similar to that of RuO_2. These alternative materials include MnO_2, NiO, Fe_3O_4, and V_2O_5.

In general, manganese oxides (MnO_x) present relatively low cost, low toxicity, and environmental safety, as well as high theoretical capacities ranging from 1100 to 1300 F g^{-1}.[268–272] Since the early report by Lee and Goodenough in 1999,[273] MnO_x has attracted major attention and is considered a promising alternative class of materials for ES applications.[45,195,274–277]

The capacitance of manganese oxides comes mainly from pseudocapacitance, which is attributed to reversible redox transitions involving the exchange of protons and/or cations with the electrolyte, as well as the transitions between Mn(III)/Mn(II), Mn(IV)/Mn(III), and Mn(VI)/Mn(IV) within the electrode potential window of the electrolyte.[278,279] The proposed mechanism is expressed in eqn (14):[269,278,280–282]

$$MnO_\alpha(OC)_\beta + \delta C^+ + \delta e^+ \leftrightarrow MnO_{\alpha-\beta}(OC)_{\beta+\delta} \quad (14)$$

where C^+ denotes the protons and alkali metal cations (Li^+, Na^+, K^+) in the electrolyte, and $MnO_\alpha(OC)_\beta$ and $MnO_{\alpha-\delta}(OC)_{\beta+\delta}$ indicate $MnO_2{\cdot}nH_2O$ in high and low oxidation states, respectively. Eqn (14) suggests that both protons and alkali cations are involved in the redox process, and that the MnO_x material must have high ionic and electronic conductivity.[270,272]

Despite the clearly redox nature of the energy storage mechanism, MnO_x-based electrodes can also demonstrate typical rectangular-shaped cyclic voltammetry curves (Fig. 10 presents an example), analogous to non-faradaic energy storage mechanisms.[283,284]

As reported in the literature,[240,272,286,287] both physical properties (*e.g.* microstructure and surface morphology) and chemical factors (valence and the hydrous state of the oxide) affect the pseudocapacitive performance of Mn oxides. It was found that the cycle stability of Mn oxides is mainly controlled by their microstructure, while their specific capacitance is governed primarily by their chemically hydrous state.[288]

3.2.2.3.1 Factors affecting the pseudocapacitance of MnO_x. We here review in detail several physical and chemical factors that affect the pseudocapacitance of MnO_x electrodes:

(1) *Crystallinity*. Similar to ruthenium oxide, if the crystallinity is too high in MnO_x, the protonation (or deprotonation) reaction will be limited. Although high crystallinity can give rise to higher conductivity, loss of surface area occurs

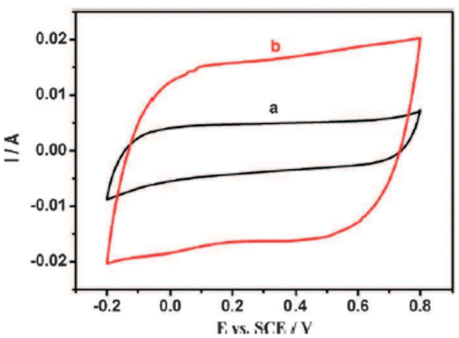

Fig. 10 Cyclic voltammograms of MnO_2-based electrodes in a 1 M Na_2SO_4 electrolyte at a potential scan rate of 5 mV s^{-1}. (a) MnO_2 obtained by using CNT and (b) MnO_2 obtained by using mesoporous carbon.[285] (Reprinted from ref. 285 with permission from Elsevier.)

simultaneously. On the other hand, although lower crystallinity can result in a highly porous microstructure, the electrical conductivity of the resulting MnO_x will be low. Consequently, there should be a trade-off between electrical conductivity in the solid phase and ionic transport in the pore. With respect to crystallinity-dependent electrical conductivity, the annealing temperature plays an important role in achieving optimal conductivity. When compared with those not heat-treated, MnO_x heat-treated at 200 °C showed a higher specific capacitance at high scan rates, and lower specific capacitance at low scan rates.[289] This phenomenon might be attributable to the fact that films treated at 200 °C possess both lower open porosity and lower surface area. At a high scan rate, diffusion of H^+ and Na^+ ions is limited and some pores and voids become inaccessible. Obviously, excellent pseudocapacitive behavior can be obtained when Mn oxide is treated at an appropriate annealing temperature.[276,290]

(2) *Crystal structure*. Crystallized MnO_2 materials have several crystalline structures, including α-, β-, γ-, and δ-MnO_2. Among them, α-, β-, and γ-MnO_2 have a tunnel structure (2 × 2 octahedral units for α-MnO_2, the relatively large tunnel structured phase; 1 × 1 octahedral units for β-MnO_2, the more compact and dense phase), and δ-MnO_2 has a relatively open layered structure (as shown in Fig. 11 by birnessite).[13,291]

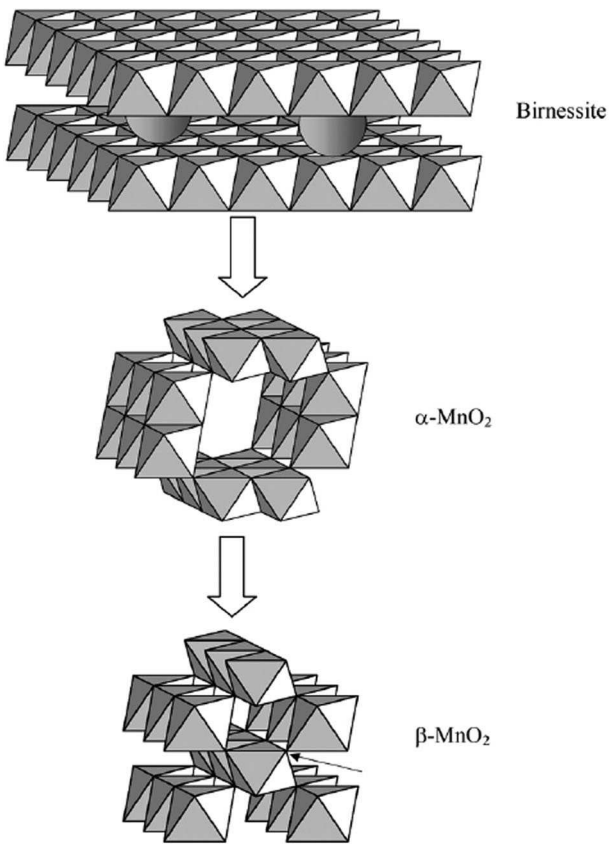

Fig. 11 Manganese dioxide structural transitions induced during material synthesis.[291] (Reprinted from ref. 291 with permission from Elsevier.)

It has been recognized that different preparation conditions can result in different MnO_x structures. For example, gradually increasing the precursor acidity can lead to a progression from layered δ-MnO_2, through the relatively large tunnel structured phase α-MnO_2, to a more compact and dense β-MnO_2. In an NaOH or KOH solution, the product is mainly a δ-MnO_2 phase. These structural changes in MnO_2 give rise to significant changes in electronic and ionic conductivity, affecting the material's pseudocapacitive behaviour.[291]

With α-MnO_2, it was reported by Hu and Tsou[278] that an amorphous hydrous manganese oxide (α-$MnO_2{\cdot}nH_2O$) fabricated from an $MnSO_4{\cdot}5H_2O$ solution *via* anodic deposition yielded a specific capacitance in the range of 265–320 F g^{-1} when measured in a potential range between 0 and 1.0 V using a 0.1 M Na_2SO_4 aqueous electrolyte solution. Furthermore, amorphous MnO_2 made from an $Mn(CH_3COO)_2$ solution showed a capacity of 195–275 F g^{-1} in a 2 M KCl solution and 310 F g^{-1} in 2 M $(NH_4)_2SO_4$. However, nanostructured α-MnO_2 synthesized *via* a hydrothermal technique under mild conditions yielded a specific capacitance of 168 F g^{-1} at a potential scan rate of 1 mV s^{-1}.[292] Single-crystal α-MnO_2 prepared by hydrothermal reaction of $KMnO_4$ under acidic conditions exhibited a specific capacitance of only 71.1 F g^{-1} at a current density of 300 mA g^{-1}.[293]

For γ-MnO_2 based materials, although one high specific capacitance of 240 F g^{-1} at a current density of 1 mA cm^{-2} was reported,[294] the majority of materials yielded specific capacitances of only 20–30 F g^{-1}.[283,295]

The two-dimensional layered structure of δ-MnO_2 can facilitate cation intercalation/deintercalation with little structural rearrangement.[296,297] Several methods for synthesizing δ-MnO_2 have been developed. δ-MnO_2 obtained *via* a hydrothermal synthesis process exhibited a much higher specific capacitance than γ-MnO_2 and β-MnO_2.[71,291] δ-MnO_2 synthesized through a redox reaction between $MnSO_4$ and $KMnO_4$ in an aqueous medium gave a specific capacitance of 236 F g^{-1} at 0.5 mA cm^{-1} in 0.1 mol L^{-1} Na_2SO_4 electrolyte.[298] Besides these two methods, a δ-MnO_2 compound was obtained using sonochemistry and exhibited a specific capacitance value exceeding 350 F g^{-1}.[299,300]

(3) *Morphology*. There is no doubt that the morphology of MnO_2 closely relates to the specific surface area and therefore the specific capacitance. Thus, the morphology of MnO_2 plays a determinant role in its electrochemical performance.[45,301] In the literature, prepared manganese oxides have many different morphologies, such as nanowires,[302–304] nanorods,[305] nanobelts,[296,306] flower-like microspheres,[291,307] nanobundles,[308] and flower-like nanowhiskers.[292] Depending on the morphology, the obtained material's specific surface area can range from 20 to 150 m^2 g^{-1}.

Normally, the morphology of MnO_x can be controlled by altering the preparation process or reaction conditions. For example, using a soft template method, various morphologies are obtainable by adjusting the precursors and conditions.[309] Using an anodic deposition method,[45] the morphology of manganese oxide prepared from manganese acetate solutions is controllable by varying the deposition current density. In a hydrothermal reaction, the morphology of MnO_2 changes by varying the reaction time at a given molar ratio of reactants,[310]

the solvent used, the temperature of the reaction, and so forth.[311] In a microemulsion process,[312] precise control of particle size and shape can be achieved. Templated electrosynthesis,[313] which is widely used as an effective pathway to form one-dimensional porous structures using anodic aluminium oxide and polycarbonate membranes, can also be employed for MnO_x synthesis.

Several morphologies of MnO_2 and their effects on specific capacitance are worth discussing here. The first is one-dimensional nanostructured MnO_x. In general, for one-dimensional nanostructured materials, short transport/diffusion path lengths for both ions and electrons can be realized, leading to faster kinetics, offering large specific surface areas, and resulting in high charge/discharge capacities.[195,314] For example, nanowires with smaller diameters can offer larger specific surface area for the access of electrolyte ions, more active sites for charge transfer, and short transport/diffusion distance for proton diffusion. That may be the reason why they have a higher capacitance of 350 F g^{-1} compared with nanorods' capacitance of 243 F g^{-1}.[315] Another example is one-dimensional nanobelt materials. They not only offer large electrode surface area and provide conducting pathways for ions, leading to high capacity and fast kinetics, but also better accommodate large volume changes, resulting in improved cycle performance for cathode materials.[316,317] The second MnO_2 morphology is porous spherical particle materials. According to Donne *et al.*,[291,301] these are better than platelet particles. The third morphology is an Mn oxide film with a rodlike structure (prepared through anodic deposition from a 0.01 M Mn acetate solution at various deposition current densities on Au-coated Si substrates), whose maximum capacitance is 185 F g^{-1}.[45] The fourth is a petal-shaped manganese oxide, which may not be a good choice for ES material because it could reduce the specific surface area, leading to capacitance fading. Further, the more ordered hexagonal NiAs-type crystal structure possesses fewer electrochemically active sites available for fast ionic transport and charge transfer. The fifth morphology is MnO_2-pillar layered manganese oxide, which shows good cycling stability because pillaring agents are not favored for significant structural or mesostructural change during the intercalation and de-intercalation processes, leading to enhanced stability of the layered structure.[318]

Based on the above and the literature, one-dimensional nanostructured materials with special morphologies and large surface areas are necessary for potential applications in ES.

(4) *Thickness of the electrode layer*. In general, the specific capacitance decreases with increasing thickness of the electrode layer (or film) due to the low conductivity of MnO_2. There are quite a number of publications on this issue. For example, when the deposited loading of nanostructured MnO_2 was increased from 50 to 200 μg cm^{-2} the specific capacitance decreased from 400 to 177 F g^{-1}.[319] For birnessite-like compounds prepared by electro-oxidation of acidic aqueous solutions of $MnSO_4$, capacities vary in the range of 70–150 F g^{-1}, depending strongly on the thickness of the electrode layer.[320] Some researchers have also pointed out that the thicker MnO_2 films deposited at higher potential are different from the thin films obtained at lower potentials. The difference between their specific capacitance can be as large as 100 F g^{-1}.[56] For instance, the specific capacitance of a MnO_2 layer prepared from the oxidation of $MnSO_4$ decreased from 220 to 50 F g^{-1} as the MnO_2 loading was increased from 100 μg cm^{-2} to 4 mg cm^{-2}.[321] Therefore, it is obvious that the thicker the film, the lower the specific capacitance.

The major benefits of thin layers can involve (i) lower series resistance due to shorter transport paths for the diffusion of protons (low concentration polarization of the electrolyte), (ii) easy access of the electrolyte to the active surface of manganese dioxide, and (iii) higher electronic conductivity. Hence, high specific capacitance and rate capability can be achieved, especially when a thin MnO_2 layer is uniformly dispersed on conductive and porous carbonaceous materials with a high surface area. For example, Prasad and Miura.[322] reported a thin amorphous MnO_2 film obtained by potentiodynamic deposition that exhibited a specific capacitance of 482 F g^{-1}. When this thin layer was used for ES electrodes, high power density and stability were achieved. Most reported MnO_2 thin layers have exhibited specific capacitances as high as ~600 F g^{-1} or more within a potential window of 0.9–1.2 V in aqueous electrolytes containing KCl, K_2SO_4, Na_2SO_4, or KOH.[52,288,323–329] A thin MnO_2 layer prepared by a sol–gel method (MnO_2 loading of ~4 μg cm^{-2}) showed a specific capacitance of 700 F g^{-1} in a potential window of 0.9 V.[269,280] A thin layer of an MnO_2 electrode prepared by dip-coating colloidal MnO_2 exhibited a specific capacitance value close to 700 F g^{-1}.[210] A specific capacitance as high as 1300 F g^{-1} was reported with thin MnO_2 deposits (on the scale of nanometres) because the reaction kinetics was no longer limited by the electrical conductivity of MnO_2.[270] Besides nearly perfect cyclic performance, the MnO_2 thin layer yielded a high specific capacitance of 149 F g^{-1} even at the high potential scan rate of 500 mV s^{-1}.[330] Unfortunately, even though this kind of MnO_2 thin layer can exhibit an extremely high specific capacitance of 1330 F g^{-1}, the entire electrode can only provide a capacitance of 0.039 F cm^2 [268] far from the requirements for practical applications, which need high power and energy.

(5) *Specific surface area and pore structure*. As with RuO_2, larger surface area implies more faradaic active sites and thereby higher pseudocapacitance. Normally, the specific capacitance of a metal oxide material will increase significantly as its surface area increases.[268,331] For example, a fibrous electrode has a high surface area and contains more active sites for redox reactions. At the same time, the porous structure of the material can offer more channels for the electrolyte, leading to less electrochemical polarization and therefore minimal dissolution of Mn oxide. Furthermore, high porosity can easily relieve the internal stress created during the charging and discharging processes, protecting the electrode from physical damage. Hence, the more fibrous or porous the oxide, the better the cycle stability is.[288]

It is worth pointing out that both the surface area and the pore-size distribution of MnO_2 can be controlled by adjusting the reaction time and the surfactant content in the aqueous phase.[332]

(6) *Chemical factors (the hydrous state of the oxide and valence)*. Physically and chemically bound water is believed to be helpful for the transportation of electrolyte ions. Thus, the loss of water content caused by heat treatment will result in

poor ion conductivity as well as loss of pseudocapacitance if the heat treatment temperature is too high.[44,333] For instance, it was reported that heat treatment at a temperature up to 200 °C could result in the removal of both physically and chemically adsorbed water.[272] Elsewhere it was also suggested that heat treatment can be optimized to possibly enhance overall pseudocapacitive behavior.[327]

The Mn oxidation state is another very critical factor affecting the electrochemical performance of Mn oxides. Owing to the Jahn–Teller distortion of the $Mn(III)O_6$ octahedron, MnO_x involving trivalent Mn(III) shows a rather lower conductivity when compared with MnO_2 or amorphous manganese oxides involving Mn(IV).[13,334] Consequently, with different nanostructured manganese oxides synthesized *via* a precipitation technique using $KMnO_4$ and various alcohols, the presence of Mn^{3+} results in reduced specific capacitance.[277] It was reported that when γ-MnO_2 was transformed to α-Mn_2O_3 and Mn_3O_4 by mechanical grinding, the specific capacitance decreased linearly as the amount of γ-MnO_2 decreased.[334] With respect to this issue, the literature also shows that MnO_2 exhibits much better performance than $Mn(OH)_2$, Mn_2O_3, and Mn_3O_4.[269,278,296]

The factors mentioned above are all related to the MnO_x preparation processes and conditions. To improve Mn oxides' pseudocapacitive performance, developing more favorable preparation processes to optimize the microstructure, crystallinity, and the chemical state of Mn oxides should be an important approach. Several typical techniques reported in the literature are thermal decomposition, co-precipitation, sol–gel processes, electrodeposition, mechanical milling processes, and hydrothermal synthesis.[50,54,269,273,278,280,288,302,311,335–338]

Among these, the hydrothermal route has been proven to be an effective and controllable method to produce Mn oxides with various nanostructures such as nanowhiskers, nanoplates, and nanorods.[302,311,339] Note that the mechanical milling process can lead to a sequential phase transition from γ-MnO_2 to the thermodynamically stable α-Mn_2O_3 and subsequently to Mn_3O_4, depending on the duration of mechanical grinding.[334]

3.2.2.3.2 Challenges for Mn oxides. Regarding Mn oxides as ES materials, several challenges must be addressed to make them usable in practice:

(1) *Dissolution problem.* Owing to the partial dissolution of MnO_2 in the electrolyte during cycling, MnO_2 oxide electrodes suffer from capacitance degradation.[295,340,341] The dissolution reactions can be expressed as eqn (15) or (16):[269]

$$Mn_2O_3(s) + 2H^+ \rightarrow Mn^{2+}_{(aq)} + MnO_2(s) + H_2O \quad (15)$$

or

$$2MnO(OH) \rightarrow Mn^{2+}_{(aq)} + MnO_2(s) + 2OH^- \quad (16)$$

Several approaches have been carried out to prevent Mn oxides from dissoluting during cycling. For example, new electrolyte salts have been developed to avoid forming acidic species in solution.[342,343] Another approach is to apply a protective shell to the Mn oxide surface. Babakhani and Ivey[16] prepared a Mn oxide/CP coaxial core/shell electrode. Mn oxide rods were first synthesized through anodic deposition from an Mn acetate solution, and then were coated using electropolymerization of a conducting polymer to yield coaxial rods. The presence of a conducting polymer suppresses the dissolution of Mn oxide and improves its resistance to failure, leading to both enhanced capacitance and high cycling rate capability.[151,344] It was demonstrated that this Mn oxide/CP coaxial core/shell electrode could exhibit a specific capacitance of 285 F g^{-1} with 92% retention after 250 cycles in 0.5 M Na_2SO_4 at 20 mV s^{-1}, which is much better than uncoated Mn oxide rods.[16] In addition to the above two methods (new electrolytes and material coating), it was reported that inert cobalt oxide also suppressed the dissolution of Mn into electrolyte and stabilized MnO_x,[345,346] leading to both high cycling stability and higher power when measured at a high scan rate of 200 mV s^{-1}.[333] However, if the cobalt oxide content was too high, a significant reduction in the specific capacitance was observed.

(2) *Low surface area and poor electronic conductivity.* Another concern is the low surface areas and poor electronic conductivity of MnO_x materials. To improve these, several approaches have been carried out in ES material development. For example, a large surface area can be achieved by introducing multilayered film electrodes containing transition-metal composite materials.[347] In this way, the formed Mn oxides have high electrochemical activities, leading to excellent electrochemical capacitance and long cycling durability. Besides this method, doping other metals into MnO_x is a proven effective way to increase the surface area. In a nanostructured nickel–manganese oxide composite, the doping nickel increased the Mn oxide surface area by about 46% and the specific capacitance by 37%.[286,348] Increase in the surface areas of MnO_x materials can also be realized by introducing Co into MnO_x or by adding a surfactant such as sodium lauryl sulfate or Triton X-100.[268,283,331] In addition, hierarchical hollow nanospheres of MnO_x yielded a specific surface area of 253 m^2 g^{-1}.[349]

To address the issue of enhancing manganese oxides' poor electrical conductivity, doping with ruthenium,[203] nickel,[51] and Mo[80] seems to be helpful. In addition to doping, highly conductive supports such as active carbon, CNTs, graphite, and conducting polymers have also been utilized to support manganese oxides in an attempt to promote their conductivity.

In actuality, the presence of conductive supports not only improves the electrical conductivity of MnO_x but also increases its active surface area. Using a supporting strategy, MnO_2 can be dispersed over a large area, preventing its further growth by agglomeration and ensuring high utilization of the active materials in addition to providing double-layer capacitance. The most important feature of the supporting strategy is that these conductive supports can form a three-dimensional porous conducting network to effectively assist electron transfer and ion transport within MnO_x.[22,51,281,333,335,347,350–360] For instance, a rectangular shape in a cyclic voltammogram[361] and a volumetric specific capacitance of 253 F cm^{-3} can be obtained from a manganese oxide/carbon composite electrode.[362] Mn oxide/CNT composite electrodes[355] reached a specific capacitance of 415 F g^{-1} because CNTs were able to provide electronic conductive paths and form a network of open mesopores. Li *et al.*[275] reported that when MnO_2

particles were partially coated on the surfaces of MCNTs through a hydrothermal process, a specific capacitance of 550 F g^{-1} was obtained. The MnO_2/C composite electrode also exhibited highly stable performance up to 10 000 cycles.[305] In addition, composites with a single-walled CNT support showed excellent cycling capability even at a high current of 2 A g^{-1}.[354]

In summary, to achieve high energy and power densities for ES, MnO_x based electrode materials can be modified through depositing MnO_x onto carbon materials with high surface areas, highly ordered mesopores, and high electrical conductivity, which can then yield high specific capacitances. However, it should be noted that the specific capacitance of the composite electrode can be compromised by the low faradaic reaction activity of the conductive supports.

(3) *Poor ionic conductivity*. The poor ionic conductivity of Mn oxides is another challenge that hinders their practical application in ES.[272,363] To improve their ionic conductivity, great effort has been invested into nanostructured MnO_x materials. For example, multilayered MnO_2 with a macropore surface and an interlayer space yielded high ionic conductivity, leading to improved pseudocapacitive behaviour with high retention of a rectangular shape during charging/discharging, even at the high potential scan rate of 100 mV s^{-1}.[284]

In addition, a nanoscopic MnO_2 phase can minimize solid-state transport distances for ions going into the oxide. For example, Mn oxide nanowire arrays with high aspect ratio and high surface area, prepared on anodic aluminium oxide templates, displayed a specific capacitance of 254 F g^{-1}.[364] Nanostructured Co- and Ni-doped MnO_2 deposited by a potentiodynamic method have also been explored, showing specific capacitances of 621 and 498 F g^{-1}, respectively, at a scan rate of 10 mV s^{-1}; at a high scan rate of 200 mV s^{-1} they yielded 377 and 307 F g^{-1}, respectively.[333] A uniformly dispersed fibrous manganese oxide electrode, which had a unique nanoporous structure, was able to deliver a high specific capacitance of 502 F g^{-1} and excellent cyclic stability.[365] This is because the high porosity structure enhanced electrolyte accessibility, promoting ionic transportation within the electrode, kinetic reversibility, and electrochemical reaction homogeneity.

3.2.2.3.3 New developments in MnO_2. In recent years, some intensive studies on MnO_2 nanostructured and MnO_2 composite materials as well as their asymmetric ES have been carried out as outlined below.

(1) *Nanostructured MnO_2*. Nanostructured MnO_2 materials have been intensively investigated.[71,366–368] Nano-MnO_2 can exhibit an electrochemical performance superior to its bulk counterpart because it possesses higher specific surface area and the short transport/diffusion path lengths of ions and electrons. Some single-crystal α-MnO_2 nanotubes,[369] which were synthesized by a hydrothermal method without the assistance of templates, surfactants and heat-treatment, could possess a high specific capacitance. α-MnO_2 nanowires with a diameter of 30 to 40 nm and mean pore diameter of 3.1 nm could give a specific capacitance of 466 Fg^{-1} and high cycling efficiency as well at a current density of 10 mA cm^{-2} [370]. α-MnO_2 nanorods with a diameter less than 50 nm showed good cycling stabilities and could deliver a maximum capacitance of 166.2 F g^{-1}.[371]

Nano-structured MnO_2 can be prepared from the reduction of $KMnO_4$ either by alcohols, such as methanol and ethanol,[277] ethylene glycol,[372] KBH_4, fumaric acid, or $MnSO_4$, and Pluronic P123 as a structure-directing agent *etc.*[309] The synthesis techniques exploited include hydrothermal,[373] electrodeposition,[374] sol–gel methods,[269] template synthesis,[375] thermal decomposition,[376] as well as sonochemical synthesis.[377] However, complicated operations, time/energy-consuming and expensive reagents seemed to be serious obstacles for the industrialization of nano-MnO_2. Therefore, it is necessary to develop some simple and cost-effective processes.

(2) *MnO_2 composite materials*. In addition to nanostructured MnO_2, the combination of MnO_2 with other materials such as graphite and CNTs has also been investigated extensively.[326,378–385]

The introduction of other materials into MnO_2 can improve the electron conductivity of the electrode, extend the working potential, and guarantee an effective utilization of MnO_2.[386] As a result, the composite electrodes can display higher specific capacitances, higher energy and higher power densities. For example, the fabrication of a flexible nanoarchitecture by coating an ultrathin film (several nanometres) of MnO_2 to highly electrical conductive Zn_2SnO_4 nanowires grown on carbon microfibers, could result in a maximum specific capacitance of 642.4 F g^{-1} at a current density of 1 A g^{-1} in 1 M Na_2SO_4, an excellent specific energy of 36.8 W h kg^{-1}, a specific power of 32 kW kg^{-1} at 40 A g^{-1} as well as a good long-term cycling stability.[387] In this case, the crystalline Zn_2SnO_4 nanowires grown on carbon microfibers served as highly electrical conductive cores to support MnO_2 shells with highly electrolytic accessible surface area and to provide reliable electrical connections to the MnO_2 shells.

Graphene–MnO_2 composites (78 wt% MnO_2), which were prepared by redox reaction between graphene and potassium permanganate under microwave irradiation, displayed a specific capacitance as high as 310 F g^{-1} at 2 mV s^{-1}, which is almost three times higher than that of pure graphene (104 F g^{-1}) and birnessite type MnO_2 (103 F g^{-1}). The improved electrochemical performance might be attributed to the increased electrode conductivity in the presence of graphene network, the increased effective interfacial area between MnO_2 and the electrolyte, as well as the contact area between MnO_2 and graphene.[388]

With respect to CNT composite materials, most of the reports dealt with non-aligned and disordered CNTs. Compared to non-aligned CNTs, aligned CNT-based electrodes could show advantages such as low contact resistance, large specific surface area, and fast electron transfer kinetics.[389,390] For example, R. Amade *et al.*[391] prepared a nanostructured composite electrode with dense, long and vertically aligned CNTs (with high specific surface area), coupled with a thinner layer of MnO_2 by optimizing the CNT preparing parameters and electrodeposition processes of MnO_2. A specific capacitance of 642 F g^{-1},[391] much higher than that of activated carbon/MnO_2 electrodes,[386] was obtained at a scan rate of 10 mV s^{-1}. This high capacitance was mainly attributed to CNT's high surface area and conductivity.[391]

To simultaneously achieve both high energy and power densities, one of the challenges is to optimize the mass proportion of the composite.[386] For an active carbon/MnO_2 composite electrode, the optimal mass proportion of active carbon in the positive electrode was found to be 15%.[392]

(3) *Asymmetric cells*. Recently, asymmetric cells coupling with electrodes operating reversibly in different potential ranges have been presented as a promising way to increase voltage in aqueous electrolyte, leading to high energy density as expressed in eqn (9). For example, as reported by Gao *et al.*,[392] a hybrid ES (with a composite MnO_2 and activated carbon as the positive electrode and activated carbon as the negative electrode) extended the operating voltage to 2 V in a 0.5 M Na_2SO_4 aqueous solution. This operating voltage window could be divided into two distinct parts: an approximate symmetric scale ranging from 0 to 1.1 V and an asymmetric scale from 1.1 to 2.0 V.

By optimizing the mass ratio (R) between the positive and negative electrodes, the best performance for asymmetric MnO_2/actived carbon ES was obtained with R = 2.5 and V (cell voltage) = 2 V, allowing the maximum potentials for both electrodes to be close to the acceptable stability values.[393] However, to reduce the R value, designing positive electrodes with enhanced capacitance according to the following formula seemed to be challengeable. Eqn (17) is based on the equivalence of charge passed through both electrodes.

$$R = \frac{m_+}{m_-} = \frac{C_- \times \Delta E_-}{C_+ \times \Delta E_+} \qquad (17)$$

where m_+ and m_- are the masses of the electrode materials, C_+ and C_- are the specific capacitances, and E_+ and E_- are the potential windows for the positive and negative electrodes, respectively.

3.2.2.4 Co_3O_4 and $Co(OH)_2$. (1) *Co_3O_4*. Co_3O_4 seems to exhibit excellent reversible redox behavior, large surface area, high conductivity, long-term performance, and good corrosion stability.[394–397] Therefore, it has been considered an alternative electrode material for ES.[398] The pseudocapacitance of Co_3O_4 originates from the following redox reaction:[399]

$$Co_3O_4 + H_2O + OH^- \leftrightarrow 3CoOOH + e^- \qquad (18)$$

With respect to this, Co_3O_4-based materials have been assessed by many groups for ES applications.[396,400,401] For example, mesoporous Co_3O_4 microspheres with a unique crater-like morphology were synthesized using mesoporous silica material as a template. When tested, this material had a smaller inner resistance of about 0.4 Ω and could provide a specific capacitance of 102 F g^{-1}.[402] A specific capacitance of 118 F g^{-1} for a cobalt oxide electrode was obtained by chemically coating cobalt oxide thin films on copper substrates.[2] Kandalkar *et al.*[75] prepared a cobalt oxide film from a cobalt chloride precursor and obtained a specific capacitance of 165 F g^{-1} in a 1.0 M aqueous KOH electrolyte at a scan rate of 10 mV s^{-1}. Shan and Gao[399] reported a MWCNT composite electrode, MWCNT/Co_3O_4, and achieved a specific capacitance of 200 F g^{-1}. A Co_3O_4 film deposited using a solution spray pyrolysis technique exhibited a specific capacitance of 74 F g^{-1}.[403] This relatively low capacitance was attributed to the anhydrous nature of Co_3O_4. A Co_3O_4 electrode prepared by a sol–gel method gave a specific capacitance of 291 F g^{-1}.[404]

Recent studies have been concentrated on Co_3O_4 with special morphology and microstructure. Microspheres, nanosheets, nanowires, nanorods, nanotubes as well as thin films are all seen in the recent studies on Co_3O_4. For example, crater-like Co_3O_4 microspheres with a BET surface area of 60 m^2 g^{-1} were synthesized by L. Wang *et al.*[402] Hexagonal Co_3O_4 nanosheets, synthesized using a facile complex–precursor solution procedure followed by a sequential thermal decomposition at atmospheric pressure, could give a specific capacitance of 227 F g^{-1} at 1 A g^{-1}.[405] Co_3O_4 nanowire arrays prepared on nickel foam, showed a maximum specific capacitance of 746 F g^{-1} at a current density of 5 mA cm^{-2}.[406] Using a facile and efficient hydrothermal method, Co_3O_4 nanorods with nanoporosity could give a specific capacitance of 280 F g^{-1} at 5 mV s^{-1} in 2 M KOH,[407] while single crystal Co_3O_4 nanorods exhibited a high capacitance of 456 F g^{-1} at a current density of 1 A g^{-1}.[37] Co_3O_4 nanotubes with an outer wall diameter of 300 nm and a wall thickness of 50 nm, synthesized by chemically depositing cobalt hydroxide in anodic aluminium oxide templates and thermally annealing, displayed a specific capacitance of 574 F g^{-1} at 0.1 A g^{-1}.[408] Co_3O_4 thin films, prepared through electrodeposition, exhibited a specific capacitance of 235 F g^{-1} at a scan rate of 20 mV s^{-1}. The specific energy power densities of such thin film-based ES were 4.0 W h kg^{-1} and 1.33 kW kg^{-1}, respectively.[409] In addition, mesoporous Co_3O_4 nanoparticles with a BET surface area of 184.8 m^2 g^{-1} showed the maximum specific capacitance of 370 F g^{-1}.[410] Aerogel-like mesoporous Co_3O_4, prepared with an addition of an epoxide, exhibited a high specific capacitance of 600 F g^{-1}.[400] These recent studies suggest that the appropriate morphology and microstructure are necessary in achieving an enhanced performance of Co_3O_4-based ES.

(2) *$Co(OH)_2$*. $Co(OH)_2$-based materials are attractive due to their layered structure and large interlayer spacing, which promises high surface area and a fast ion insertion/desertion rate.[411–413] Two plausible reactions can occur, as expressed in eqn (19) and (20):[178,414,415]

$$Co(OH)_2 + OH^- \leftrightarrow CoOOH + H_2O + e^- \qquad (19)$$

$$CoOOH + OH^- \leftrightarrow CoO_2 + H_2O + e^- \qquad (20)$$

Some publications exist on $Co(OH)_2$-based materials for ES. For example, a flexible nanoflake film of porous cobalt hydroxide was deposited by galvanostatic electrodeposition on a stainless-steel mesh, giving a high capacitance of 609 F g^{-1}.[416] To further improve the specific capacitance, some modifications were carried out on the microstructure of cobalt hydroxide, resulting in an incremental increase in specific capacitance.[417] It seems that $Co(OH)_2$-based materials show much higher specific capacitances than Co_3O_4-based materials.

It should be noted that a specific capacitance higher than that of RuO_2 can be achieved in many cases where Co oxide based materials are in the electrode. For example, Al-substituted

α-cobalt hydroxide, prepared by a potentiostatic deposition process, yielded a specific capacitance of 843 F g^{-1} in a potential window between 0 and 0.4 V.[413] One of the most impressive results was obtained by Zhou *et al.*,[418] who presented a specific capacitance up to 2646 F g^{-1} when an ordered mesoporous cobalt hydroxide film electrodeposited on foamed Ni mesh was used as the electrode material. This exceptionally high specific capacitance was attributed to the special ordered mesoporous nanostructure of Co oxides. Unfortunately, most of the specific energy achieved is located in low potential ranges.[419,420] Therefore, an increase in the specific energy in the high potential range would be the key for their practical application in ES.

In summary, $Co(OH)_2$-based ES electrodes can give much higher specific capacitances than Co_3O_4. However, such high specific capacitance is only located in low potential ranges, which limits the materials' practical application in ES.

3.2.2.5 NiO/Ni(OH)$_2$. (1) *NiO*. Nickel oxide is considered an alternative electrode material for ES in alkaline electrolytes due to its easy synthesis, relatively high specific capacitance (theoretical specific capacitance of 3750 F g^{-1}),[421–424] environment friendliness, and low cost.[425] The redox reaction of nickel oxide in a KOH electrolyte can be expressed as eqn (21):[426–428,74]

$$NiO + OH^- \leftrightarrow NiOOH^- + e^- \quad (21)$$

It is recognized that the electrochemical surface reactivity of nickel oxide is strongly dependent on its crystallinity. As shown in Table 3,[429] during synthesis the calcination temperature can significantly affect the crystalline structure of NiO_x, the value of x, and the specific capacitance. At above 280 °C, more crystallization takes place and the value of x decreases. As a result, a maximum specific capacitance of 696 F g^{-1} can be reached at 250 °C. However, when a $Ni(OH)_2$/CNT electrode is heated to 300 °C, the capacitance decreases significantly.

To improve the unsatisfactory porous structures of Ni oxides, which can limit the transportation of electrolyte ions, leading to slow electrochemical processes in charge storage and delivery, nickel oxides with a hierarchical porous texture have been developed.[430] As a result, the capacitance retention ratio of nickel oxide improved at a high potential scan rate because the open hierarchical porous texture permitted ions easy access to the electrode/electrolyte interface.

It has also been shown that the preparation process can strongly influence the electrochemical behavior of NiO.[74] For example, NiO with a cubic structure, synthesized *via* a chemical process, had a maximum specific capacitance of 167 F g^{-1}, while porous NiO[428] obtained by a sol–gel method exhibited a specific capacitance of 200–250 F g^{-1}, and after being annealed at 250 °C its specific capacitance reached 696 F g^{-1}.[429]

The challenges in using NiO-based electrode materials for ES involve:

(i) *Poor cycle performance*. For example, a hexagonal nanoporous $Ni(OH)_2$ film prepared by electrodeposition gave a specific capacitance of 578 F g^{-1}. However, after 400 cycles, approximately 4.5% of the specific capacitance was lost due to degradation of the material's microstructure.[178] Another example is a nickel oxide film prepared *via* an electrochemical method, which also exhibited poor cycle performance.[431] At a current density of 0.49 mA cm^{-2} its specific capacitance decreased from 160 to 140 F g^{-1} after 5000 cycles, losing 12.5% of its initial capacitance. To address this degradation, a supporting strategy was explored using Co and CNT as supports to form a composite. The composite material, which was formed by thermally decomposing nickel and cobalt nitrates directly onto the surface of a CNT/graphite electrode, showed a high specific capacitance of 569 F g^{-1} at a discharge current density of 10 mA cm^{-2} in a 1 M KOH aqueous solution. This composite electrode displayed excellent cycle stability as well. Only 0.2% of the specific capacitance was lost after 1000 cycles at a current density of 10 mA cm^{-2}.[432]

(ii) *High resistivity*. Another challenge for NiO electrodes is their high resistivity (low electrical conductivity). To address this issue, making composites of NiO with conductive carbon materials seems to be an effective approach. In a nickel oxide/CNT nanocomposite,[46] the CNT conducting network significantly improved the electrical conductivity of the host NiO. CNTs' high specific surface area can also increase the active sites for redox reactions. As a result, the NiO_x-normalized specific capacitance of a NiO_x/CNT electrode can reach a specific capacitance as high as 1000 F g^{-1}, which is approximately three times higher than the ~350 F g^{-1} obtained for a NiO_x thin-film electrode.[433]

The conductivity of nickel oxide can also be improved by introducing cobalt ions into the nickel oxide matrix.[432,434] For example, nanostructured Co–Ni/Co–Ni oxides with a cauliflower shape, as shown in Fig. 12, exhibited low resistance and a high-specific capacitance of 331 F g^{-1} as well as high cyclic stability.[423] The electrochemical behaviour of Ni–Co oxides was found to be dependent on the composition of the oxides. For instance, a specific capacitance as high as 541 F g^{-1} was achieved, even at a discharge current density of 100 mA cm^{-2} as was excellent charge–discharge cycle stability.[432]

A recent trend in NiO is to develop nanostructured materials. The prepared nano-NiO materials include nanocolumns, nanosheets, nanoflakes, nanorings, hierarchical porous nanoflowers, nano/microspheres, porous nanowall arrays as well as hollow nanospheres.[435–441] In particular, the porous structure of hollow nanospheres can act as an "ion reservoir",

Table 3 Effect of calcination temperature on the specific capacitance calculated from constant current discharge curves (charging at 0.6 V *vs.* Hg/HgO for 10 minutes)[429] (reprinted from ref. 429 with permission from Elsevier)

	Specific capacitance/F g^{-1} (0.60–0.00 V *vs.* Hg/HgO)			
Heating temperature/°C	2 mA cm^{-2}	10 mA cm^{-2}	20 mA cm^{-2}	x in NiO_x
110	592	419	377	2.32
200	636	469	404	2.06
250	696	521	479	1.50
280	586	420	373	1.36
300	546	383	340	1.19
350	494	302	269	1.18
400	382	270	235	1.15
450	157	106	88.8	1.08

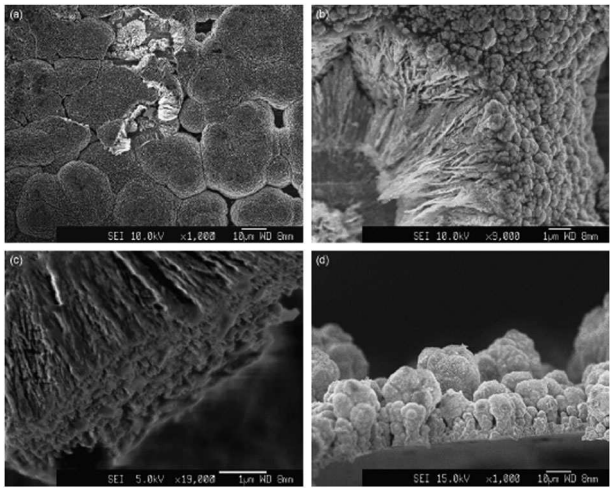

Fig. 12 (a)–(d) SEM images of nanostructured Co–Ni oxides at different magnifications.[423] (Reprinted from ref. 423 with permission from Elsevier.)

leading to not only high surface area but also better mass transportation, ensuring steady supply of ions for Faradic reactions at high current densities.[442] Regarding the synthesis, the template-based method is the most common method for preparing NiO hollow nanospheres. However, this method is usually too complicated and time-consuming because of the process of acid/base erosion or calcinations. Recently, a microwave-assisted gas/liquid interfacial method, which is a simple and template-free hydrothermal method, was used to prepare a flowerlike NiO hollow nanosphere, showing high specific capacitances of 770 F g^{-1} and 585 F g^{-1} at the discharge currents of 2 A g^{-1} and 5 A g^{-1}, respectively, and excellent cycling stability as well.[440]

(2) *$Ni(OH)_2$*. It has been determined that $Ni(OH)_2$ and a $Co(OH)_2$–$Ni(OH)_2$ composite can yield much higher specific capacitances than NiO.[443,444] Hu *et al.*[443] reported that an electrodeposited nickel hydrous oxide film could exhibit a specific capacitance as high as *ca.* 1000 F g^{-1}. In the case of $Co(OH)_2$–$Ni(OH)_2$/Y-zeolite composites, the specific capacitance was estimated to be as high as 1710 F g^{-1}.[445] For a $Co_{0.41}Ni_{0.59}$ layered double hydroxide the specific capacitance reached 1809 F g^{-1} at 1 A g^{-1}.[446]

For further improvement, if the micropore structure of this kind of materials is optimized, much better performance can be achieved. For example, Kong *et al.*[444] reported a nickel hydroxide material with a mesoporous structure of interconnected nanoflakes, which was capable of delivering a specific capacitance of 2055 F g^{-1} at 0.625 A g^{-1}. After introducing mesoporous carbon into the Ni hydroxide to form a nickel hydroxide/mesoporous carbon composite, the charge-transfer resistance was greatly reduced, resulting in an extremely high specific capacitance of 2570 F g^{-1} at a current density of 5 mA cm^{-2}.[447] Therefore, in terms of specific capacitance, both $Ni(OH)_2$ and $Co(OH)_2$–$Ni(OH)_2$ should be satisfactory materials for ES. Unfortunately, the potential window of these materials is too narrow.[443]

In summary, due to the low cost of raw materials and high specific capacitance, Co/Ni composites should be promising materials in ES applications as long as a wide potential window can be obtained and the composition of binary oxides can be accurately controlled.

3.2.2.6 V_2O_5. Vanadium oxides have also been investigated for their potential use in ES due to their variable oxidation states, which can yield surface/bulk redox reactions.[448,449] For example, Lee and Goodenough[450] prepared amorphous V_2O_5 by quenching V_2O_5 powders heated at 950 °C, then studied the behavior of this material in aqueous KCl solutions. The specific capacitance obtained was 350 F g^{-1}. A V_2O_5 sample prepared by a sol–gel method[451] exhibited a maximum specific capacitance of 214 F g^{-1} at a scan rate of 5 mV s^{-1} in a 2 M KCl solution.

Fig. 13 [451] shows that the specific capacitance of V_2O_5 is dependent on the electrolyte used. Among the aqueous electrolytes employed, a solution of 2 M KCl seems to be the best. This result was also supported by Wee *et al.*[452] In their work, V_2O_5 nanofibres showed the highest specific capacitance, 190 F g^{-1}, in aqueous 2 M KCl electrolyte, compared to 1 M H_2SO_4 (106 F g^{-1}) and 2 M KOH (8 F g^{-1}). In addition, the specific capacitance of V_2O_5 material was further improved to 250 F g^{-1} in an organic solution containing an $LiClO_4$ electrolyte.[452]

The challenge for V_2O_5 is its low conductivity. In an attempt to improve electronic conductance, V_2O_5-based composites, which contain materials with higher electronic conductivity such as metal fibres, metal oxides, or carbonaceous materials, have been developed.[453–457] For example, CNTs have been explored as a compositing material to form V_2O_5/CNT composites, which have a larger specific capacitance than pure V_2O_5. Jayalakshmi *et al.*[457] demonstrated that at a scan rate of 100 mV s^{-1}, in dilute KCl solution, the addition of CNT could increase the capacitance to almost three-fold that of simple vanadium oxide. Similarly, a $V_2O_5{\cdot}xH_2O$/CNT film electrode also showed a high specific capacitance of 910 F g^{-1} at a potential scan rate of 10 mV s^{-1}, three times higher than that of a $V_2O_5{\cdot}xH_2O$ thin-film electrode (300 F g^{-1}).[458] SnO_2 has also been explored as a composite material, as it is semiconductive and has conventional redox properties. When it was combined with V_2O_5 to form a composite, the electronic properties were significantly improved. For example, a SnO_2–V_2O_5–CNT electrode provided a specific capacitance

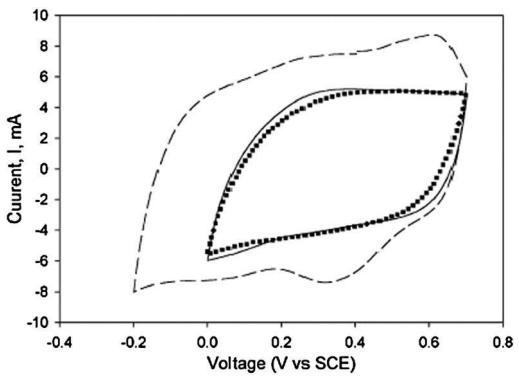

Fig. 13 CV curves of V_2O_5 in 2 M KCl (—), 2 M LiCl (—), and 2 M NaCl (·····) electrolytes at a scan rate of 5 mV s^{-1}.[451] (Reprinted from ref. 451 with permission from Elsevier.)

of 121.4 F g^{-1} at a scan rate of 100 mV s^{-1}, much higher than a V_2O_5–CNT electrode.[457]

The above results demonstrate that the electronic properties of V_2O_5 can be favorably changed with a suitable choice of additive in the electrode material.

3.2.2.7 SnO_2. SnO_2 has also been explored as an alternative ES electrode material. However, its specific capacitance is much lower than other metal oxides'. For example, a SnO_2 composite electrode synthesized by impregnating tin oxide sol into resorcinol–formaldehyde wet gels or by impregnating tin tetrachloride solution into carbon aerogel electrodes displayed a specific capacitance of only 66–70 F g^{-1}.[459] A Sb-doped SnO_2 nanocrystallite synthesized by a sol–gel process[460] had a specific capacitance of only 16 F g^{-1} in a 1 M KOH electrolyte even at a low scan rate of 4 mV s^{-1}. Even a SnO_2/RuO_2 composite could only give a specific capacitance of 33 F g^{-1} at a scan rate of 50 mV s^{-1}.[225] However, amorphous nanostructured SnO_2 synthesized using electrochemical deposition showed a specific capacitance value as high as 285 F g^{-1} at a scan rate of 10 mV s^{-1}, and 101 F g^{-1} at a high scan rate of 200 mV s^{-1}.[461] Furthermore, the specific capacitance of a nanoscaled SnO_2–Al_2O_3 composite can reach 119 F g^{-1} in a 0.1 M NaCl solution, which is much greater than pure SnO_2.[462]

Again, the major disadvantage for SnO_2 material is its small potential, although the introduction of Al_2O_3 into SnO_2 can expand its potential window.[462]

3.2.2.8 Iron oxides (Fe_2O_3 and Fe_3O_4). α-Fe_2O_3 is another candidate for ES electrode material, offering low cost and minimal environmental impact. However, poor electronic conductivity restricts its applications in high-power storage devices. The incorporation of MCNTs into α-Fe_2O_3 nanospheres seems to be a way to improve its conductivity, leading to better ion diffusion. It was reported that a hybrid supercapacitor consisting of MCNTs and α-Fe_2O_3/MCNT thin-film electrodes yielded a high specific energy density of 50 W h kg^{-1} at a specific power density of 1000 W kg^{-1} over the potential range of 0–2.8 V.[463] However, owing to poorer electron transport within the α-Fe_2O_3 film and the reaction's comparatively sluggish kinetics, the specific capacitance was reduced by 90% when the potential scan rate was increased. When the scan rate was changed from 2 to 200 mV s^{-1}, the specific capacitance dropped from 100 to 8 F g^{-1}.[463]

Fe_3O_4 is another inexpensive material exhibiting pseudocapacitance in alkali sulfite electrolytes. However, its low specific capacitance is a limitation for practical application. For example, a Fe_3O_4 electrode synthesized using electrocoagulation and a reflux method exhibited a specific capacitance of only 5.3 F g^{-1} in a 1 M Na_2SO_4 solution.[464] Recently, a Fe_3O_4 film prepared *via* a hydrothermal process displayed a typical pseudocapacitive behavior in a 1 M Na_2SO_3 solution, a specific capacitance of 118.2 F g^{-1} between −1 and 0.1 V, and a capacitive retention of 88.8% after 500 cycles of charging/discharging.[465]

Neither Fe_2O_3 nor Fe_3O_4 seem realistic materials for ES due to their poor capacitance and cycle stability.

3.2.2.9 Other materials. (1) *Other metal oxides.* Many other metal oxide materials, such as IrO_2, Bi_2O_3, and MoO_2, have also been explored as electrode materials for ES. The oxides of multivalent metal iridium exhibit a large faradaic pseudocapacitance, similar to RuO_2.[15] For example, hydrous IrO_2 showed a specific capacitance close to 550 F g^{-1}.[466] However, its price is even higher than that of RuO_2. A Bi_2O_3 electrode exhibits good electrochemical supercapacitive characteristics as well as high stability in aqueous NaOH solution. The highest specific capacitance achieved with electrodeposited Bi_2O_3 films was 98 F g^{-1}.[467] One-dimensional MoO_2 nanorods, prepared by thermal decomposition of tetrabutylammonium hexamolybdate ($((C_4H_9)_4N)_2Mo_6O_{19}$) in an inert atmosphere, yielded a specific capacitance of 140 F g^{-1}.[468] All of these metal oxide materials present faradaic pseudocapacitance to a moderate extent, but they suffer from one problem or another. Their application as ES electrode materials seems unrealistic at the present stage of technology.

(2) *Transition metal nitrides.* In recent years, transition metal nitride materials have attracted much attention due to their high electrical conductivity ($\sim 10^6$ Ω^{-1} m^{-1}) and chemical stability (excellent resistance to common acids and alkali). For example, molybdenum nitride (MoN) was explored as an ES electrode material in sulfuric acid solution.[469] Its specific capacitance behavior was found to be comparable to that of RuO_2. Unfortunately, MoN has a substantially smaller operating voltage range (only 0.7 V) due to its electrochemical decomposition. Vanadium nitride seems to be a promising ES electrode material. Its specific capacitance was found to be 161 F g^{-1} at 30 mV s^{-1}, and it retained 70% of its original capacitance value even when the potential scan rate was increased from 30 to 300 mV s^{-1}.[79] Using a nanostructured vanadium nitride, a high specific capacitance of 1200–1400 F g^{-1} was obtained when tested at a scan rate of 2 mV s^{-1},[470] while 554 F g^{-1} was achieved at a high scan rate of 100 mV s^{-1}.[471]

(3) *New materials.* Recently, lithium-ion ES technology has been introduced. This device shows advantages such as reduced mass and volume as well as increased operating voltage over traditional ES technology.[472] The new materials investigated include $MnFe_2O_4$, $LiMn_2O_4$ and $NaMn_2O_4$.

Unlike MnO_2-based materials, whose pseudo-capacitance essentially comes from amorphous MnO_2, $MnFe_2O_4$ exhibits pseudo-capacitance in crystalline form.[472] It exhibits high power delivering capability and superior cycling stability in aqueous electrolytes.[473,474] This nanocrystalline $MnFe_2O_4$, acting as an anode material, showed a specific capacitance of 99 F g^{-1}.[472] An $LiMn_2O_4$ cathode showed a specific capacity of 130–100 mA h g^{-1} at 10–100 C rate within −0.3–0.9 V (*vs.* Ag/AgCl/saturated $KCl_{(aq.)}$).[472] The energy density of $LiMn_2O_4$ decreased very fast with rising current density because the large diameter of the solvated Li^+ could lead to difficulty of Li^+ solvation and desolvation at high current densities.[475] The asymmetric ES cell containing $LiMn_2O_4$ (cathode) and $MnFe_2O_4$ (anode) showed a maximum operating voltage window of *ca.* 1.3 V. This cell could reach the maximum specific power and energy densities when the mass ratio between the anode and the cathode was ~4.0. In this case, the specific cell energy density, based on the total mass of two electrodes, was 10 and 5.5 W h kg^{-1} at 0.3 and 1.8 kW kg^{-1}, respectively.

Meanwhile, the cell also exhibited a low self-discharge rate as well as a good cycling stability.[472] An $NaMnO_2$ cathode showed two redox couples in 0.5 M Na_2SO_4 within the potential range of 0–1.1 V, which were ascribed to the intercalation–deintercalation of Na^+ into and from the solid lattice. The specific capacitance of the $NaMnO_2$ electrode was found to be 140 F g^{-1}. The asymmetric ES containing active carbon and $NaMnO_2$ electrodes exhibited a specific capacitance of 38.9 F g^{-1} and an energy density of 19.5 W h kg^{-1} at a power density of 130 W kg^{-1}. These values are based on the total mass of the active electrode materials (including anode and cathode).[475]

4. Trends in ES

With increasing demands for clean, sustainable energy, the advantages of high power density, high efficiency, and long life expectancy have made electrochemical supercapacitors one of the major emerging devices for energy storage and power supply. In particular, their feasibility for practical applications in hybrid power sources, backup power sources, starting power for fuel cells, and burst-power generation in electronic devices has been demonstrated.

However, one of the key challenges for ES is their limited energy density, which has hindered their wider application in the field of energy storage. To overcome this challenge, a major focus of ES research and development should be to discover new electrode materials with high capacitance and a wide potential window. In the design of ES electrode materials, the favored properties of ES electrode materials include: (1) high specific surface area, meaning more active sites, (2) suitable pore-size distribution, pore network, and pore length for facilitating the diffusion of ions at a high rate, (3) low internal electrical resistance for efficient charge transport in the composite electrode, and (4) better electrochemical and mechanical stability for good cycling performance. The porosity of ES materials should be particularly emphasized here. Nano-micropores are necessary to achieve higher specific surface area, and these micropores must be ensured to be electrochemically accessible for ions. Hence, pore network, the availability and wettability of pores, with dimensions matching the size of solvated anions and cations are crucial for ES electrode materials.

Several important ES electrode materials that should be mentioned are carbon-based materials, conductive polymers, and metal oxides. For carbon materials, higher specific surface area and rational pore distribution have been achieved, and given the commercially available ES, although their capacitances (or energy densities) are still low. Regarding conductive polymers, which show high specific capacitances, the major challenges are their swelling and shrinking during charge/recharge, leading to a short ES lifetime. With respect to metal oxides, amorphous structures can possess high specific surface areas and favor the diffusion of ions into the material's bulk, and the combined water is believed to be helpful for ion transport. In the case of RuO_2-based materials, although they have high capacitances, their costliness prevents their practical application in ES.

It is worth pointing out that although thin films can achieve very high surface area, high specific capacitance (> 2000 F g^{-1}), and rate capability due to increased electrical conductivity, in a real ES they may not necessarily be ideal electrode materials. This is because when a film is used to construct a thicker electrode layer, the electrochemical utilization of the material and ionic transport throughout the internal volume of the thicker electrode layer will be limited, becoming a large obstacle to the film's practical use in ES electrodes.

To develop new materials with optimal performance, two important research directions in ES electrode exploration are:

(1) *Composite materials*. Regardless of the materials for ES electrodes, combining different materials to form composites should be an important approach because the individual substances in the composites can have a synergistic effect through minimizing particle size, enhancing specific surface area, inducing porosity, preventing particles from agglomerating, facilitating electron and proton conduction, expanding active sites, extending the potential window, protecting active materials from mechanical degradation, improving cycling stability, and providing extra pseudocapacitance. As a result, the obtained composites can overcome the drawbacks of the individual substances and embody the advantages of all constituents. High capacities over 1700 F g^{-1} have been reported on the basis of composite materials.[445–447] But it is worth to point out that the reverse effects may also take place in the process of making composites. Consequently, there should be a compromise among the composition of individual substances and an optimized molar ratio of constituents for every composite material.

(2) *Nanomaterials*. Recent trends in ES also involve the development of nanostructured materials, such as nanoaerogels, nanotubes/rods, nanoplates, nanospheres, and so on. Nanostructured materials possess high specific surface area. They can provide short transport/diffusion path lengths for ions and electrons, leading to faster kinetics, more efficient contact of electrolyte ions, and more electroactive sites for faradaic energy storage, resulting in high charge/discharge capacities even at high current densities. Material morphology is closely related to the specific surface area and the diffusion of ions in the electrode, and one-dimensional nanostructure materials seem to be very promising for ES application due to their reduced diffusion paths and larger specific surface areas.

References

1 C. Largeot, C. Portet, J. Chmiola, P. Taberna, Y. Gogotsi and P. Simon, *J. Am. Chem. Soc.*, 2008, **130**, 2730.
2 S. Kandalkar, D. Dhawale, C. Kim and C. Lokhande, *Synth. Met.*, 2010, **160**, 1299.
3 R. Kötz and M. Carlen, *Electrochim. Acta*, 2000, **45**, 2483.
4 R. Kötz, S. Müller, M. Bärtschi, B. Schnyder, P. Dietrich, F. N. Büchi, A. Tsukada, G. G. Scherer, P. Rodatz, O. Garcia, P. Barrade, V. Hermann and R. Gallay, *Electrochem. Soc. Proc.*, 2001, **21**, 564.
5 P. Simon and Y. Gogotsi, *Nat. Mater.*, 2008, **7**, 845.
6 E. Frackowiak, *Phys. Chem. Chem. Phys.*, 2007, **9**, 1774.
7 L. Zhang and X. S. Zhao, *Chem. Soc. Rev.*, 2009, **38**, 2520.
8 H. Pan, J. Li and Y. Feng, *Nanoscale Res. Lett.*, 2010, **5**, 654.
9 M. Inagaki, H. Konno and O. Tanaike, *J. Power Sources*, 2010, **195**, 7880.
10 E. Frackowiak and F. Beguin, *Carbon*, 2001, **39**, 937.
11 A. G. Pandolfo and A. Hollenkamp, *J. Power Sources*, 2006, **157**, 11.

12 P. Simon and A. Burke, *Interface*, 2008, **17**, 38.
13 S. W. Zhang and G. Z. Chen, *Energy Mater.*, 2008, **3**, 186.
14 A. Burke, *J. Power Sources*, 2000, **91**, 37.
15 B. E. Conway, *Electrochemical Supercapacitors*, Kluwer Academic/Plenum Press, New York, 1999.
16 B. Babakhani and D. G. Ivey, *Electrochim. Acta*, 2010, **55**, 4014.
17 S. Sarangapani, B. V. Tilak and C. P. Chen, *J. Electrochem. Soc.*, 1996, **143**, 3791.
18 J. P. Zheng, J. Huang and T. R. Jow, *J. Electrochem. Soc.*, 1997, **144**, 2026.
19 Y. M. Vol'fkovich and T. M. Serdyuk, *Russ. J. Electrochem.*, 2002, **38**, 935.
20 M. S. Wu and P. C. Chiang, *Electrochem. Solid-State Lett.*, 2004, **7**, A123.
21 W. Sugimoto, H. Iwata, Y. Murakami and Y. Takasu, *J. Electrochem. Soc.*, 2004, **151**, A1181.
22 X. Dong, W. Shen, J. Gu, L. Xiong, Y. Zhu, H. Li and J. Shi, *J. Phys. Chem. B*, 2006, **110**, 6015.
23 Y. Zhang, H. Feng, X. Wu, L. Wang, A. Zhang, T. Xia, H. Dong, X. Li and L. Zhang, *Int. J. Hydrogen Energy*, 2009, **34**, 4889.
24 B. E. Conway, V. Birss and J. Wojtowicz, *J. Power Sources*, 1997, **66**, 1.
25 C. Ming Chuang, C. W. Huang, H. Teng and J. M. Ting, *Energy Fuels*, 2010, **24**, 6476.
26 M. Kisacikoglu, M. Uzunoglu and M. Alam, *Int. J. Hydrogen Energy*, 2009, **34**, 1497.
27 S. Ma, K. Nam, W. Yoon, X. Yang, K. Ahn, K. Oh and K. Kim, *Electrochem. Commun.*, 2007, **9**, 2807.
28 H. Ohno and K. Fukumoto, *Electrochemistry*, 2008, **76**, 16.
29 G. A. Snook, P. Kao and A. S. Best, *J. Power Sources*, 2011, **196**, 1.
30 M. Galiński, A. Lewandowski and I. Stępniak, *Electrochim. Acta*, 2006, **51**, 5567.
31 J. Carche, C. K. Dyer, P. T. Moseley, Z. Ogumi, D. A. J. Rand and B. Scrosati, *Encyclopedia of Electrochemical Power Sources*, Elsevier B.V., 2009.
32 A. Lewandowski and M. Galiński, *J. Phys. Chem. Solids*, 2004, **64**, 281.
33 A. Balducci, W. A. Henderson, M. Mastragostino, S. Passerini, P. Simon and F. Soavi, *Electrochim. Acta*, 2005, **50**, 2233.
34 H. Randriamahazaka, C. Plesse, D. Teyssie and C. Chevrot, *Electrochim. Acta*, 2005, **50**, 1515.
35 H. Liu, P. He, Z. Li, Y. Liu and J. Li, *Electrochim. Acta*, 2006, **51**, 1925.
36 W. Sun, R. Zheng and X. Chen, *J. Power Sources*, 2010, **195**, 7120.
37 L. Cui, J. Li and X. G. Zhang, *J. Appl. Electrochem.*, 2009, **39**, 1871.
38 H. K. Song, H. Y. Hwang, K. H. Lee and L. H. Dao, *Electrochim. Acta*, 2000, **45**, 2241.
39 A. Kusko and J. Dedad, *IEEE Ind. Appl. Mag.*, 2007, **13**, 66.
40 M. Uzunoglu and M. S. Alam, *IEEE Trans. Energy Convers.*, 2008, **23**, 263.
41 P. Thounthong, V. Chunkag, P. Sethakul, B. Davat and M. Hinaje, *IEEE Trans. Veh. Technol.*, 2009, **58**, 3892.
42 J. R. Miller and A. F. Burke, *Electrochem. Soc. Interface*, 2008, **17**, 53.
43 H. Chen, T. N. Cong, W. Yang, C. Tan, Y. Li and Y. Ding, *Prog. Nat. Sci.*, 2009, **19**, 291.
44 R. N. Reddy and R. G. Reddy, *J. Power Sources*, 2004, **132**, 315.
45 B. Babakhani and D. G. Ivey, *J. Power Sources*, 2010, **195**, 2110.
46 J. Lee, K. Liang, K. An and Y. Lee, *Synth. Met.*, 2005, **150**, 153.
47 J. R. Miller, *Electrochim. Acta*, 2006, **52**, 1703.
48 J. P. Zheng, *J. Electrochem. Soc.*, 2005, **152**, A1864.
49 C. Yuan, B. Gao and X. Zhang, *J. Power Sources*, 2007, **173**, 606.
50 Y. U. Jeong and A. Manthiram, *J. Electrochem. Soc.*, 2002, **149**, A1419.
51 Y. Chen and C. Hu, *Electrochem. Solid-State Lett.*, 2003, **6**, A210.
52 C. C. Hu and C. C. Wang, *J. Electrochem. Soc.*, 2003, **150**, A1079.
53 H. P. Park, O. O. Park, K. H. Shin, C. S. Jin and J. H. Kim, *Electrochem. Solid-State Lett.*, 2002, **5**, H7.
54 R. N. Reddy and R. G. Reddy, *J. Power Sources*, 2003, **124**, 330.
55 J. Lai, S. Levy and M. Rose, *IEEE Aerosp. Electron. Syst. Mag.*, 1992, **7**, 14.
56 Q. Huang, X. Wang and J. Li, *Electrochim. Acta*, 2006, **52**, 1758.
57 P. Sharma and T. S. Bhatti, *Energy Convers. Manage.*, 2010, **51**, 2901.
58 A. S. Aricò, P. Bruce, B. Scrosati, J. Tarascon and W. V. Chalkwijk, *Nat. Mater.*, 2005, **4**, 366.
59 H. Lee, M. S. Cho, I. H. Kim, J. D. Nam and Y. Lee, *Synth. Met.*, 2010, **160**, 1055.
60 D. Choi and P. N. Kumta, *J. Electrochem. Soc.*, 2006, **153**, A2298.
61 E. Frackowiak, S. Delpeux, K. Jurewicz, K. Szostak, D. Cazorla-Amoros and F. Béguin, *Chem. Phys. Lett.*, 2002, **361**, 35.
62 V. Ruiz, C. Blanco, E. R. Piñero, V. Khomenko, F. Béguin and R. Santamaría, *Electrochim. Acta*, 2007, **52**, 4969.
63 C. Peng, S. W. Zhang and D. Jewell, *Prog. Nat. Sci.*, 2008, **18**, 777.
64 C. Peng, J. Jin and G. Chen, *Electrochim. Acta*, 2007, **53**, 525.
65 A. Malinauskas, J. Malinauskiene and A. Ramanavicius, *Nanotechnology*, 2005, **16**, 51.
66 S. Cho and S. B. Lee, *Acc. Chem. Res.*, 2008, **41**, 699.
67 D. Belanger, T. Brousse and J. W. Long, *Electrochem. Soc. Interface*, 2008, **17**, 49.
68 Y. R. Ahn, M. Y. Song, S. M. Jo and C. R. Park, *Nanotechnology*, 2006, **17**, 2865.
69 V. D. Patake, C. D. Lokhande and O. S. Joo, *Appl. Surf. Sci.*, 2009, **255**, 4192.
70 C. C. Hu, Y. H. Huang and K. H. Chang, *J. Power Sources*, 2002, **108**, 117.
71 J. Yan, T. Wei, J. Cheng, Z. Fan and M. Zhang, *Mater. Res. Bull.*, 2010, **45**, 210.
72 J. Jiang and A. Kucernak, *Electrochim. Acta*, 2002, **27**, 2381.
73 P. A. Nelson and J. R. Owen, *J. Electrochem. Soc.*, 2003, **150**, 1313.
74 U. M. Patil, R. R. Salunkhe, K. V. Gurav and C. D. Lokhande, *Appl. Surf. Sci.*, 2008, **255**, 2603.
75 S. G. Kandalkar, J. L. Gunjakar and C. D. Lokhande, *Appl. Surf. Sci.*, 2008, **254**, 5540.
76 N. Miura, S. Oonishi and K. Rajendra, *Electrochem. Solid-State Lett.*, 2004, **7**, 247.
77 C. C. Hu, C. M. Huang and K. H. Chang, *J. Power Sources*, 2008, **185**, 1594.
78 D. L. Silva, R. G. Delattore and G. Pattanaik, *J. Electrochem. Soc.*, 2008, **155**, 14.
79 X. Zhou, H. Chen, D. Shu and C. He, *J. Phys. Chem. Solids*, 2009, **70**, 495.
80 M. Nakayama, A. Tanaka and Y. Sato, *Langmuir*, 2005, **21**, 5907.
81 Q. Li, Z. Li, L. Lin, X. Wang, Y. Wang, C. Zhang and H. Wang, *Chem. Eng. J.*, 2010, **156**, 500.
82 M. Endo, T. Maeda, T. Takeda, Y. J. Kim, K. Koshiba, H. Hara and M. S. Dresselhaus, *J. Electrochem. Soc.*, 2001, **148**, A910.
83 D. Qu and H. Shi, *J. Power Sources*, 1998, **74**, 99.
84 E. Raymundo-Pinero, K. Kierzek, J. Machnikowski and F. Beguin, *Carbon*, 2006, **44**, 2498.
85 O. Barbieri, M. Hahn, A. Herzog and R. Kotz, *Carbon*, 2005, **43**, 1303.
86 G. Salitra, A. Soffer, L. Eliad, Y. Cohen and D. Aurbach, *J. Electrochem. Soc.*, 2000, **147**, 2486.
87 K. Kierzek, E. Frackowiak, G. Lota, G. Gryglewicz and J. Machnikowski, *Electrochim. Acta*, 2004, **49**, 515.
88 B. Fang and L. Binder, *J. Power Sources*, 2006, **163**, 616.
89 S. Shiraishi, H. Kurihara, K. Okabe, D. Hulicova and A. Oya, *Electrochem. Commun.*, 2002, **4**, 593.
90 J. N. Barisci, G. G. Wallace and R. H. Baughman, *J. Electrochem. Soc.*, 2000, **147**, 4580.
91 C. Portet, Z. Yang, Y. Korenblit, Y. Gogotsi, R. Mokaya and G. Yushin, *J. Electrochem. Soc.*, 2009, **156**, A1.
92 J. Lee, J. Kim and T. Hyeon, *Adv. Mater.*, 2006, **18**, 2073.
93 T. Morishita, Y. Soneda, T. Tsumura and M. Inagaki, *Carbon*, 2006, **44**, 2360.
94 T. Morishita, T. Tsumura, M. Toyoda, J. Przepiórski, A. W. Morawski, H. Konno and M. Inagaki, *Carbon*, 2010, **48**, 2690.
95 B. Xu, F. Wu, R. Chen, G. Cao, S. Chen, Z. Zhou and Y. Yang, *Electrochem. Commun.*, 2008, **10**, 795.
96 E. Raymundo-Piñero, D. Cazorla-Amoros, A. Linares-Solano, S. Delpeux, E. Frackowiak, K. Szostak and F. Béguin, *Carbon*, 2002, **40**, 1614.
97 D. Lozano-Castello, M. A. Lillo-Rodenas, D. Cazorla-Amoros and A. Linares-Solano, *Carbon*, 2001, **39**, 741.

98 K. H. An, W. S. Kim, Y. S. Park, Y. C. Choi, S. M. Lee, D. C. Chung, D. J. Bae and S. C. Lim, *Adv. Mater.*, 2001, **13**, 497.
99 K. H. An, W. S. Kim, Y. S. Park, J. M. Moon, D. J. Bae, S. C. Lim, Y. S. Lee and Y. H. Lee, *Adv. Funct. Mater.*, 2001, **11**, 387.
100 C. Zhou, S. Kumar, C. D. Doyle and J. M. Tour, *Chem. Mater.*, 2005, **17**, 1997.
101 K. Xia, Q. Gao, J. Jiang and J. Hu, *Carbon*, 2008, **46**, 1718.
102 K. Jurewicz, K. Babel, A. Zioekowski and H. Wachowska, *J. Phys. Chem. Solids*, 2004, **65**, 269.
103 M. J. Bleda-Martinez, J. A. Macia-Agullo, D. Lozano-Castello, E. Morallon, D. Cazorla-Amoros and A. Linares-Solano, *Carbon*, 2005, **43**, 2677.
104 Y. Zhu, S. Murali, M. D. Stoller, K. J. Ganesh, W. Cai, P. J. Ferreira, A. Pirkle, R. M. Wallace, K. A. Cychosz, M. Thommes, D. Su, E. A. Stach and R. S. Ruoff, *Sci. Express*www.sciencexpress.org/10.1126/science.1200770.
105 C. O. Ania, V. Khomenko, E. Raymundo-Pinero, J. B. Parra and F. Beguin, *Adv. Funct. Mater.*, 2007, **17**, 1828.
106 F. Regisser, M. Laveoio, D. Champagne and D. Belanger, *J. Electroanal. Chem.*, 1996, **415**, 47.
107 A. Momma, X. Lin, T. Osaka, Y. Ushio and Y. Sawada, *J. Power Sources*, 1996, **60**, 249.
108 F. Béguin, K. Szostak, G. Lota and E. Frackowiak, *Adv. Mater.*, 2005, **17**, 2380.
109 D. Hulicova, J. Yamashita, Y. Soneda, H. Hatori and M. Kodama, *Chem. Mater.*, 2005, **17**, 1241.
110 D. Hulicova, M. Kodama and H. Hatori, *Chem. Mater.*, 2006, **18**, 2318.
111 G. Lota, B. Grzyb, H. Machnikowska, J. Machnikowski and E. Frackowiak, *Chem. Phys. Lett.*, 2005, **404**, 53.
112 E. Raymundo-Pinero, F. Leroux and F. Béguin, *Adv. Mater.*, 2006, **18**, 1877.
113 E. Frackowiak, G. Lota, J. Machnikowski, K. Kierzek, C. Vix and F. Béguin, *Electrochim. Acta*, 2005, **51**, 2209.
114 K. Leitner, A. Lerf, M. Winter, J. O. Besenhard, S. Villar-Rodil, F. Suarez-Garcia, A. Martinez-Alonso and J. M. D. Tascon, *J. Power Sources*, 2006, **153**, 419.
115 M. Seredych, D. Hulicova-Jurcakova, G. Q. Lu and T. J. Bandosz, *Carbon*, 2008, **46**, 1475.
116 H. Pan, C. K. Poh, Y. P. Feng and J. Lin, *Chem. Mater.*, 2007, **19**, 6120.
117 K. Jurewicz, K. Babel, A. Ziolkowski and H. Wachowska, *Electrochim. Acta*, 2003, **48**, 1491.
118 W. Li, D. Chen, Z. Li, Y. Shi, Y. Wan, J. Huang, J. Yang, D. Zhao and Z. Jiang, *Electrochem. Commun.*, 2007, **9**, 569.
119 S. Shiraishi, M. Kibe, T. Yokoyama, H. Kurihara, N. Patel, A. Oya, Y. Kaburagi and Y. Hishiyama, *Appl. Phys. A*, 2006, **82**, 585.
120 D.-W. Wang, F. Li, Z.-G. Chen, G. Q. Lu and H.-M. Cheng, *Chem. Mater.*, 2008, **20**, 7195.
121 M. Hughes, M. S. P. Shaffer, A. C. Renouf, C. Singh, G. Z. Chen, D. J. Fray and A. H. Windle, *Adv. Mater.*, 2002, **14**, 382.
122 M. Hughes, G. Z. Chen, M. S. P. Shaffer, D. J. Fray and A. H. Windle, *Chem. Mater.*, 2002, **14**, 1610.
123 G. Arabale, D. Wagh, M. Kulkarni, I. S. Mulla, S. P. Vernekar, K. Vijayamohanan and A. M. Rao, *Chem. Phys. Lett.*, 2003, **376**, 207.
124 D. Qu, *J. Power Sources*, 2002, **109**, 403.
125 G. Yu, W. Chen, Y. Zheng, J. Zhao, X. Li and Z. Xu, *Mater. Lett.*, 2006, **60**, 2453.
126 C. Hu, C. Wang and K. Chang, *Electrochim. Acta*, 2007, **52**, 2691.
127 K. R. Prasad, K. Koga and N. Miura, *Chem. Mater.*, 2004, **16**, 1845.
128 M. Kalaji, P. J. Murphy and G. O. Williams, *Synth. Met.*, 1999, **102**, 1360.
129 Y. Zhou, B. He, W. Zhou, J. Huang, X. Li, B. Wu and H. Li, *Electrochim. Acta*, 2004, **49**, 257.
130 V. Gupta and N. Miura, *Mater. Lett.*, 2006, **60**, 1466.
131 L. Fan and J. Maier, *Electrochem. Commun.*, 2006, **8**, 937.
132 F. Fusalba, N. E. Mehdi, L. Breau and D. Belanger, *Chem. Mater.*, 1999, **11**, 2743.
133 K. Naoi, S. Suematsu and A. Manago, *J. Electrochem. Soc.*, 2000, **147**, 420.
134 K. S. Ryu, K. M. Kim, Y. J. Park, N. G. Park, M. G. Kang and S. H. Chang, *Solid State Ionics*, 2002, **152**, 861.
135 S. A. Hashmi and H. M. Upadhyaya, *Solid State Ionics*, 2002, **152**, 883.
136 C. Arbizzani, M. Mastragostino, L. Meneghello and R. Paraventi, *Adv. Mater.*, 1996, **8**, 331.
137 D. Villers, D. Jobin, C. Soucy, D. Cossement, R. Chahine, L. Breau and D. Belanger, *J. Electrochem. Soc.*, 2003, **150**, A747.
138 P. Sivaraman, A. Thakur, R. K. Kushwaha, D. Ratna and A. B. Samui, *Electrochem. Solid-State Lett.*, 2006, **9**, A435.
139 A. Rudge, J. Davey, I. Raistrick, S. Gottesfeld and J. P. Ferraris, *J. Power Sources*, 1994, **47**, 89.
140 K. S. Ryu, K. M. Kim, N.-G. Park, Y. J. Park and S. H. Chang, *J. Power Sources*, 2002, **103**, 305.
141 A. Clémente, S. Panero, E. Spila and B. Scrosati, *Solid State Ionics*, 1996, **85**, 273.
142 A. Laforgue, P. Simon, C. Sarrazin and J.-F. Fauvarque, *J. Power Sources*, 1999, **80**, 142.
143 C. Arbizzani, M. Mastragostino and F. Soavi, *J. Power Sources*, 2001, **100**, 164.
144 M. Mastragostino, R. Paraventi and A. Zanelli, *J. Electrochem. Soc.*, 2000, **147**, 3167.
145 M. Q. Wu, G. A. Snook, V. Gupta, M. Shaffer, D. J. Fray and G. Z. Chen, *J. Mater. Chem.*, 2005, **15**, 2297.
146 K. Lota, V. Khomenko and E. Frackowiak, *J. Phys. Chem. Solids*, 2004, **65**, 295.
147 J. H. Kim, Y. S. Lee, A. K. Sharma and C. Liu, *Electrochim. Acta*, 2006, **52**, 1727.
148 H. Li, J. Wang, Q. Chu, Z. Wang, F. Zhang and S. Wang, *J. Power Sources*, 2009, **190**, 578.
149 W. Li, J. Chen, J. Zhao, R. Zhang and J. Zhu, *Mater. Lett.*, 2005, **59**, 800.
150 M. E. Roberts, D. R. Wheeler, B. B. McKenzie and B. C. Bunker, *J. Mater. Chem.*, 2009, **19**, 6977.
151 R. K. Sharma, A. C. Rastogi and S. B. Desu, *Electrochim. Acta*, 2008, **53**, 7690.
152 L. Li, C. Loveday, D. S. K. Mudigonda and J. P. Ferraris, *J. Electrochem. Soc.*, 2002, **149**, A1201.
153 E. Naudin, N. Mehdi, C. Soucy, L. Breau and D. Bélanger, *Chem. Mater.*, 2001, **13**, 634.
154 C. P. Fonseca, J. E. Benedetti and S. Neves, *J. Power Sources*, 2006, **158**, 789.
155 Z. Zhu, G. Wang, M. Sun, X. Li and C. Li, *Electrochim. Acta*, 2011, **56**, 1366.
156 Y. G. Wang, H. Q. Li and Y. Y. Xia, *Adv. Mater.*, 2006, **18**, 2619.
157 A. Laforgue, P. Simon, J. F. Fauvarque, M. Mastragostino, F. Soavi, J. F. Sarrau, P. Lailler, M. Conte, E. Rossi and S. Saguatti, *J. Electrochem. Soc.*, 2003, **150**, A645.
158 A. Laforgue, P. Simon, J. F. Fauvarque, J. F. Sarrau and P. Lallier, *J. Electrochem. Soc.*, 2001, **148**, A1130.
159 A. D. Pasquier, A. Laforgue, P. Simon, G. C. Amatucci and J. F. Fauvarque, *J. Electrochem. Soc.*, 2002, **149**, A302.
160 A. Di Fabio, A. Giorgi, M. Mastragostino and F. Soavi, *J. Electrochem. Soc.*, 2001, **148**, A845.
161 K. Jurewicz, S. Delpeux, V. Bertagna, F. Béguin and E. Frackowiak, *Chem. Phys. Lett.*, 2001, **347**, 36.
162 Q. Xiao and X. Zhou, *Electrochim. Acta*, 2003, **48**, 575.
163 V. Khomenko, E. Frackowiak and F. Beguin, *Electrochim. Acta*, 2005, **50**, 2499.
164 H. Zhang, G. Cao, Z. Wang, Y. Yang, Z. Shi and Z. Gu, *Electrochem. Commun.*, 2008, **10**, 1056.
165 E. Frackowiak, V. Khomenko, K. Jurewicz, K. Lota and F. Béguin, *J. Power Sources*, 2006, **153**, 413.
166 H. Zhang, G. Cao and Y. Yang, *J. Power Sources*, 2007, **172**, 476.
167 D. R. Rolison, *Science*, 2003, **299**, 1698.
168 J. Wang, Y. L. Xu, X. Chen and X. F. Du, *J. Power Sources*, 2007, **163**, 1120.
169 Q. Xiao and X. Zhou, *Electrochim. Acta*, 2003, **48**, 57.
170 H. An, Y. Wang, X. Wang, L. Zheng, X. Wang, L. Yi, L. Bai and X. Zhang, *J. Power Sources*, 2010, **195**, 6964.
171 S. Biswas and L. T. Drzal, *Chem. Mater.*, 2010, **22**, 5667.
172 Y. Fang, J. Liu, D. J. Yu, J. P. Wicksted, K. Kalkan, C. O. Topal, B. N. Flanders, J. Wu and J. Li, *J. Power Sources*, 2010, **195**, 674.
173 C. Yang and P. Liu, *Synth. Met.*, 2010, **160**, 768.
174 J. F. Zang, S. J. Bao, C. M. Li, H. J. Bian, X. Q. Cui, Q. L. Bao, C. Q. Sun, J. Guo and K. R. Lian, *J. Phys. Chem. C*, 2008, **112**, 14843.

175 S. H. Mujawar, S. B. Ambade, T. Battumur, R. B. Ambade and S. H. Lee, *Electrochim. Acta*, 2011, **56**, 4462.
176 K. Zhang, L. L. Zhang, X. S. Zhao and J. Wu, *Chem. Mater.*, 2010, **22**, 1392.
177 Q. Liu, M. H. Nayfeh and S. T. Yau, *J. Power Sources*, 2010, **195**, 3956.
178 D. D. Zhao, S. J. Bao, W. J. Zhou and H. L. Li, *Electrochem. Commun.*, 2007, **9**, 869.
179 I. H. Kim and K. B. Kim, *J. Electrochem. Soc.*, 2006, **153**, A383.
180 Q. X. Jia, S. G. Song, X. D. Wu, J. H. Cho, S. R. Foltyn, A. T. Findikoglu and J. L. Smith, *Appl. Phys. Lett.*, 1996, **68**, 1069.
181 K. Sakiyama, S. Onishi, K. Ishihara, K. Orita, T. Kajiyama, N. Hosoda and T. Hara, *J. Electrochem. Soc.*, 1993, **140**, 834.
182 J. P. Zheng, P. J. Cygan and T. R. Jow, *J. Electrochem. Soc.*, 1995, **142**, 2699.
183 N. Wu, S. Kuo and M. Lee, *J. Power Sources*, 2002, **104**, 62.
184 S. Trasatti, *Electrochim. Acta*, 1991, **36**, 225.
185 C. Hu, C. Lee and T. Wen, *J. Appl. Electrochem.*, 1996, **26**, 72.
186 M. Ramani, B. S. Haran, R. E. White and B. N. Popov, *J. Electrochem. Soc.*, 2001, **148**, A374.
187 S. Ferro and A. De Battisti, *J. Phys. Chem. B*, 2002, **106**, 2249.
188 T. Wen and C. Hu, *J. Electrochem. Soc.*, 1992, **139**, 2158.
189 Y. Su, F. Wu, L. Bao and Z. Yang, *New Carbon Mater.*, 2007, **22**, 53.
190 M. Seo, A. Saouab and S. Park, *Mater. Sci. Eng., B*, 2010, **167**, 65.
191 Y. Zheng, H. Ding and M. Zhang, *Thin Solid Films*, 2008, **516**, 7381.
192 Y. Kim, K. Tadai and T. Mitani, *J. Mater. Chem.*, 2005, **15**, 4914.
193 J. K. Lee, H. M. Pathan, K. D. Jung and O. S. Joo, *J. Power Sources*, 2006, **159**, 1527.
194 S. Sarangapani, J. Forchione, A. Griffith and A. LaConti, Proceedings of The Second International Seminar on Double Layer Capacitors and Similar Energy Storage Devices, Beerfield Beach, FL, Dec. 9–11, 1991.
195 C.-C. Hu, K.-H. Chang, M.-C. Lin and Y.-T. Wu, *Nano Lett.*, 2006, **6**, 2690.
196 R. Fu, Z. Ma and J. Zheng, *J. Phys. Chem. B*, 2002, **106**, 3592.
197 K. E. Swider, C. I. Merzbacher, P. L. Hagans and D. R. Rolison, *Chem. Mater.*, 1997, **9**, 1248.
198 T. C. Liu, W. G. Pell and B. E. Conway, *Electrochim. Acta*, 1997, **42**, 3541.
199 L. A. Doubova, A. De Battisti, S. Daolio, C. Pagura, S. Barison, R. Gerbasi, G. Bat-tiston, P. Guerriero and S. Trasatti, *Russ. J. Electrochem.*, 2004, **40**, 1115.
200 W. Sugimoto, K. Yokoshima, Y. Murakami and Y. Takasu, *Electrochim. Acta*, 2006, **52**, 1742.
201 J. W. Long, K. E. Swider, C. I. Merzbacher and D. R. Rolison, *Langmuir*, 1999, **15**, 780.
202 W. Sugimoto, H. Iwata, K. Yokoshima, Y. Murakami and Y. Takasu, *J. Phys. Chem. B*, 2005, **109**, 7330.
203 J. Wen, X. Ruan and Z. Zhou, *J. Phys. Chem. Solids*, 2009, **70**, 816.
204 A. Foelske, O. Barbieri, M. Hahn and R. Kötz, *Electrochem. Solid-State Lett.*, 2006, **9**, A268.
205 J. P. Zheng and Y. Xin, *J. Power Sources*, 2002, **110**, 1050.
206 F. Pico, E. Morales, J. A. Fernandez, T. A. Centeno, J. Ibañez, R. M. Rojas, J. M. Amarilla and J. M. Rojo, *Electrochim. Acta*, 2009, **54**, 2239.
207 H. Kim and B. N. Popov, *J. Power Sources*, 2002, **104**, 52.
208 Y. Liu, W. Zhao and X. Zhang, *Electrochim. Acta*, 2008, **53**, 3296.
209 Z. Sun, Z. Liu, B. Han, S. Miao, J. Du and Z. Miao, *Carbon*, 2006, **44**, 888.
210 W. Sugimoto, H. Iwata, Y. Yasunaga, Y. Murakami and Y. Takasu, *Angew. Chem., Int. Ed.*, 2003, **42**, 4092.
211 V. Subramanian, S. C. Hall, P. H. Smith and B. Rambabu, *Solid State Ionics*, 2004, **175**, 511.
212 M. Egashira, Y. Matsuno, N. Yoshimoto and M. Morita, *J. Power Sources*, 2010, **195**, 3036.
213 M. Ramani, B. S. Haran, R. E. White, B. N. Popov and L. Arsov, *J. Power Sources*, 2001, **93**, 209.
214 G. Cui, X. Zhou, L. Zhi, T. Arne and M. Klaus, *New Carbon Mater.*, 2007, **22**, 302.
215 Y. Lin, K. Lee, K. Chen and Y. Huang, *Appl. Surf. Sci.*, 2009, **256**, 1042.
216 J. P. Zheng and T. R. Jow, *J. Power Sources*, 1996, **62**, 155.
217 T. R. Jow and J. P. Zheng, *J. Electrochem. Soc.*, 1998, **145**, 49.
218 J. P. Zheng, *Electrochem. Solid-State Lett.*, 1999, **2**, 359.
219 Q. L. Fang, D. A. Evans, S. L. Roberson and J. P. Zheng, *J. Electrochem. Soc.*, 2001, **148**, A833.
220 Y. U. Jeong and A. Manthiram, *Electrochem. Solid-State Lett.*, 2000, **3**, 205.
221 Y. U. Jeong and A. Manthiram, *J. Electrochem. Soc.*, 2001, **148**, A189.
222 C. C. Hu and Y. H. Huang, *Electrochim. Acta*, 2001, **46**, 3431.
223 Y. Takasu, T. Nakamura, H. Ohkawauchi and Y. Murakami, *J. Electrochem. Soc.*, 1997, **144**, 2601.
224 Y. Takasu, T. Ohnuma, S. Mizutani, W. Sugimoto and Y. Murakami, *Electrochemistry*, 2001, **69**, 493.
225 S. L. Kuo and N. L. Wu, *Electrochem. Solid-State Lett.*, 2003, **6**, A85.
226 Y. Wang and X. Zhang, *Electrochim. Acta*, 2004, **49**, 1957.
227 W. Sugimoto, T. Shibutani, Y. Murakami and Y. Takasu, *Electrochem. Solid-State Lett.*, 2002, **5**, A170.
228 Y. Takasu and Y. Murakami, *Electrochim. Acta*, 2000, **45**, 4135.
229 J. M. Miller, B. Dunn, T. D. Tran and R. W. Pekala, *J. Electrochem. Soc.*, 1997, **144**, L309.
230 C. Hu and C. Wang, *Electrochem. Commun.*, 2002, **4**, 554.
231 V. Panic, T. Vidakovic, S. Gojkovic, A. Dekanski, S. Milonjic and B. Nikolic, *Electrochim. Acta*, 2003, **48**, 3805.
232 J. H. Jang, S. H. Han, T. Hyeon and S. M. Oh, *J. Power Sources*, 2003, **123**, 79.
233 X. Qin, S. Durbach and G. T. Wu, *Carbon*, 2004, **42**, 451.
234 G. H. Deng, X. Xiao, J. H. Chen, X. B. Zeng, D. L. He and Y. F. Kuang, *Carbon*, 2005, **43**, 1557.
235 B. Gao, X. Zhang, C. Yuan, J. Li and L. Yu, *Electrochim. Acta*, 2006, **52**, 1028.
236 C. C. Hu, K. H. Chang and C. C. Wang, *Electrochim. Acta*, 2007, **52**, 4411.
237 C. C. Hu, W. C. Chen and K. H. Chang, *J. Electrochem. Soc.*, 2004, **151**, A281.
238 I. H. Kim and K. B. Kim, *Electrochem. Solid-State Lett.*, 2001, **4**, A62.
239 W. Dmowski, T. Egami, K. E. Swider-Lyons, C. T. Love and D. R. Rolison, *J. Phys. Chem. B*, 2002, **106**, 12677.
240 D. A. McKeown, P. L. Hagans, L. P. L. Carette, A. E. Russell, K. E. Swider and D. R. Rolison, *J. Phys. Chem. B*, 1999, **103**, 4825.
241 B. C. Kim, G. G. Wallace, Y. I. Yoon, J. M. Ko and C. O. Too, *Synth. Met.*, 2009, **159**, 1389.
242 M. T. Brumbach, T. M. Alam, R. H. Nilson, P. G. Kotula, B. B. McKenzie, R. G. Tissot and B. C. Bunker, *Mater. Chem. Phys.*, 2010, **124**, 359..
243 K. Yokoshima, T. Shibutani, M. Hirota, W. Sugimoto, Y. Murakami and Y. Takasu, *J. Power Sources*, 2006, **160**, 1480.
244 C. C. Wang and C. C. Hu, *J. Electrochem. Soc.*, 2005, **152**, A370.
245 M. Ito, Y. Murakami, H. Kaji, K. Yahikozawa and Y. Takasu, *J. Electrochem. Soc.*, 1996, **143**, 32.
246 C. C. Hu and W. C. Chen, *Electrochim. Acta*, 2004, **49**, 3469.
247 C. Lin, J. A. Ritter and B. N. Popov, *J. Electrochem. Soc.*, 1999, **146**, 3155.
248 Y. Sato, K. Yomogida, T. Nanaumi, K. Kobayakawa, Y. Ohsawa and M. Kawai, *Electrochem. Solid-State Lett.*, 2000, **3**, 113.
249 J. Zhang, D. Jiang, B. Chen, J. Zhu, L. Jiang and H. Fang, *J. Electrochem. Soc.*, 2001, **148**, A1362.
250 M. S. Dandekar, G. Arabale and K. Vijayamohanan, *J. Power Sources*, 2005, **141**, 198.
251 Y. Zhao, L. Liu, J. Xu, J. Yang, M. Yan and Z. Jiang, *J. Solid State Electrochem.*, 2007, **11**, 283.
252 Y. Takasu, C. Matsuo, T. Ohnuma, M. Ueno and Y. Murakami, *Chem. Lett.*, 1998, 1235.
253 H. Li, R. Wang and R. Cao, *Microporous Mesoporous Mater.*, 2008, **111**, 32.
254 T. Nanaumi, Y. Ohsawa, K. Kobayakawa and Y. Sato, *Electrochemistry*, 2002, **70**, 681.
255 W. C. Chen, C. C. Hu, C. C. Wang and C. K. Min, *J. Power Sources*, 2004, **125**, 292.
256 M. Min, K. Machida, J. H. Jang and K. Naoi, *J. Electrochem. Soc.*, 2006, **153**, A334.

257 A. L. M. Reddy and S. Ramaprabhu, *J. Phys. Chem. C*, 2007, **111**, 7727.
258 W. Sugimoto, T. Kizaki, K. Yokoshima, Y. Murakami and Y. Takasu, *Electrochim. Acta*, 2004, **49**, 313.
259 I. H. Kim, J. H. Kim, Y. H. Lee and K. B. Kim, *J. Electrochem. Soc.*, 2005, **152**, A2170.
260 J. H. Park, J. M. Ko and O. O. Park, *J. Electrochem. Soc.*, 2003, **150**, A864.
261 B. J. Lee, S. R. Sivakkumar, J. M. Ko, J. H. Kim, S. M. Jo and D. Y. Kim, *J. Power Sources*, 2007, **168**, 546.
262 F. Pico, J. Ibañez, M. A. Lillo-Rodenas, A. Linares-Solano, R. M. Rojas, J. M. Amarilla and J. M. Rojo, *J. Power Sources*, 2008, **176**, 417.
263 V. Barranco, F. Pico, J. Ibañez, M. A. Lillo-Rodenas, A. Linares-Solano, M. Kimura, A. Oya, R. M. Rojas, J. M. Amarilla and J. M. Rojo, *Electrochim. Acta*, 2009, **54**, 7452.
264 L. M. Huang, H. Z. Lin, T. C. Wen and A. Gopalan, *Electrochim. Acta*, 2006, **52**, 1058.
265 R. Liu, J. Duay, T. Lane and S. B. Lee, *Phys. Chem. Chem. Phys.*, 2010, **12**, 4309.
266 K. Machida, K. Furuchi, M. Min and K. Naoi, *Electrochemistry*, 2004, **72**, 402.
267 Y. S. Hu, L.-Z. Fan, J. Maier, P. Adelhelm, B. Smarsly and M. Antonietti, *Adv. Funct. Mater.*, 2007, **17**, 3083.
268 S. Devaraj and N. Munichandraiah, *Electrochem. Solid-State Lett.*, 2005, **8**, A373.
269 S. C. Pang, M. A. Anderson and T. W. Chapman, *J. Electrochem. Soc.*, 2000, **147**, 444.
270 M. Toupin, T. Brousse and D. Bélanger, *Chem. Mater.*, 2004, **16**, 3184.
271 J. K. Chang, M. T. Lee and W. T. Tsai, *J. Power Sources*, 2007, **166**, 590.
272 M. Toupin, T. Brousse and D. Bélanger, *Chem. Mater.*, 2002, **14**, 3946.
273 H. Lee and J. Goodenough, *J. Solid State Chem.*, 1999, **144**, 220.
274 S. E. Chun, S. I. Pyun and G. J. Lee, *Electrochim. Acta*, 2006, **51**, 6479.
275 L. Li, Z. Y. Qin, L. F. Wang, H. J. Liu and M. F. Zhu, *J. Nanopart. Res.*, 2010, **12**, 2349.
276 J. K. Chang, Y. L. Chen and W. T. Tsai, *J. Power Sources*, 2004, **135**, 344.
277 V. Subramanian, H. Zhu and B. Wei, *Chem. Phys. Lett.*, 2008, **453**, 242.
278 C. C. Hu and T. W. Tsou, *Electrochem. Commun.*, 2002, **4**, 105.
279 B. Messaoudi, S. Joiret, M. Keddam and H. Takenouti, *Electrochim. Acta*, 2001, **46**, 2487.
280 S. C. Pang and M. A. Anderson, *J. Mater. Res.*, 2000, **15**, 2096.
281 E. Raymundo-Pinero, V. Khomenko, E. Frackowiak and F. Beguin, *J. Electrochem. Soc.*, 2005, **152**, A229.
282 C. Ye, Z. M. Lin and S. Z. Hui, *J. Electrochem. Soc.*, 2005, **152**, A1272.
283 E. Machefaux, T. Brousse, D. Bélanger and D. Guyomard, *J. Power Sources*, 2007, **165**, 651.
284 M. Nakayama, T. Kanaya and R. Inoue, *Electrochem. Commun.*, 2007, **9**, 1154.
285 M. W. Xua, W. Jia, S. J. Bao, Z. Su and B. Dong, *Electrochim. Acta*, 2010, **55**, 5117.
286 H. Kim and B. N. Popov, *J. Electrochem. Soc.*, 2003, **150**, D56.
287 M. T. Lee, J. K. Chang and W. T. Tsai, *J. Electrochem. Soc.*, 2007, **154**, A875.
288 J. K. Chang, C. H. Huang, M. T. Lee, W. T. Tsai, M. J. Deng and I. W. Sun, *Electrochim. Acta*, 2009, **54**, 3278.
289 J. Wei, N. Nagarajan and I. Zhitomirsky, *J. Mater. Process. Technol.*, 2007, **186**, 356.
290 C. K. Lin, K. H. Chuang, C. Y. Lin, C. Y. Tsay and C. Y. Chen, *Surf. Coat. Technol.*, 2007, **202**, 1272.
291 S. W. Donne, A. F. Hollenkamp and B. C. Jones, *J. Power Sources*, 2010, **195**, 367.
292 V. Subramanian, H. W. Zhu and B. Q. Wei, *J. Power Sources*, 2006, **159**, 361.
293 H. G. Wang, Z. G. Lu, D. Qian, Y. J. Li and W. Zhang, *Nanotechnology*, 2007, **18**, 115616.
294 S. L. Chou, F. Y. Cheng and J. Chen, *J. Power Sources*, 2006, **162**, 727.
295 T. Brousse, M. Toupin, R. Dugas, L. Athouel, O. Crosnier and D. Belanger, *J. Electrochem. Soc.*, 2006, **153**, A2171.
296 R. H. Ma, Y. Bando, L. Q. Zhang and T. Sasaki, *Adv. Mater.*, 2004, **16**, 918.
297 L. Athouel, F. Moser, R. Dugas, O. Crosnier, D. Belanger and T. Brousse, *J. Phys. Chem. C*, 2008, **112**, 7270.
298 S. Devaraj and N. Munichandraiah, *J. Phys. Chem. C*, 2008, **112**, 4406.
299 A. Zolfaghari, F. Ataherian, M. Ghaemi and A. Gholami, *Electrochim. Acta*, 2007, **52**, 2806.
300 M. Ghaemi, F. Ataherian, A. Zolfaghari and S. M. Jafari, *Electrochim. Acta*, 2008, **53**, 4607.
301 E. Beaudrouet, A. LeGalLaSalle and D. Guyomard, *Electrochim. Acta*, 2009, **54**, 1240.
302 L. I. Hill, A. Verbaere and D. Guyomard, *J. Electrochem. Soc.*, 2003, **150**, D135–D148.
303 M. S. Wu, P. C. J. Chiang, J. T. Lee and J. C. Lin, *J. Phys. Chem. B*, 2005, **109**, 23279.
304 L. Zhang, Z. H. Liu, H. Lv, X. Tang and K. Ooi, *J. Phys. Chem. C*, 2007, **111**, 8418.
305 R. K. Sharma, H. S. Oh, Y. G. Shul and H. Kim, *J. Power Sources*, 2007, **173**, 1024.
306 Z. P. Liu, R. Z. Ma, Y. Ebina, K. Takada and T. Sasaki, *Chem. Mater.*, 2007, **19**, 6504.
307 L. C. Zhang, L. P. Kang, H. Lv, Z. K. Su, K. Ooi and Z. H. Liu, *J. Mater. Res.*, 2008, **23**, 780.
308 J. C. Ge, L. H. Zhuo, F. Yang, B. Tang, L. Z. Wu and C. Tung, *J. Phys. Chem. B*, 2006, **110**, 17854.
309 R. Jiang, T. Huang, J. Liu, J. Zhuang and A. Yu, *Electrochim. Acta*, 2009, **54**, 3047.
310 Y. Yang and C. Huang, *J. Solid State Electrochem.*, 2010, **14**, 1293.
311 V. Subramanian, H. Zhu, R. Vajtai, P. M. Ajayan and B. Wei, *J. Phys. Chem. B*, 2005, **109**, 20207.
312 S. Devaraj and N. Munichandraiah, *J. Electrochem. Soc.*, 2007, **154**, A80.
313 M. Lai and D. J. Riley, *J. Colloid Interface Sci.*, 2008, **323**, 203.
314 R. Liu and S. B. Lee, *J. Am. Chem. Soc.*, 2008, **130**, 2942.
315 M. S. Wu, *Appl. Phys. Lett.*, 2005, **87**, 153102.
316 F. Cheng, J. Zhao, W. Song, C. Li, H. Ma, J. Chen and P. Shen, *Inorg. Chem.*, 2006, **45**, 2038.
317 J. H. Kim, T. Ayalasomayajula, V. Gona and D. Choi, *J. Power Sources*, 2008, **183**, 366.
318 J. Yuan, Z. H. Liu, S. Qiao, X. Ma and N. Xu, *J. Power Sources*, 2009, **189**, 1278.
319 N. Nagarajan, M. Cheong and I. Zhitomirsky, *Mater. Chem. Phys.*, 2007, **103**, 47.
320 Y. K. Zhou, M. Toupin, D. Bélanger, T. Brousse and F. Favier, *J. Phys. Chem. Solids*, 2006, **67**, 1351.
321 J. N. Broughton and M. J. Brett, *Electrochim. Acta*, 2005, **50**, 4814.
322 K. R. Prasad and N. Miura, *J. Power Sources*, 2004, **135**, 354.
323 N. Nagarajan, H. Humadi and I. Zhitomirsky, *Electrochim. Acta*, 2006, **51**, 3039.
324 J. K. Chang and C. H. Huang, *Electrochim. Acta*, 2008, **53**, 4447.
325 F. J. Liu, *J. Power Sources*, 2008, **182**, 383.
326 K. W. Nam and C. W. Lee, *J. Power Sources*, 2009, **188**, 323.
327 S. F. Chin, S. C. Pang and M. A. Anderson, *J. Electrochem. Soc.*, 2002, **149**, A379.
328 T. Shinomiya, V. Gupta and N. Miura, *Electrochim. Acta*, 2006, **51**, 4412.
329 J. N. Broughton and M. J. Brett, *Electrochim. Acta*, 2004, **49**, 4439.
330 Y. Dai, K. Wang, J. Zhao and J. Xie, *J. Power Sources*, 2006, **161**, 737.
331 S. Devaraj and N. Munichandraiah, *J. Electrochem. Soc.*, 2007, **154**, A901.
332 X. H. Yang, Y. G. Wang, H. M. Xiong and Y. Y. Xia, *Electrochim. Acta*, 2007, **53**, 752.
333 K. R. Prasad and N. Miura, *Electrochem. Commun.*, 2004, **6**, 1004.
334 A. Taguchi, S. Inoue, S. Akamaru, M. Hara, K. Watanabe and T. Abe, *J. Alloys Compd.*, 2006, **414**, 137.
335 J. Li, X. Wang, Q. Huang, S. Gamboa and P. J. Sebastian, *J. Power Sources*, 2006, **160**, 1501.
336 X. Y. Chen, X. Li and Y. Jiang, *Solid State Commun.*, 2005, **136**, 94.

337 C. Tsang, J. Kim and A. Manthiram, *J. Solid State Chem.*, 1998, **137**, 28.
338 J. K. Chang and W. T. Tsai, *J. Electrochem. Soc.*, 2003, **150**, A1333.
339 X. Wang and Y. Li, *Chem. Commun.*, 2002, 764.
340 Y. C. Hsieh, K. T. Lee, Y. P. Lin, N. L. Wu and S. W. Donne, *J. Power Sources*, 2008, **177**, 660.
341 Q. Li, K. Li, J. Gu and H. Fan, *J. Phys. Chem. Solids*, 2008, **69**, 1733.
342 W. Xu and C. A. Angell, *Electrochem. Solid-State Lett.*, 2001, **4**, E1.
343 K. Xu, S. Zhang, B. A. Poese and T. R. Jow, *Electrochem. Solid-State Lett.*, 2002, **5**, A259.
344 S. Komaba, A. Ogata and T. Tsuchikawa, *Electrochem. Commun.*, 2008, **10**, 1435.
345 J. K. Chang, M. T. Lee, C. H. Huang and W. T. Tsai, *Mater. Chem. Phys.*, 2008, **108**, 124.
346 P. Y. Chuang and C. C. Hu, *Mater. Chem. Phys.*, 2005, **92**, 138.
347 H. Zheng, F. Tang and M. Lim, *J. Power Sources*, 2010, **195**, 680.
348 E. H. Liu, W. Li, J. Li, X. Y. Meng, R. Ding and S. T. Tan, *Mater. Res. Bull.*, 2009, **44**, 1122.
349 X. Tang, Z. Liu, C. Zhang, Z. Yang and Z. Wang, *J. Power Sources*, 2009, **193**, 939.
350 S. L. Kuo and N. L. Wu, *J. Power Sources*, 2006, **162**, 1437.
351 X. Liu, S. Fu and C. Huang, *Powder Technol.*, 2005, **154**, 120.
352 H. Zhang, G. Cao, Z. Wang, Y. Yang, Z. Shi and Z. Gu, *Nano Lett.*, 2008, **8**, 2664.
353 S. B. Ma, K. Y. Ahn, E. S. Lee, K. H. Oh and K. B. Kim, *Carbon*, 2007, **45**, 375.
354 V. Subramanian, H. Zhu and B. Wei, *Electrochem. Commun.*, 2006, **8**, 827.
355 C. Y. Lee, H. M. Tsai, H. J. Chuang, S. Y. Li, P. Lin and T. Y. Tseng, *J. Electrochem. Soc.*, 2005, **152**, A716.
356 L. J. Sun, X. X. Liu, K. K. T. Lau, L. Chen and W. M. Gu, *Electrochim. Acta*, 2008, **53**, 3036.
357 X. Zhang, L. Ji, S. Zhang and W. Yang, *J. Power Sources*, 2007, **173**, 1017.
358 S. R. Sivakkumar, J. M. Ko, D. Y. Kim, B. C. Kim and G. G. Wallace, *Electrochim. Acta*, 2007, **52**, 7377.
359 T. Brousse, M. Toupin and D. Bélanger, *J. Electrochem. Soc.*, 2004, **151**, A614.
360 K. R. Prasad and N. Munichandraiah, *J. Electrochem. Soc.*, 2002, **149**, A1393.
361 J. K. Chang, C. T. Lin and W. T. Tsai, *Electrochem. Commun.*, 2004, **6**, 666.
362 L. L. Zhang, T. Wei, W. Wang and X. S. Zhao, *Microporous Mesoporous Mater.*, 2009, **123**, 260.
363 H. Y. Lee, S. W. Kim and H. Y. Lee, *Electrochem. Solid-State Lett.*, 2001, **4**, A19.
364 C. L. Xu, S. J. Bao, L. B. Kong, H. Li and H. L. Li, *J. Solid State Chem.*, 2006, **179**, 1351.
365 J. K. Chang, S. H. Hsu, W. T. Tsai and I. W. Sun, *J. Power Sources*, 2008, **177**, 676.
366 H. S. Nama, J. K. Yoon, J. M. Ko and J. D. Kim, *Mater. Chem. Phys.*, 2010, **123**, 331.
367 H. Xia, J. K. Feng, H. L. Wang, M. Lai and L. Lu, *J. Power Sources*, 2010, **195**, 4410.
368 D. P. Dubal, D. S. Dhawale, R. R. Salunkhe and C. D. Lokhande, *J. Alloys Compd.*, 2010, **496**, 370.
369 W. Xiao, H. Xia, J. Fuh and L. Lu, *J. Power Sources*, 2009, **193**, 935.
370 Z. Jiang, J. Han and X. Liu, *Adv. Mater. Res.*, 2010, **152–153**, 1551.
371 Y. Li, H. Xie, J. Wang and L. Chen, *Mater. Lett.*, 2011, **65**, 403.
372 P. Ragupathy, D. H. Park, G. Campet, H. N. Vasan, S. J. Hwang, J. H. Choy and N. Munichandraiah, *J. Phys. Chem. C*, 2009, **113**, 6303.
373 N. Tang, X. K. Tian, C. Yang and Z. B. Pi, *Mater. Res. Bull.*, 2009, **44**, 2062.
374 H. Adelkhani1, M. Ghaemi and M. Ruzbehani, *Int. J. Electrochem. Sci.*, 2011, **6**, 123.
375 X. Y. Wang, X. Y. Wang, W. G. Huang, P. J. Sebastian and S. Gamboa, *J. Power Sources*, 2005, **140**, 211.
376 H. Q. Wang, Z. S. Li, J. H. Yang, Q. Y. Li and X. X. Zhong, *J. Power Sources*, 2009, **194**, 1218.
377 H. Q. Wang, G. F. Yang, Q. Y. Li, X. X. Zhong, F. P. Wang, Z. S. Li and Y. h. Li, *New J. Chem.*, 2011, **35**, 469.
378 S. W. Lee, J. Kim, S. Chen, P. T. Hammond and Y. S. Horn, *ACS Nano*, 2010, **4**, 3889.
379 Y. Hou, Y. W. Cheng, T. Hobson and J. Liu, *Nano Lett.*, 2010, **10**, 2727.
380 T. Bordjiba and D. Belanger, *J. Electrochem. Soc.*, 2009, **156**, A378.
381 S. Chen, J. W. Zhu, X. D. Wu, Q. F. Han and X. Wang, *ACS Nano*, 2010, **4**, 2822.
382 C. Liu, F. Li, L. P. Ma and H. M. Cheng, *Adv. Mater.*, 2010, **22**, E1.
383 Y. Wang, C. Y. Foo, T. K. Hoo, M. Ng and J. Lin, *Chem.–Eur. J.*, 2010, **16**, 3598.
384 J. M. Ko and K. M. Kim, *Mater. Chem. Phys.*, 2009, **114**, 837.
385 J. Yan, Z. Fan, T. Wei, J. Cheng, B. Shao, K. Wang, L. Song and M. Zhang, *J. Power Sources*, 2009, **194**, 1202.
386 A. Malak-Polaczyk, C. Matei-Ghimbeu, C. Vix-Guterl and E. Frackowiak, *J. Solid State Chem.*, 2010, **183**, 969.
387 L. Bao, J. Zang and X. Li, *Nano Lett.*, 2011, **11**, 1215.
388 J. Yan, Z. Fan, T. Wei, W. Qian, M. Zhang and F. Wei, *Carbon*, 2010, **48**, 3825.
389 J. Liu, J. Essner and J. Li, *Chem. Mater.*, 2010, **22**, 5022.
390 W. D. Zhang and J. Chen, *Pure Appl. Chem.*, 2009, **81**, 2317.
391 R. Amade, E. Jover, B. Caglar, T. Mutlu and E. Bertran, *J. Power Sources*, 2011, **196**, 5779.
392 P. C. Gao, A. H. Lu and W. C. Li, *J. Power Sources*, 2011, **196**, 4095.
393 L. Demarconnay, E. Raymundo-Piñero and F. Béguin, *J. Power Sources*, 2011, **196**, 580.
394 P. J. Kulesza, S. Zamponi, M. A. Malik, M. Berrettoni, A. Wolkiewicz and R. Marassi, *Electrochim. Acta*, 1998, **43**, 919.
395 Z. Xun, C. Cai, W. Xing and T. H. Lu, *J. Electroanal. Chem.*, 2003, **545**, 19.
396 V. Srinivasan and J. W. Weidner, *J. Power Sources*, 2002, **108**, 15.
397 H. Kim, T. Seong, J. Lim and W. Cho, *J. Power Sources*, 2001, **102**, 167.
398 T. C. Liu, W. G. Pell and B. E. Conway, *Electrochim. Acta*, 1999, **44**, 2829.
399 Y. Shan and L. Gao, *Mater. Chem. Phys.*, 2007, **103**, 206.
400 T. Y. Wei, C. H. Chen, K. H. Chang, S. Y. Lu and C. C. Hu, *Chem. Mater.*, 2009, **21**, 3228.
401 F. F. Tao, C. L. Gao, Z. H. Wen, Q. Wang, J. H. Li and Z. Xu, *J. Solid State Chem.*, 2009, **182**, 1055.
402 L. Wang, X. Liu, X. Wang, X. Yang and L. Lu, *Curr. Appl. Phys.*, 2010, **10**, 1422.
403 V. R. Shinde, S. B. Mahadik, T. P. Gujar and C. D. Lokhande, *Appl. Surf. Sci.*, 2006, **252**, 7487.
404 C. Lin, J. A. Ritter and B. N. Popov, *J. Electrochem. Soc.*, 1998, **145**, 4097.
405 F. Zhang, L. Hao, Q. B. Fu and X. G. Zhang, *Chin. J. Inorg. Chem.*, 2010, **26**, 827.
406 Y. Y. Gao, S. L. Chen, D. X. Cao, G. L. Wang and J. L. Yin, *J. Power Sources*, 2010, **195**, 1757.
407 G. Wang, X. Shen, J. Horvat, B. Wang, H. Liu, D. Wexler and J. Yao, *J. Phys. Chem. C*, 2009, **113**, 4357.
408 J. Xu, L. Gao, J. Cao, W. Wang and Z. Chen, *Electrochim. Acta*, 2010, **56**, 732.
409 S. G. Kandalkar, H. Lee, H. Chae and C. Kim, *Mater. Res. Bull.*, 2011, **46**, 48.
410 M. Zheng, J. Cao, S. Liao, J. Liu, H. Chen, Y. Zhao, W. Dai, G. Ji, J. Cao and J. Tao, *J. Phys. Chem. C*, 2009, **113**, 3887.
411 V. Gupta, T. Kusahara, H. Toyama, S. Gupta and N. Miura, *Electrochem. Commun.*, 2007, **9**, 2315.
412 R. S. Jayashree and P. V. Kamath, *J. Mater. Chem.*, 1999, **9**, 961.
413 V. Gupta, S. Gupta and N. Miura, *J. Power Sources*, 2008, **177**, 685.
414 L. Cao, F. Xu, Y. Y. Liang and H. L. Li, *Adv. Mater.*, 2004, **16**, 1853.
415 D. A. Wruck and M. Rubin, *J. Electrochem. Soc.*, 1993, **140**, 1097.
416 F. Fusalba, P. Gouérec, D. Villers and D. Bélanger, *J. Electrochem. Soc.*, 2001, **148**, A1.
417 P. K. Rajendra and N. Munichandraiah, *J. Power Sources*, 2002, **112**, 443.

418 W. J. Zhou, M. W. Xu, D. D. Zhao, C. L. Xu and H. L. Li, *Microporous Mesoporous Mater.*, 2009, **117**, 55.
419 V. Gupta and N. Miura, *Electrochem. Commun.*, 2007, **9**, 2316.
420 P. K. Nayak and N. Munichandraiah, *J. Electrochem. Soc.*, 2008, **155**, A855.
421 E. B. Castro, S. G. Real and L. F. D. Pinheiro, *Int. J. Hydrogen Energy*, 2004, **29**, 255.
422 M. S. Wu, Y. A. Huang, J. J. Jow, W. D. Yang, C. Y. Hsieh and H. M. Tsai, *Int. J. Hydrogen Energy*, 2008, **33**, 2921.
423 V. Gupta, T. Kawaguchi and N. Miura, *Mater. Res. Bull.*, 2009, **44**, 202.
424 R. S. Jayashree and P. V. Kamth, *J. Appl. Electrochem.*, 2001, **31**, 1315.
425 K. W. Nam, K. H. Kim, E. S. Lee, W. S. Yoon, X. Q. Yang and K. B. Kim, *J. Power Sources*, 2008, **182**, 642.
426 Y. G. Wang and Y. Y. Xia, *Electrochim. Acta*, 2006, **51**, 3223.
427 H. Li, Y. Li, R. Wang and R. Cao, *J. Alloys Compd.*, 2009, **481**, 100.
428 K. C. Liu and M. A. Anderson, *J. Electrochem. Soc.*, 1996, **143**, 124.
429 J. Cheng, G. P. Cao and Y. S. Yang, *J. Power Sources*, 2006, **159**, 734.
430 D. W. Wang, F. Li and H. M. Cheng, *J. Power Sources*, 2008, **185**, 1563.
431 M. S. Wu, Y. A. Huang, C. H. Yang and J. J. Jow, *Int. J. Hydrogen Energy*, 2007, **32**, 4153.
432 Z. Fan, J. Chen, K. Cui, F. Sun, Y. Xu and Y. Kuang, *Electrochim. Acta*, 2007, **52**, 2959.
433 K. W. Nam, E. S. Lee, J. H. Kim, Y. H. Lee and K. B. Kim, *J. Electrochem. Soc.*, 2005, **152**, A2129.
434 L. Cao, M. Lin and H. L. Li, *J. Electrochem. Soc.*, 2005, **152**, A806.
435 X. Zhang, W. Shi, J. Zhu, W. Zhao, J. Ma, S. Mhaisalkar, T. L. Maria, Y. Yang, H. Zhang, H. H. Hng and Q. Yan, *Nano Res.*, 2010, **3**, 643.
436 J. W. Lang, L. B. Kong, W. J. Wu, Y. C. Luo and L. Kang, *Chem. Commun.*, 2008, 4213.
437 Y. Ren and L. Gao, *J. Am. Ceram. Soc.*, 2010, **93**, 3560.
438 C. Yuan, X. Zhang, L. Su, B. Gao and L. Shen, *J. Mater. Chem.*, 2009, **19**, 5772.
439 J. Zhu, J. Jiang, J. Liu, R. Ding, H. Ding, Y. Feng, G. Wei and X. Huang, *J. Solid State Chem.*, 2011, **184**, 578.
440 C. Y. Cao, W. Guo, Z. M. Cui, W. G. Song and W. Cai, *J. Mater. Chem.*, 2011, **21**, 3204.
441 X. Song and L. Gao, *J. Phys. Chem. C*, 2008, **112**, 15299.
442 D. W. Wang, F. Li, M. Liu, G. Lu and H. M. Cheng, *Angew. Chem., Int. Ed.*, 2008, **47**, 373.
443 Y. Hu, Y. V. Tolmachev and D. A. Scherson, *J. Electroanal. Chem.*, 1999, **468**, 64.
444 L. B. Kong, W. J. Wu, M. Liu, Y. C. Luo and L. Kang, *J. Solid State Electrochem.*, 2009, **13**, 333.
445 Y. Y. Liang, S. J. Bao and H. L. Li, *J. Solid State Electrochem.*, 2007, **11**, 571.
446 Z. A. Hu, Y. L. Xie, Y. X. Wang, H. Y. Wu, Y. Y. Yang and Z. Y. Zhang, *Electrochim. Acta*, 2009, **54**, 2737.
447 J. Zhang, L. B. Kong, J. J. Cai, H. Li, Y. C. Luo and L. Kang, *Microporous Mesoporous Mater.*, 2010, **132**, 154.
448 W. Dong, D. R. Rolison and B. Dunn, *Electrochem. Solid-State Lett.*, 2000, **3**, 457.
449 T. Kudo, Y. Ikeda, T. Watanabe, M. Hibino, M. Miyayama, H. Abe and K. Kajita, *Solid State Ionics*, 2002, **152**, 833.
450 H. Y. Lee and J. B. Goodenough, *J. Solid State Chem.*, 1999, **148**, 81.
451 R. N. Reddy and R. G. Reddy, *J. Power Sources*, 2006, **156**, 700.
452 G. Wee, H. Z. Soh, Y. L. Cheah, S. G. Mhaisalkar and M. Srinivasan, *J. Mater. Chem.*, 2010, **20**, 6720.
453 M. J. Parent, S. Passerini, B. B. Owens and W. H. Smyrl, *J. Electrochem. Soc.*, 1999, **146**, 1346.
454 G. Wang, M. Qu, Z. Yu and R. Yuan, *Mater. Chem. Phys.*, 2007, **105**, 169.
455 S. Passerini, J. J. Ressler, D. B. Le, B. B. Owens and W. H. Smyrl, *Electrochim. Acta*, 1999, **44**, 2209.
456 A. Dobley, K. Ngala, S. Yang, P. Y. Zavalij and M. S. Whittingham, *Chem. Mater.*, 2001, **13**, 4382.
457 M. Jayalakshmi, M. Mohan Rao, N. Venugopal and K. B. Kim, *J. Power Sources*, 2007, **166**, 578.
458 I. H. Kim, J. H. Kim, B. W. Cho, Y. H. Lee and K. B. Kim, *J. Electrochem. Soc.*, 2006, **153**, A989.
459 S. W. Hwang and S. H. Hyun, *J. Power Sources*, 2007, **172**, 451.
460 N. L. Wu, *Mater. Chem. Phys.*, 2002, **75**, 6.
461 K. R. Prasad and N. Miura, *Electrochem. Commun.*, 2004, **6**, 849.
462 M. Jayalakshmi, N. Venugopal, K. P. Raja and M. M. Rao, *J. Power Sources*, 2006, **158**, 1538.
463 X. Zhao, C. Johnston and P. S. Grant, *J. Mater. Chem.*, 2009, **19**, 8755.
464 H. Zhu, D. Yang and L. Zhu, *Surf. Coat. Technol.*, 2007, **201**, 5870.
465 J. Chen, K. Huang and S. Liu, *Electrochim. Acta*, 2009, **55**, 1.
466 A. A. F. Grupioni, E. Arashiro and T. A. F. Lassali, *Electrochim. Acta*, 2002, **48**, 407.
467 T. P. Gujar, V. R. Shinde, C. D. Lokhande and S. H. Han, *J. Power Sources*, 2006, **161**, 1479.
468 J. Rajeswari, P. S. Kishore, B. Viswanathan and T. K. Varadarajan, *Electrochem. Commun.*, 2009, **11**, 572.
469 T. C. Liu, W. G. Pell and B. E. Conway, *J. Electrochem. Soc.*, 1998, **145**, 1882.
470 D. W. Choi, G. E. Blomgren and P. N. Kumta, *Adv. Mater.*, 2006, **18**, 1178.
471 D. W. Choi and P. N. Kumta, *Electrochem. Solid-State Lett.*, 2005, **8**, A418.
472 Y. Lin and N. Wu, *J. Power Sources*, 2011, **196**, 851.
473 S. L. Kuo and N. L. Wu, *J. Power Sources*, 2006, **162**, 1437.
474 S. L. Kuo, J. F. Lee and N. L. Wu, *J. Electrochem. Soc.*, 2007, **154**, A34.
475 Q. T. Qua, Y. Shi, S. Tian, Y. H. Chen, Y. P. Wu and R. Holze, *J. Power Sources*, 2009, **194**, 1222.

